Doctoral Dissertation

Design of Nanoporous and Chemical Structures in Carbonized Bionanofiber Paper for Solar Thermal Heating

太陽光熱変換に向けた炭化バイオナノファイバーペーパーのナノ細孔構造と化学構造制御

Thanakorn Yeamsuksawat

June 2023

Graduate School of Engineering,
Osaka University

Contents

General Introduction

The efficient utilization of renewable energy resources, particularly solar energy, is widely recognized as a promising approach to addressing global warming and promoting sustainable development for human activity.[1,2] In recent years, the adoption of solar energy has gained significant momentum, driven by ongoing research and the need for alternative power sources in response to concerns about the limited availability of fossil fuels.[3,4] In this regard, solar thermal heating, holds great significance in a broad range of applications[5,6], including solar-driven water vaporization,[7–11] desalination[9,10,12], wastewater purification[9,13,14], deicing[15–17], the catalytic production of fuels and chemicals[18–21], energy storage[22–24], wearable heating,[25–27] wound healing,[28] sterilization[29–33], etc. This approach involves the conversion of solar light energy into thermal energy by using photothermal materials such as plasmonic metal nanoparticles, metal oxide semiconductors, and carbon materials.[5,6] Among these, the carbon materials have gained significant attention due to their proficiency in harvesting a broader range of wavelengths compared to other materials[5,34–37]. This characteristic makes them highly advantageous for absorbing solar light within the 300–2500 nm wavelength range[38] **(Fig. 1)**.

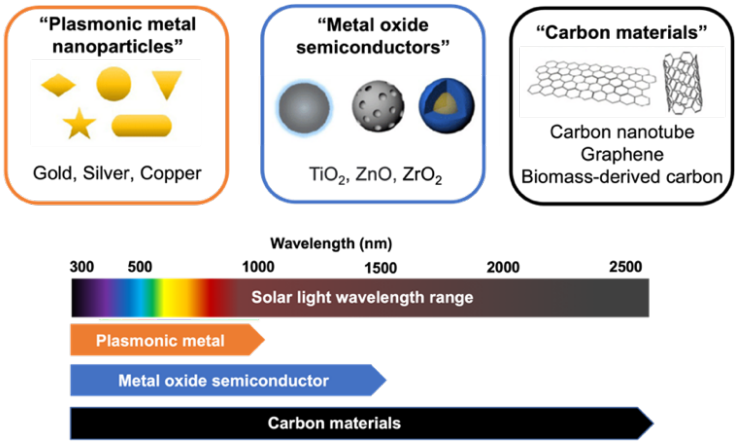

Fig. 1 Type of photothermal materials and solar light absorption wavelength range for each photothermal material.

Photothermal materials possess the remarkable capability to absorb optical energy and convert it into heat.[5,39] The general mechanism behind solar thermal heating involves the absorption of solar light by such photothermal materials. When illuminated, the electrons within the photothermal material are promoted from the ground state to the excited state. After that, the excited electrons relax back to the ground state, releasing energy in the form of heat[5,40] **(Fig. 2)**. Therefore, if photothermal materials can absorb a greater amount of solar light, the heat generated via the photothermal conversion process will increase proportionally.[41–43] Hence, it is necessary to develop photothermal materials with improved structural and functional properties in order to enhance their solar thermal heating performance so as to use solar light energy more efficiently[34] **(Fig. 3)**.

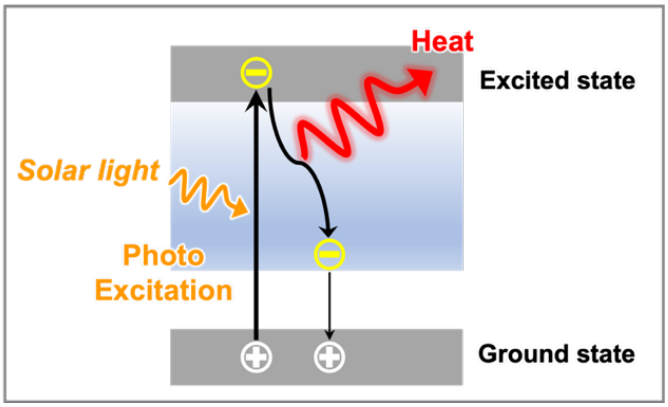

Fig. 2 General mechanism of solar thermal heating

One effective approach to harnessing visible light in the 400–700 nm range is through the customization of subwavelength nanoporous structures.[44] These structures have been extensively utilized in plasmonic metal nanoparticles and metal oxide semiconductors, making it possible to enhance the light absorption while simultaneously suppressing the reflection of light from the outer surface. This phenomenon is commonly referred to as the "light confinement effect".[45–47] For carbon-based materials derived primarily from organic sources, the energy gaps between the bonding (σ) and antibonding (σ^*) orbitals in single carbon bonds such as C–C, C–H, and C–O are significant.[5] Consequently, the transition from σ to σ^* cannot occur under solar light irradiation. To address this limitation, it is necessary to design carbon structures with sp^2-hybridization[48,49]

and heteroatom doping.[50,51] These modifications involve the formation of pi (π) bonds via the promotion of an electron from an s orbital to a 2p atomic orbital, and the manipulation of the band energy. Because the electrons are less strongly bonded, the resulting π bonds are typically weaker than σ bonds. Hence, the excitation of these electrons from the π to the π^* orbital requires lower energy input. By increasing the number of π bonds and incorporating doping components, the energy gap between the highest-occupied molecular orbital (HOMO) and the lowest unoccupied molecular orbital (LUMO) is decreased.[48–51] As a result, the solar light absorption is enhanced, particularly at longer wavelengths. This, in turn, facilitates the conversion of the absorbed light into heat through vibrational relaxation.[43,52] Therefore, a rational strategy for maximizing solar thermal heating would involve tuning both the subwavelength nanoporous structures and chemical structures of carbon-based photothermal materials.

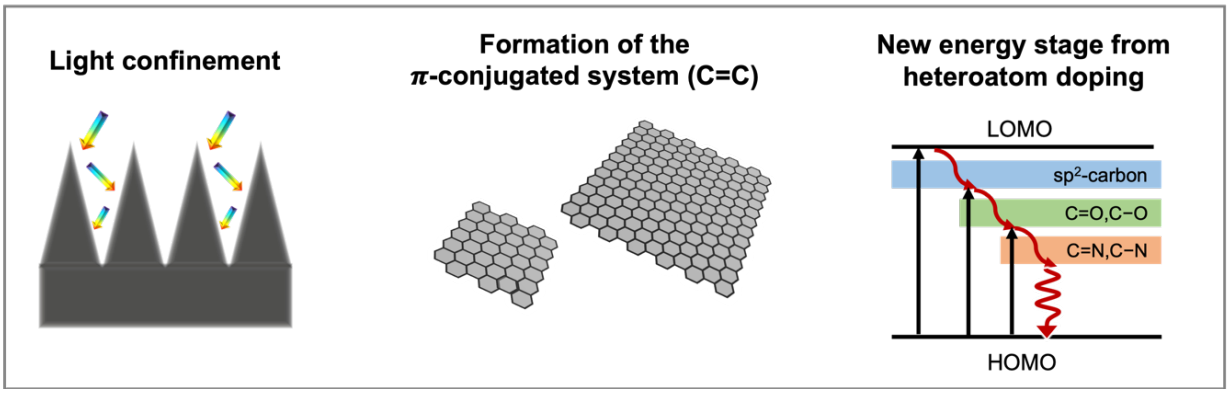

Fig. 3 Strategies to improve solar thermal heating performance of photothermal materials.

Recently, there has been growing interest in biomass-derived carbon materials due to their unique physical and chemical properties, porous structures with high specific surface areas, and sustainability.[53,54] Due to these advantages, biomass-derived carbon materials such as carbonized wood[55–59], mushroom[60], sugarcane[61–64], cotton[65,66], daikon[67], agave flower stalk[68], corncob[69–71], bamboo[72–74], rice straw,[75,76] loofah,[77] lotus,[78–80] carrot,[81] pomelo peel,[82] durian,[83] eggplant,[84] and

sunflower head[85] have been investigated as sustainable photothermal materials for solar thermal heating applications **(Fig. 4)**. However, previous studies have encountered certain limitations such as difficulties in designing subwavelength nanoporous structures and suitable carbonization conditions. Consequently, the design of biomass-derived carbon materials that exhibit desirable nanoporous and chemical structures for solar thermal heating applications has proven challenging.

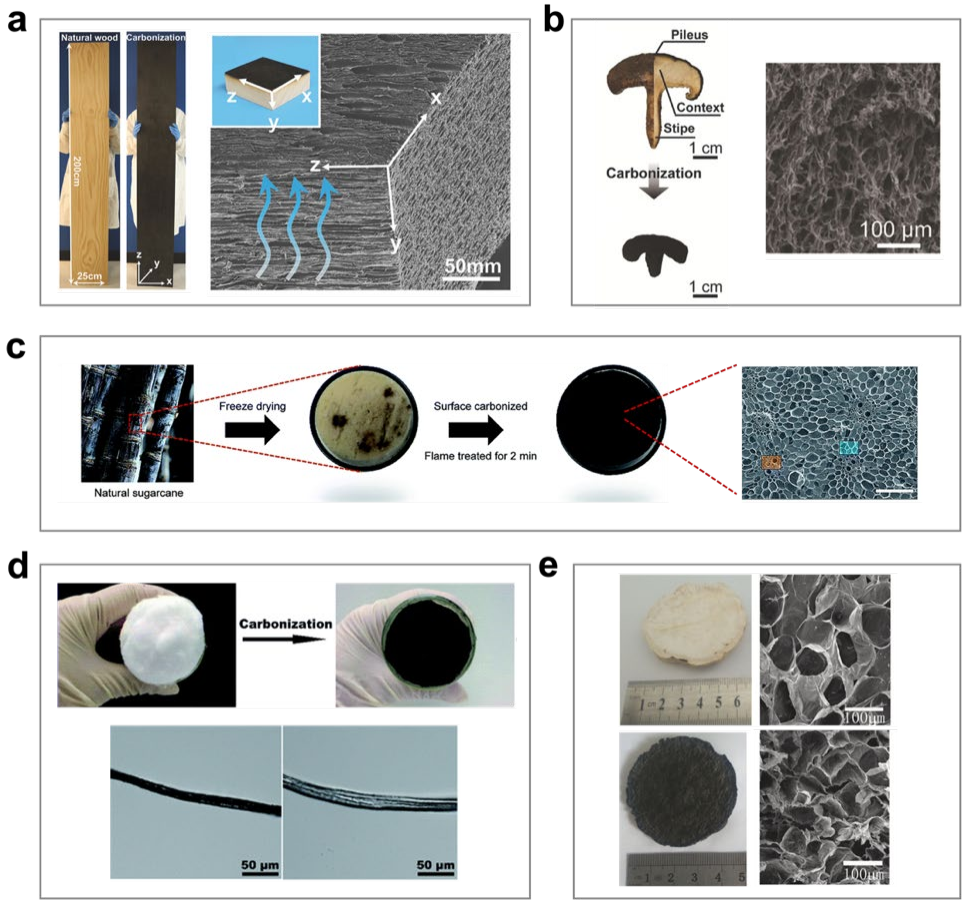

Fig. 4 Example of biomass-derived carbon for solar thermal heating application. (a) Carbonized wood Reproduced with permission[54]. Copyright 2018, Wiley-VCH; (b) Carbonized mushroom Reproduced with permission[59]. Copyright 2017, Wiley-VCH; (c) Carbonized sugarcane Reproduced with permission[60]. Copyright 2019, Royal Society of Chemistry; (d) Carbonized cotton Reproduced with permission[64]. Copyright 2018, Royal Society of Chemistry; and (e) Carbonized daikon Reproduced with permission[66]. Copyright 2019, Elsevier BV.

To address the above-mentioned limitations, significant attention has focused on bionanofiber materials, which have excellent physical properties, sustainability, and nanostructures.[86–89] Cellulose nanofibers are composed of ordered linear chains of β-(1,4)-linked D-glucose, and can be fabricated from wood pulp fibers by reducing their diameters (ranging from less than 100 μm to around 2–4 nm)[87,90–92] **(Fig. 5a)**. In addition, chitin (β-(1→4)-linked N-acetyl anhydroglucosamine)[93] can be isolated as nanofibers from the exoskeletons of crustacean wastes such as crab shells[94,95], squid pens[96,97], and prawns[98,99] **(Fig. 5b)**. The nanofiber morphologies of cellulose and chitin make them ideal building blocks for the fabrication of nanostructures. Furthermore, because the sp^3-hybridized carbon structures of cellulose and chitin are both rich in oxygen and hydrogen, and chitin is also rich in nitrogen,[88,100,101] carbonization can be employed to tune their chemical structures over a wide range[102–104]. Therefore, cellulose and chitin are promising precursors for fabricating carbon materials with optimized nanoporous and chemical structures for the development of high-performance photothermal materials for solar thermal heating applications.

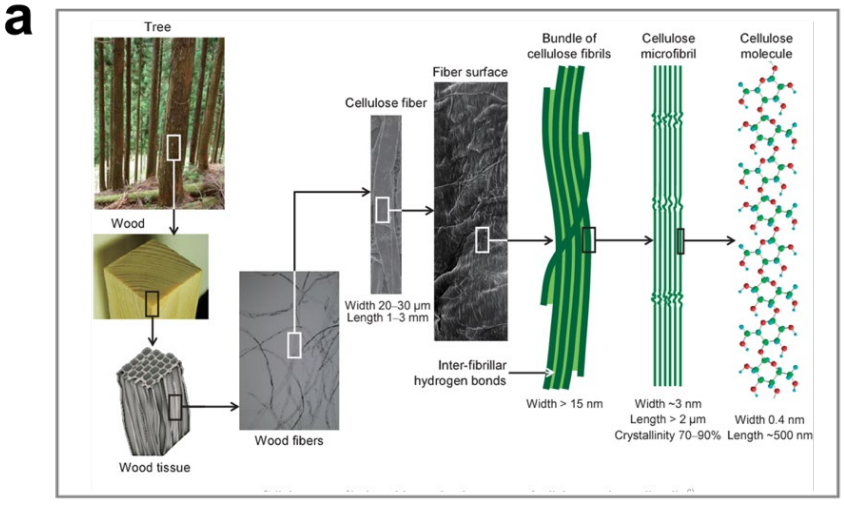

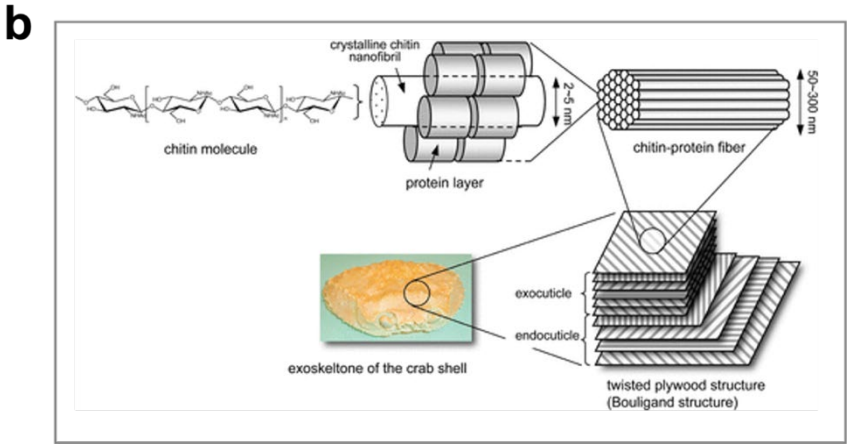

Fig. 5 The hierarchical structure of bionanofiber materials. (a) Cellulose nanofiber in wood. Reproduced with permission[86]. Copyright 2009, Royal Society of Chemistry; (b) Chitin nanofiber in the exoskeleton structure of crustacean shell. Reproduced with permission[93]. Copyright 2009, American Chemical Society.

Outline of this dissertation

Sustainable biomass-derived carbon materials have garnered significant research attention due to their potential application in solar thermal heating. These materials possess the remarkable ability to absorb and convert solar light energy into thermal energy with high efficiency. However, the customization of their carbon-based chemical and nanoporous structures for enhanced solar thermal heating performance has not progressed sufficiently. This dissertation focuses on the utilization of cellulose and chitin nanofibers due to their fascinating nanofiber morphologies and intrinsic chemical structures, which can be customized via conventional high-temperature and CO_2-laser-induced carbonization techniques. In this work, the bionanofiber materials are fabricated in the form of a paper, denoted as nanopaper, that exhibits controllable subwavelength nanoporous structure by adjusting the pore spaces between the bio-nanofibers, followed by

carbonization. Subsequently, the solar thermal heating performance of the carbonized bionanofiber papers are investigated.

Chapter 1

The solar thermal heating performances of carbonized cellulose nanopapers with dense and subwavelength nanoporous structures are compared. It is confirmed that the subwavelength nanoporous structures enhance the light absorption and improve the solar thermal heating performance. Then, the cellulose nanopapers with subwavelength nanoporous structures are carbonized at various temperatures to control the chemical structure. As a result, the semi-carbonized structure obtained at 500 °C is found to be suitable for light absorption and exhibits the optimal solar thermal heating performance

Chapter 2

The findings of Chapter 1 are applied to chitin nanopaper. The carbonized chitin nanopaper exhibits better solar thermal heating than the carbonized cellulose nanopaper. This result is attributed to the nitrogen component in the chitin molecule, which contributes to the retention of the subwavelength nanoporous structure and the enhancement in solar absorption after carbonization.

Chapter 3

The rapid carbonization of chitin nanopaper is successfully achieved by CO_2 laser irradiation. The addition of calcium chloride is shown to improve the flame retardancy and facilitate the CO_2 laser carbonization process. As a result, the CO_2-laser-carbonized chitin paper exhibits a comparable solar thermal heating performance to that of bio-nanopaper carbonized at high-temperature.

References

1 S. Mekhilef, R. Saidur and A. Safari, *Renew. Sustain. Energy Rev.*, 2011, **15**, 1777–1790.

2 M. S. Guney, *Renew. Sustain. Energy Rev.*, 2016, **57**, 776–785.

3 G. W. Crabtree and N. S. Lewis, *Phys. Today*, 2007, **60**, 37–42.

4 N. Abas, A. Kalair and N. Khan, *Futures*, 2015, **69**, 31–49.

5 M. Gao, L. Zhu, C. K. Peh and G. W. Ho, *Energy Environ. Sci.*, 2019, **12**, 841–864.

6 Y. Li, X. Bai, D. Yuan, F. Zhang, B. Li, X. San, B. Liang, S. Wang, J. Luo and G. Fu, *Nat. Commun.*, 2022, **13**, 776.

7 R. Fillet, V. Nicolas, V. Fierro and A. Celzard, *Sol. Energy Mater. Sol. Cells*, 2021, **219**, 110814.

8 L. Zhu, M. Gao, C. K. N. Peh and G. W. Ho, *Nano Energy*, 2019, **57**, 507–518.

9 W. Guan, Y. Guo and G. Yu, *Small*, 2021, **17**, 2007176.

10 I. Ibrahim, D. H. Seo, A. M. McDonagh, H. K. Shon and L. Tijing, *Desalination*, 2021, **500**, 114853.

11 Y. Lin, H. Xu, X. Shan, Y. Di, A. Zhao, Y. Hu and Z. Gan, *J. Mater. Chem. A*, 2019, **7**, 19203–19227.

12 F. Nawaz, Y. Yang, S. Zhao, M. Sheng, C. Pan and W. Que, *J. Mater. Chem. A*, 2021, **9**, 16233–16254.

13 A. M. Saleque, N. Nowshin, Md. N. A. S. Ivan, S. Ahmed and Y. H. Tsang, *Sol. RRL*, 2022, **6**, 2100986.

14 S. Cao, A. Thomas. A and C. Li, *Angew. Chem.*, 2023, **135,** e202214391

15 S. Dash, J. De Ruiter and K. K. Varanasi, *Sci. Adv.*, 2018, **4**, eaat0127.

16 Y. Wu, L. Dong, X. Shu, Y. Yang, P. Feng and Q. Ran, *Chem. Eng. J.*, 2023, **469**, 143924.

17 S. Jiang, Y. Diao and H. Yang, *Adv. Colloid Interface Sci.*, 2022, **308**, 102756.

18 X. Meng, T. Wang, L. Liu, S. Ouyang, P. Li, H. Hu, T. Kako, H. Iwai, A. Tanaka and J. Ye, *Angew. Chem.*, 2014, **126**, 11662–11666.

19 E. T. Kho, T. H. Tan, E. Lovell, R. J. Wong, J. Scott and R. Amal, *Green Energy Environ.*, 2017, **2**, 204–217.

20 S. Zhou, L. Zhou, Y. Zhang, J. Sun, J. Wen and Y. Yuan, *J. Mater. Chem. A*, 2019, **7**, 4217–4229.

21 Z. Wang, Y. Liu, B. Huang, Y. Dai, Z. Lou, G. Wang, X. Zhang and X. Qin, *Phys. Chem. Chem. Phys.*, 2014, **16**, 2758–2774.

22 Z. Wang, Z. Tong, Q. Ye, H. Hu, X. Nie, C. Yan, W. Shang, C. Song, J. Wu, J. Wang, H. Bao, P. Tao and T. Deng, *Nat. Commun.*, 2017, **8**, 1478.

23 L. Tang, X. Zhao, C. Feng, L. Bai, J. Yang, R. Bao, Z. Liu, M. Yang and W. Yang, *Sol. Energy Mater. Sol. Cells*, 2019, **203**, 110174.

24 C. Chang, X. Nie, X. Li, P. Tao, B. Fu, Z. Wang, J. Xu, Q. Ye, J. Zhang, C. Song, W. Shang and T. Deng, *J. Mater. Chem. A*, 2020, **8**, 20970–20978.

25 Y. Cheng, H. Zhang, R. Wang, X. Wang, H. Zhai, T. Wang, Q. Jin and J. Sun, *ACS Appl. Mater. Interfaces*, 2016, **8**, 32925–32933.

26 Y. Huang, X. Chen, J. Yu and L.-Q. Tao, *Mater. Lett.*, 2021, **284**, 128869.

27 H. Yi, Y. Zhao and S. Song, *Appl. Clay Sci.*, 2021, **200**, 105886.

28 Y. Gao, H. Du, Z. Xie, M. Li, J. Zhu, J. Xu, L. Zhang, J. Tao and J. Zhu, *J. Mater. Chem. B*, 2019, **7**, 3644–3651.

29 J. Li, M. Du, G. Lv, L. Zhou, X. Li, L. Bertoluzzi, C. Liu, S. Zhu and J. Zhu, *Adv. Mater.*, 2018, **30**, 1805159.

30 L. Wang, Y. Feng, K. Wang and G. Liu, *Nano Energy*, 2021, **87**, 106158.

31 J. Huo, Q. Jia, H. Huang, J. Zhang, P. Li, X. Dong and W. Huang, *Chem. Soc. Rev.*, 2021, **50**, 8762–8789.

32 Y. Lu, H. Zhang, D. Fan, Z. Chen and X. Yang, *J. Hazard. Mater.*, 2022, **423**, 127128.

33 Q. Xin, H. Shah, A. Nawaz, W. Xie, M. Z. Akram, A. Batool, L. Tian, S. U. Jan, R. Boddula, B. Guo, Q. Liu and J. R. Gong, *Adv. Mater.*, 2019, **31**, 1804838.

34 J. U. Kim, S. Lee, S. J. Kang and T. Kim, *Nanoscale*, 2018, **10**, 21555–21574.

35 X. Wu, G. Y. Chen, G. Owens, D. Chu and H. Xu, *Mater. Today Energy*, 2019, **12**, 277–296.

36 L. Wang, M. Hasanzadeh Kafshgari and M. Meunier, *Adv. Funct. Mater.*, 2020, **30**, 2005400.

37 K. W. Tan, C. M. Yap, Z. Zheng, C. Y. Haw, P. S. Khiew and W. S. Chiu, *Adv. Sustain. Syst.*, 2022, **6**, 2100416.

38 ASTM G173-03., *Standard Tables for Reference Solar Spectral Irradiances: Direct Normal and Hemispherical on 37° Tilted Surface*, ASTM International: West Conshohocken, PA, 2012.

39 G. Ni, G. Li, S. V. Boriskina, H. Li, W. Yang, T. Zhang and G. Chen, *Nat. Energy*, 2016, **1**, 16126.

40 C. Chen, Y. Kuang and L. Hu, *Joule*, 2019, **3**, 683–718.

41 J. Li, W. Zhang, W. Ji, J. Wang, N. Wang, W. Wu, Q. Wu, X. Hou, W. Hu and L. Li, *J. Mater. Chem. B*, 2021, **9**, 7909–7926.

42 X. Cui, Q. Ruan, X. Zhuo, X. Xia, J. Hu, R. Fu, Y. Li, J. Wang and H. Xu, *Chem. Rev.*, 2023, acs.chemrev.3c00159.

43 G. Liu, J. Xu and K. Wang, *Nano Energy*, 2017, **41**, 269–284.

44 K. Aydin, V. E. Ferry, R. M. Briggs and H. A. Atwater, *Nat. Commun.*, 2011, **2**, 517.

45 X. Zheng and L. Zhang, *Energy Environ. Sci.*, 2016, **9**, 2511–2532.

46 P. Kumar, R. Boukherroub and K. Shankar, *J. Mater. Chem. A*, 2018, **6**, 12876–12931.

47 H. Dotan, O. Kfir, E. Sharlin, O. Blank, M. Gross, I. Dumchin, G. Ankonina and A. Rothschild, *Nat. Mater.*, 2013, **12**, 158–164.

48 L.-L. Ma, W.-J. Liu, X. Hu, P. K. S. Lam, J. R. Zeng and H.-Q. Yu, *Chem. Eng. J.*, 2020, **400**, 125969.

49 Y. Zou, W. Li, L. Yang, F. Xiao, G. An, Y. Wang and D. Wang, *Chem. Eng. J.*, 2019, **370**, 1286–1297.

50 Y. Ito, Y. Tanabe, J. Han, T. Fujita, K. Tanigaki and M. Chen, *Adv. Mater.*, 2015, **27**, 4302–4307.

51 J. Yang, Y. Pang, W. Huang, S. K. Shaw, J. Schiffbauer, M. A. Pillers, X. Mu, S. Luo, T. Zhang, Y. Huang, G. Li, S. Ptasinska, M. Lieberman and T. Luo, *ACS Nano*, 2017, **11**, 5510–5518.

52 G. Feng, G.-Q. Zhang and D. Ding, *Chem. Soc. Rev.*, 2020, **49**, 8179–8234.

53 B. Szczęśniak, J. Phuriragpitikhon, J. Choma and M. Jaroniec, *J. Mater. Chem. A*, 2020, **8**, 18464–18491.

54 Y. Wang, M. Zhang, X. Shen, H. Wang, H. Wang, K. Xia, Z. Yin and Y. Zhang, *Small*, 2021, **17**, 2008079.

55 H. Liu, C. Chen, G. Chen, Y. Kuang, X. Zhao, J. Song, C. Jia, X. Xu, E. Hitz, H. Xie, S. Wang, F. Jiang, T. Li, Y. Li, A. Gong, R. Yang, S. Das and L. Hu, *Adv. Energy Mater.*, 2018, **8**, 1701616.

56 G. Xue, K. Liu, Q. Chen, P. Yang, J. Li, T. Ding, J. Duan, B. Qi and J. Zhou, *ACS Appl. Mater. Interfaces*, 2017, **9**, 15052–15057.

57 P. Qiu, F. Liu, C. Xu, H. Chen, F. Jiang, Y. Li and Z. Guo, *J. Mater. Chem. A*, 2019, **7**, 13036–13042.

58 C. Jia, Y. Li, Z. Yang, G. Chen, Y. Yao, F. Jiang, Y. Kuang, G. Pastel, H. Xie, B. Yang, S. Das and L. Hu, *Joule*, 2017, **1**, 588–599.

59 X. Pan, N. Zhang, Y. Yuan, X. Shao, W. Zhong and L. Yang, *Sol. Energy*, 2021, **230**, 269–277.

60 N. Xu, X. Hu, W. Xu, X. Li, L. Zhou, S. Zhu and J. Zhu, *Adv. Mater.*, 2017, **29**, 1606762.

61 J. Liu, Q. Liu, D. Ma, Y. Yuan, J. Yao, W. Zhang, H. Su, Y. Su, J. Gu and D. Zhang, *J. Mater. Chem. A*, 2019, **7**, 9034–9039.

62 C. Xiao, L. Chen, P. Mu, J. Jia, H. Sun, Z. Zhu, W. Liang and A. Li, *ChemistrySelect*, 2019, **4**, 7891–7895.

63 W. Zhang, L. Zhang, T. Li, D. Wu, C. Zhang and H. Zhu, *J. Water Process Eng.*, 2022, **49**, 102991.

64 Q. Zhang, X. Yang, H. Deng, Y. Zhang, J. Hu and R. Tian, *Desalination*, 2022, **526**, 115544.

65 X. Wu, L. Wu, J. Tan, G. Y. Chen, G. Owens and H. Xu, *J. Mater. Chem. A*, 2018, **6**, 12267–12274.

66 H. M. Wilson, S. Rahman A.R., A. E. Parab and N. Jha, *Desalination*, 2019, **456**, 85–96.

67 M. Zhu, J. Yu, C. Ma, C. Zhang, D. Wu and H. Zhu, *Sol. Energy Mater. Sol. Cells*, 2019, **191**, 83–90.

68 E. G. Villabona-Leal, A. G. Escobar-Villanueva, E. B. Pérez-Pérez, H. Martínez-Gutiérrez and V. M. Ovando-Medina, *Int. J. Energy Res.*, 2021, **45**, 19521–19534.

69 Y. Sun, Z. Zhao, G. Zhao, L. Wang, D. Jia, Y. Yang, X. Liu, X. Wang and J. Qiu, *Carbon*, 2021, **179**, 337–347.

70 H. Zhang, L. Li, B. Jiang, Q. Zhang, J. Ma, D. Tang and Y. Song, *ACS Appl. Mater. Interfaces*, 2020, **12**, 16503–16511.

71 J. He, J. Ge, Y. Pang, L. Shen, Y. Wu, Y. Lv, B. Zhang, L. Peng, J. Yang and M. Qu, *Sol. Energy*, 2023, **252**, 39–49.

72 Z. Li, C. Wang, T. Lei, H. Ma, J. Su, S. Ling and W. Wang, *Adv. Sustain. Syst.*, 2019, **3**, 1800144.

73 Y. Bian, Q. Du, K. Tang, Y. Shen, L. Hao, D. Zhou, X. Wang, Z. Xu, H. Zhang, L. Zhao, S. Zhu, J. Ye, H. Lu, Y. Yang, R. Zhang, Y. Zheng and S. Gu, *Adv. Mater. Technol.*, 2019, **4**, 1800593.

74 J. Liu, J. Yao, Y. Yuan, Q. Liu, W. Zhang, X. Zhang and J. Gu, *Adv. Sustain. Syst.*, 2020, **4**, 2000126.

75 Q. Fang, T. Li, Z. Chen, H. Lin, P. Wang and F. Liu, *ACS Appl. Mater. Interfaces*, 2019, **11**, 10672–10679.

76 D. P. Storer, J. L. Phelps, X. Wu, G. Owens, N. I. Khan and H. Xu, *ACS Appl. Mater. Interfaces*, 2020, **12**, 15279–15287.

77 Y. Lu, X. Wang, D. Fan, H. Yang, H. Xu, H. Min and X. Yang, *Sustain. Mater. Technol.*, 2020, **25**, e00180.

78 J. Fang, J. Liu, J. Gu, Q. Liu, W. Zhang, H. Su and D. Zhang, *Chem. Mater.*, 2018, **30**, 6217–6221.

79 H.-Y. Zhao, J. Zhou, Z.-L. Yu, L.-F. Chen, H.-J. Zhan, H.-W. Zhu, J. Huang, L.-A. Shi and S.-H. Yu, *Cell Rep. Phys. Sci.*, 2020, **1**, 100074.

80 L. Zhang, C. Sha, B. Li and W. Wang, *Energy Sources A: Recovery Util. Environ. Eff.*, 2023, **45**, 3359–3368.

81 Y. Long, S. Huang, H. Yi, J. Chen, J. Wu, Q. Liao, H. Liang, H. Cui, S. Ruan and Y.-J. Zeng, *J. Mater. Chem. A*, 2019, **7**, 26911–26916.

82 C. Zhang, P. Xiao, F. Ni, L. Yan, Q. Liu, D. Zhang, J. Gu, W. Wang and T. Chen, *ACS Sustain. Chem. Eng.*, 2020, **8**, 5328–5337.

83 L. Zeng, D. Deng, L. Zhu, H. Wang, Z. Zhang and Y. Yao, *Energy*, 2023, **273**, 127170.

84 R. Zhu, D. Wang, J. Zhang, Z. Yu, M. Liu and S. Fu, *Desalination*, 2022, **527**, 115585.

85 P. Sun, W. Zhang, I. Zada, Y. Zhang, J. Gu, Q. Liu, H. Su, D. Pantelić, B. Jelenković and D. Zhang, *ACS Appl. Mater. Interfaces*, 2020, **12**, 2171–2179.

86 B. Thomas, M. C. Raj, A. K. B, R. M. H, J. Joy, A. Moores, G. L. Drisko and C. Sanchez, *Chem. Rev.*, 2018, **118**, 11575–11625.

87 A. Isogai, T. Saito and H. Fukuzumi, *Nanoscale*, 2011, **3**, 71–85.

88 D. Klemm, B. Heublein, H.-P. Fink and A. Bohn, *Angew. Chem. Int. Ed.*, 2005, **44**, 3358–3393.

89 S. Ifuku and H. Saimoto, *Nanoscale*, 2012, **4**, 3308–3318.

90 A. Isogai and L. Bergström, *Curr. Opin. Green Sustain. Chem.*, 2018, **12**, 15–21.

91 S. J. Eichhorn, A. Dufresne, M. Aranguren, N. E. Marcovich, J. R. Capadona, S. J. Rowan, C. Weder, W. Thielemans, M. Roman, S. Renneckar, W. Gindl, S. Veigel, J. Keckes, H. Yano, K. Abe, M. Nogi, A. N. Nakagaito, A. Mangalam, J. Simonsen, A. S. Benight, A. Bismarck, L. A. Berglund and T. Peijs, *J. Mater. Sci.*, 2010, **45**, 1–33.

92 I. Siró and D. Plackett, *Cellulose*, 2010, **17**, 459–494.

93 M. Rinaudo, *Prog. Polym. Sci.*, 2006, **31**, 603–632.

94 S. Ifuku, M. Nogi, K. Abe, M. Yoshioka, M. Morimoto, H. Saimoto and H. Yano, *Biomacromolecules*, 2009, **10**, 1584–1588.

95 T. Setoguchi, T. Kato, K. Yamamoto and J. Kadokawa, *Int. J. Biol. Macromol.*, 2012, **50**, 861–864.

96 Y. Fan, T. Saito and A. Isogai, *Biomacromolecules*, 2008, **9**, 1919–1923.

97 A. K. Dutta, H. Izawa, M. Morimoto, H. Saimoto and S. Ifuku, *J. Chitin Chitosan Sci.*, 2013, **1**, 186–191.

98 J. D. Goodrich and W. T. Winter, *Biomacromolecules*, 2007, **8**, 252–257.

99 S. Ifuku, M. Nogi, K. Abe, M. Yoshioka, M. Morimoto, H. Saimoto and H. Yano, *Carbohydr. Polym.*, 2011, **84**, 762–764.

100 H. He, R. Zhang, P. Zhang, P. Wang, N. Chen, B. Qian, L. Zhang, J. Yu and B. Dai, *Adv. Sci.*, 2023, **10**, 2205557.

101 A. Berthod, *Anal. Chem.*, 2006, **78**, 2093–2099.

102 H. Koga, K. Nagashima, K. Suematsu, T. Takahashi, L. Zhu, D. Fukushima, Y. Huang, R. Nakagawa, J. Liu, K. Uetani, M. Nogi, T. Yanagida and Y. Nishina, *ACS Nano*, 2022, **16**, 8630–8640.

103 L. Zhu, Y. Huang, Y. Morishita, K. Uetani, M. Nogi and H. Koga, *J. Mater. Chem. C*, 2021, **9**, 4444–4452.

104 X. Li, L. Zhu, T. Kasuga, M. Nogi and H. Koga, *Chem. Eng. J.*, 2022, **450**, 137943.

Chapter 1

Semicarbonized Subwavelength-Nanopore-Structured Nanocellulose Paper for Applications in Solar Thermal Heating

1.1 Introduction

Biomass-derived carbon materials have recently attracted increased interest owing to their unique physical and chemical properties, intrinsic high-specific-surface-area porous structures, and sustainability.[1,2] The potential applications of biomass-derived carbon materials include adsorption,[3] separation,[4] sensing,[5,6] energy storage,[7,8] and photothermal heating,[9] among which photothermal heating has recently garnered the most attention for converting renewable solar light energy into heat.[10–15] Photothermal heating is achieved using photothermal materials that enable light to be absorbed and then converted into heat. Biomass-derived carbons are promising photothermal materials because carbon materials absorb light over a broader wavelength range (approximately 300–2500 nm) than other materials like plasmonic metal nanoparticles (approximately 300–1000 nm) and metal oxide semiconductors (approximately 300–1500 nm),[16] which is beneficial for absorbing solar light in the wavelength range of 300–2500 nm (*e.g.*, ASTM G173-03, AM1.5G).[17]

To use solar light energy more efficiently, photothermal materials must be structurally and functionally designed to improve their solar thermal heating performances.[16] For example, subwavelength nanoporous structures have been extensively tailored for application as plasmonic metal nanoparticles and metal oxide semiconductors to enhance light absorption by suppressing light reflection to the outer surface, which is known as “light confinement”.[18] For carbon-based photothermal materials, their sp^2-hybridized carbon-based chemical structures, such as the distribution of the highest occupied molecular orbital (HOMO) and the lowest unoccupied

molecular orbital (LUMO), must also be designed because they not only affect the light-absorption wavelength range but also convert absorbed light into heat via vibrational relaxation.[19] Therefore, tailoring both the subwavelength nanoporous and chemical structures of biomass-derived carbon materials would be a rational strategy to optimize solar thermal heating.

Recently, various biomass-derived carbon materials, such as carbonized wood,[10] cotton,[11] mushroom,[12] sugarcane,[13] daikon,[14] and agave flower stalk,[15] have been reported for solar thermal applications. Because these natural biomass materials inherently exhibit microstructures, their carbonized derivatives also intrinsically exhibit them, thereby hindering the design of subwavelength nanoporous structures. Carbonized biomass materials form sp^2-hybridized carbon-based chemical structures to absorb light over a broad wavelength range. However, these chemical structures have not been tailored to optimize solar light absorption yet because the materials are frequently carbonized under specific conditions. Thus, the design of biomass-derived carbon materials exhibiting nanoporous and chemical structures desirable for solar thermal heating applications has proven difficult.

Herein, a cellulose nanofiber-derived carbon material exhibiting tailored nanoporous and chemical structures is proposed for effective solar thermal heating. Cellulose nanofiber, which is mainly extracted from wood cell walls, has attracted significant attention as a fascinating biomass nanomaterial because of its excellent physical properties, nanostructures, abundance, and sustainability.[20–22] At present, cellulose nanofiber can be produced in a large-scale industrial operation, and its market is estimated to reach USD 963 million by 2026.[23] Cellulose nanofiber can be used as a building block to fabricate nanostructures because of its nanofiber morphology. Moreover, because the cellulose sp^3-hybridized carbon structure contains high oxygen and hydrogen contents,[24] carbonization can be used to tune cellulose nanofiber chemical structures over

a wide range.[25] Carbonized cellulose nanofiber materials have been reported for adsorption and electronic applications.[25–28] To our best knowledge, however, their application in solar thermal heating has been unexplored. In this chapter, cellulose nanofiber is fabricated into a paper (hereafter denoted as "nanopaper"), exhibiting nanoporous structures by tailoring the pore spaces between cellulose nanofibers and is subsequently carbonized at controlled temperatures to gradually grow sp^2-hybridized carbon domains. The carbonized cellulose nanopaper, fabricated with the as-tailored nanoporous and chemical structures, exhibits excellent solar thermal heating performance, which is superior even to the state-of-the-art nanocarbon materials such as carbon nanotube (CNT) and graphene films.

1.2 Experimental Section

Materials

According to the method detailed in our previous report,[25] never-dried softwood bleached kraft pulp and a high-pressure water-jet system equipped with a counter-collision chamber (Star Burst, HJP-25005E, Sugino Machine Co., Ltd., Uozu, Japan) were used to prepare a cellulose nanofiber/water dispersion. Briefly, the pulp suspension was ejected from a ⌀0.12-mm nozzle at 245 MPa for 100 passes. Iodine (>99.8% purity) and *tert*-butyl alcohol (*t*-BuOH, >99.0% purity) were purchased from Nacalai Tesque, Inc., Kyoto, Japan. A CNT black body was obtained from MICROPHASE Co., Ltd., Tsukuba, Japan. A graphite sheet (EYGS121810) was purchased from Panasonic Corp., Osaka, Japan. A graphene paper (900451-1EA) and a graphene oxide film (798991-1EA) were obtained from Merck KGaA, Darmstadt, Germany.

Cellulose nanopaper preparation and carbonization

The cellulose nanopaper was prepared and carbonized according to the method detailed in our previous report.[25] Briefly, a cellulose nanofiber/water dispersion (0.2 wt.%, 200 mL) was suction filtered through a hydrophilic polytetrafluoroethylene (PTFE) filter (H020A090C, pore diameter of 0.2 μm, Toyo Roshi Kaisha, Ltd., Tokyo, Japan), rinsed with *t*-BuOH (200 mL), and suction filtered again. The wet sheet was peeled off the PTFE filter, immersed in liquid nitrogen for 1 min, and freeze-dried (EYELA, FDU-2200, Tokyo Rikakikai Co., Ltd., Tokyo, Japan) overnight to prepare a cellulose nanopaper exhibiting a nanoporous structure. A cellulose nanopaper exhibiting a dense structure was prepared without using any *t*-BuOH by hot pressing at 110 °C and 1.1 MPa for 30 min (AYSR-5, Shinto Metal Industries, Ltd., Osaka, Japan). Prior to carbonization, cellulose nanopapers were treated with I_2 gas (the same weight as the paper) at 100 °C for 24 h in a sealed flask to retain the original morphology during carbonization.[25] The I_2-treated papers were then carbonized in a furnace (KDF-75, DENKEN-HIGHDENTAL Co., Ltd., Kyoto, Japan) in three stages under nitrogen flowing at 500 mL min^{-1}, while removing the generated corrosive HI gas in the furnace. First, the temperature was increased at 2 °C min^{-1} from room temperature to 240 °C and was maintained there for 17 h. This treatment is also effective to avoid destruction of the original fibrous morphology during carbonization.[29] Then, the temperature was increased at 2 °C min^{-1} to peak carbonization temperatures in the range 300–1100 °C and was maintained there for 1 h. Finally, the carbonized cellulose nanopaper was cooled at 2 °C min^{-1} to room temperature. Regardless of the peak carbonization temperature, the dimensions of the carbonized cellulose papers were set at approximately 1 cm × 1 cm by adjusting the original paper size.

Carbonized cellulose nanopaper thermal heating performance evaluated under solar light irradiation

The solar thermal heating performances of the carbonized cellulose nanopaper were evaluated by measuring the nanopaper surface temperatures under solar light irradiation, according to a method detailed in our previous report.[30] Prior to the temperature measurements, the emissivity of each sample was evaluated using black body tape exhibiting an emissivity of 0.95 (HB-250, OPTEX Co., Ltd., Shiga, Japan) as a reference. The nanopaper and black tape were heated using a temperature controller (SBX-303, Sakaguchi E.H. VOC Corp., Tokyo, Japan) to 75 °C. The nanopaper emissivity was estimated by adjusting the nanopaper temperature measured using an infrared thermal camera (FLIR ETS320, FLIR Systems, Inc., Wilsonville, USA) according to the black tape reference temperature. For the surface temperature measurements, a solar simulator (AM1.5G, HAL-320W, Asahi Spectra Co., Ltd., Tokyo, Japan) was used as the light source. The samples (1 cm × 1 cm) were put on an acrylic plate (3 cm × 3 cm) exhibiting a central hole (0.7 cm × 0.7 cm), and the surface temperature changes of the samples illuminated using the solar simulator (light intensity: 1 sun) were recorded using the infrared thermal camera according to the nanopaper-calibrated emissivity. The equilibrium surface temperature of the samples was calculated as the average surface temperature during 1 sun-irradiation time of 500–600 s (approximately 850 plots). For data reproducibility and statistical analyses, more than 6 samples were prepared for each condition; a p value less than 0.05 was considered statistically significant. The solar thermal heating performance was measured at 25 °C and 65% relative humidity. The CNT black body, graphite sheet, graphene paper, and graphene oxide film solar thermal heating performances were similarly evaluated for comparison.

Carbonized cellulose nanopaper application to solar-driven thermoelectric power generation

The nanopaper (3.5 cm × 3.5 cm) carbonized at 500 °C was attached to a commercial thermoelectric power generator (4.0 cm × 4.0 cm, 66900, Artec Co., Ltd., Osaka, Japan) using a heat-dissipation adhesive (COM-G52, COM Institute, Inc., Osaka, Japan) to fabricate a thermoelectric power generation module, three of which were integrated into one solar-driven thermoelectric power generation device. A propeller motor (P70-3935, working voltage and current ranges of 0.4–1.5 V and 16–20 mA, respectively, Narika Corp., Tokyo, Japan) was used to generate electrical energy. On a sunny day (October 21, 2020; 24.5 °C, 34°49′30″ N, 135°31′28″ E), natural sunlight was irradiated on one side of the nanopaper carbonized at 500 °C while the other side was cooled using an ice pack.

Characterization

The nanopaper surface morphology was observed using FE-SEM (SU-8020, Hitachi High-Tech Science Corp., Tokyo, Japan) at an accelerate voltage of 2 kV to avoid damage to cellulose nanofibers. The pore size distribution was evaluated at 77 K based on nitrogen adsorption analysis using the BET theory and the DFT method (NOVA 4200e, Quantachrome Instruments, Kanagawa, Japan). The light transmittance, reflectance, and absorption were measured using UV–vis–NIR spectroscopy (UV-3600i Plus, Shimadzu Corporation, Kyoto, Japan) with an integrating sphere attachment (ISR-603, Shimadzu Corp., Kyoto, Japan). Absorption spectra were calculated from total transmittance and total reflectance spectra. For data reproducibility and statistical analyses, more than 6 samples were prepared for each condition; a p value less than 0.05 was considered statistically significant. The FT-IR (KJP-05120S, PerkinElmer Japan Co., Ltd., Kanagawa, Japan) spectra were recorded in attenuated total reflection (ATR) mode. The Raman spectra were

recorded using a RAMAN-touch apparatus (Nanophoton Corp., Osaka, Japan) and a 532-nm incident laser. To analyze the carbon fragment crystal structures, the XRD (Ultima IV, Rigaku Corporation, Tokyo, Japan) spectra were recorded using Ni-filtered Cu-Kα radiation (1.5418 Å), and the nanopapers were scanned in the range 2θ = 5–80° at 30-kV acceleration and 40 mA. The graphitic carbon fragment crystallite sizes in the stacking (L_c) and in-plane (L_a) directions were estimated using the XRD spectra and the Scherrer formula $L = k\lambda/\beta\cos\theta$, where λ, β, and θ are the X-ray wavelength, full width at half maximum, and Bragg angle, respectively. L_c and L_a were estimated using the crystalline reflections (002) and the two-dimensional reflections (10) with k = 0.89 and 1.84, respectively, according to the method described in a previous report.[31] HR-TEM (JEM-ARM 200F, JEOL Ltd., Tokyo, Japan) observation was operated at 200 kV. The photoluminescence spectra were recorded using a Quantaurus-QY instrument (C11347-01, HAMAMATSU PHOTONICS K. K., Shizuoka, Japan). The nanopaper thermal conductivity was calculated based on the following equation:

$$K = \alpha \cdot \rho \cdot C_p \qquad (1)$$

where K, α, ρ, and C_p indicate the nanopaper thermal conductivity (W m^{-1} K^{-1}), thermal diffusivity (mm^2 s^{-1}), density (g cm^{-3}), and specific heat capacity (J g^{-1} K^{-1}), respectively. The through-plane thermal diffusivity (α) was measured using a light flash apparatus (LFA447 HyperFlash, NETZSCH, Selb, Germany). The specific heat capacity (C_p) was measured using differential scanning calorimetry (Thermo Plus EVO II, Rigaku Corp., Tokyo, Japan). Al_2O_3 was used as a reference, and the thermograms were generated by heating the nanopapers at 10 °C min^{-1} in the temperature range 0–110 °C in a N_2 atmosphere[32].

1.3 Results and Discussion

Tailoring carbonized cellulose nanopaper nanoporous structures for application to solar thermal heating

To elucidate the nanostructure impact on the light absorption and solar thermal heating performances, the carbonized cellulose nanopaper nanoporous structures were first tailored based on the workflow shown in **Fig. 1–1a**. Cellulose nanofibers (width = 22 ± 8 nm) were prepared from never-dried softwood bleached kraft pulp by aqueous counter collision.[25] Subsequently, an aqueous cellulose nanofiber dispersion was dewatered, dried by hot pressing, treated with iodine (I_2), and then carbonized at 500 °C to produce an approximately 55-µm-thick carbonized nanopaper exhibiting dense structures (**Fig. 1–1b,d**) because the cellulose nanofibers had aggregated during hot-press drying to evaporate high-surface-tension water (72.14 mN m^{-1} at 25 °C).[33] To suppress cellulose nanofiber aggregation, the water was exchanged for low-surface-tension (19.96 mN m^{-1} at 25 °C)[33] *tert*-butyl alcohol (*t*-BuOH) prior to freeze drying, the I_2 treatment, and then carbonizing the cellulose nanopaper. The as-prepared approximately 180-µm-thick carbonized cellulose nanopaper exhibited 3D nanoporous structures, which had been derived from the pore spaces between the layered cellulose nanofibers (**Fig. 1–1c**). The nitrogen adsorption analysis using the Brunauer-Emmett-Teller (BET) theory and the Density Functional Theory (DFT) method indicated that the carbonized cellulose nanopaper exhibiting nanoporous structures contains mesopores **(Fig. 1–1d)**, while field-emission scanning electron microscopy (FE-SEM) images suggested that it also contains macropores smaller than approximately 100 nm **(Fig. 1–1c)**. The I_2 pretreatment was preformed to maintain the nanoporous structures of the cellulose nanopaper after carbonization, because the simple carbonization of the cellulose nanopaper deteriorates the morphology of cellulose nanofibers.[25] Although high-temperature treatment of

cellulose removes carbon and hydrogen as a hydrocarbon gas and weakens its carbon frameworks, the I_2 pretreatment could overcome this problem; carbon removal during the high-temperature treatment was successfully suppressed by the I_2 treatment,[25] possibly owing to the preferential formation of HI.[34]

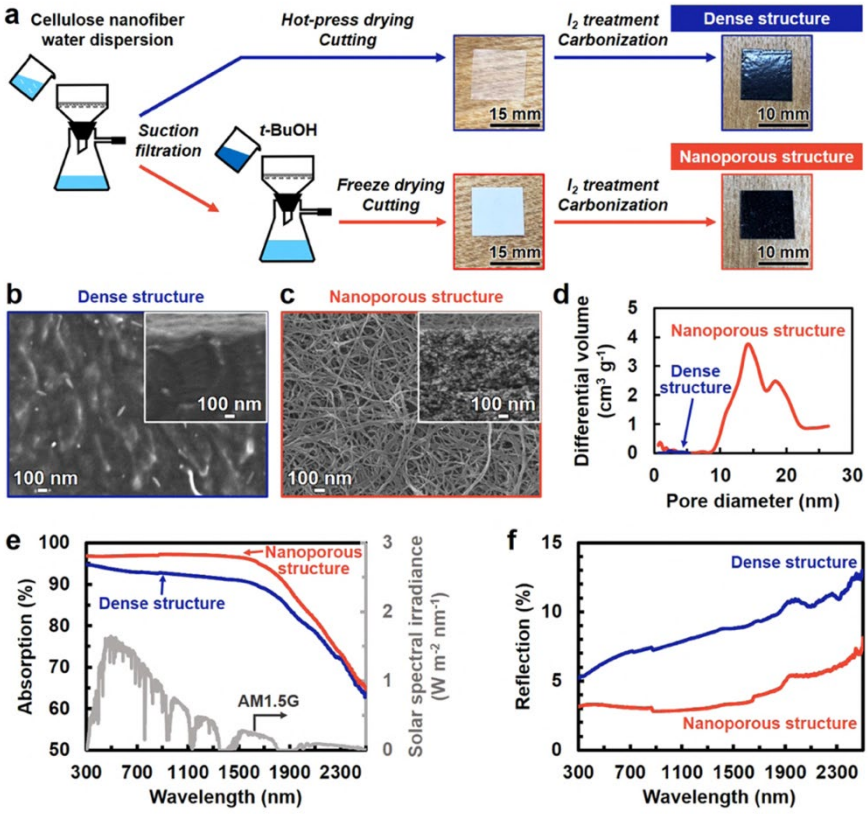

Fig. 1–1 Preparation, porous structures, and light absorption properties of cellulose nanopapers carbonized at 500 °C. (a) Preparation schematic and optical images, (b, c) cross-section (inset) and surface field-emission scanning electron microscopy (FE-SEM) images, respectively, (d) pore size distribution of carbonized cellulose nanopaper exhibiting dense or nanoporous structures, (e) solar spectral irradiance (AM1.5G) and ultraviolet–visible–near infrared (UV–vis–NIR) absorption, and (f) reflection of carbonized cellulose nanopaper exhibiting dense or nanoporous structures.

The carbonized cellulose nanopaper exhibiting the nanoporous structures showed greater light absorption (up to 97.2%) than that exhibiting the dense structures in the entire examined wavelength range (300–2500 nm), indicating that the nanoporous structures are beneficial for absorbing solar light **(Fig. 1–1e)**. As shown in **Fig. 1–1a,f** the dense structures gave the nanopaper a glossy appearance because of light reflecting off the structure surfaces. The nanoporous structures, on the other hand, gave the nanopaper a dark appearance by suppressing the light reflection **(Fig. 1–1a,f)**, albeit some light was transmitted at wavelengths above 1500 nm. Moreover, regardless of the porous structure of the carbonized cellulose nanopaper, the Raman, XRD, and FT-IR spectra of both carbonized cellulose nanopapers were similar. In the Raman spectra **(Fig. 1–2a)**, the G and the D bands were associated with the graphitic sp^2-hybridized carbon domains and the disordered graphitic carbon structures (e.g., edge of graphitic domains and in-plane imperfections), respectively. There was no large difference of the intensity ratio of D and G band peaks (I_D/I_G) between the carbonized cellulose nanopapers exhibiting nanoporous (I_D/I_G: 0.748) and dense structures (I_D/I_G: 0.766). In the XRD spectra **(Fig. 1–2b)**, two broad peaks associated with the crystalline reflections (002) and the two-dimensional reflections (10) of graphite appeared at approximately 22° and 44°.[31] The graphite crystallite sizes in the stacking and in-plane directions (L_c and L_a, respectively) were estimated using these peaks and Scherrer's formula. There was no large difference of the graphite crystallite sizes between the carbonized nanopapers exhibiting nanoporous (L_c: 0.87 nm, L_a: 1.84 nm) and dense structures (L_c: 0.85 nm, L_a: 1.83 nm). FT-IR spectra also suggested that the chemical structures of the carbonized nanopapers were similar **(Fig. 1–2c)**. These results indicated that the nanopapers exhibited negligibly different chemical structures, possibly due to being carbonized at the same temperature. Thus, the nanoporous structures enhanced the carbonized cellulose nanopaper light absorption by

suppressing the light reflection. These results indicated that the tailored carbonized cellulose nanopaper subwavelength nanoporous structures deserved the light confinement effect[35], wherein the incident light is effectively captured owing to multiple light reflections and scattering in the nanopaper matrix.

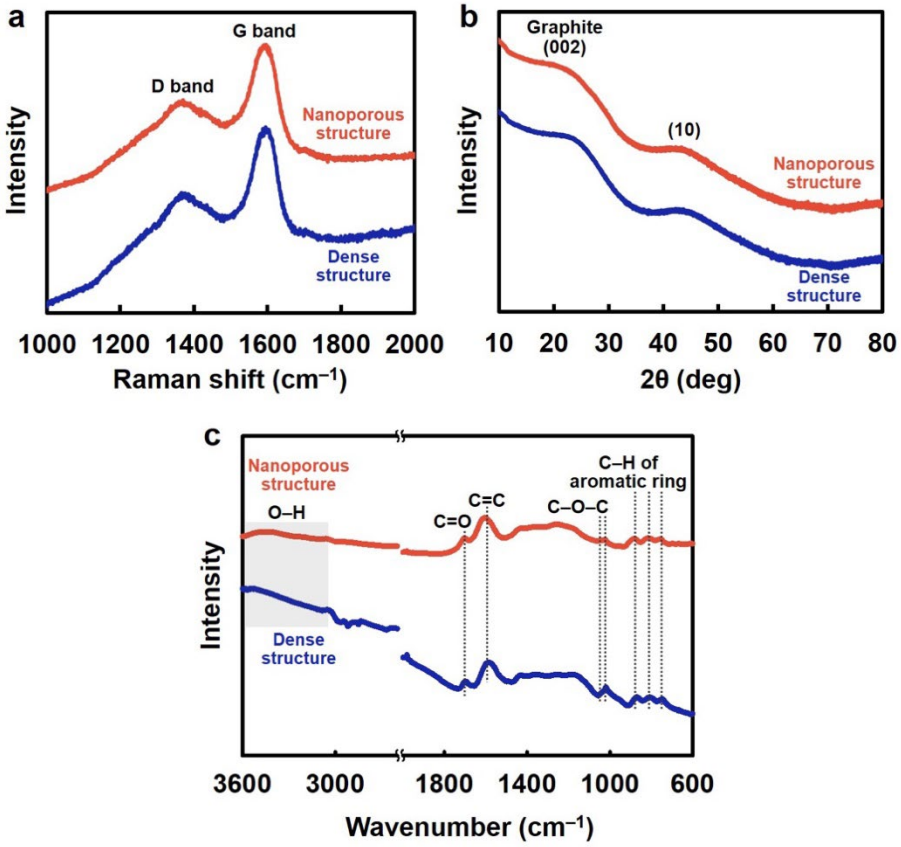

Fig. 1–2 Chemical structures of carbonized cellulose nanopapers exhibiting nanoporous and dense structures. (a) Raman, (b) X-ray diffraction (XRD), and (c) Fourier-transform infrared (FT-IR) spectra of cellulose nanopaper carbonized at 500 °C exhibiting nanoporous or dense structures.

Subsequently, the solar thermal heating performances of the carbonized cellulose nanopaper were evaluated under simulated solar light irradiation [AM1.5G, light intensity: 1.0 kW m^{-2} (1 sun)]. The change in surface temperature of the carbonized cellulose nanopaper irradiated under 1

sun was measured using a thermal camera **(Fig. 1–3a)**. The carbonized cellulose nanopaper temperature immediately increased upon 1 sun irradiation and saturated within 600 s **(Fig. 1–3b)**. Then, the equilibrium surface temperature of the carbonized cellulose nanopaper exhibiting the nanoporous structures reached 73.9 ± 0.80 °C, which was higher than that of the carbonized cellulose nanopaper exhibiting the dense structures (69.2 ± 0.65 °C). These results indicated that the nanoporous structures gave the cellulose nanopaper superior solar thermal heating compared to the dense structures. Thus, designing subwavelength nanoporous structures in the carbonized cellulose nanopaper resulted in effective solar thermal heating by enhancing the solar absorption.

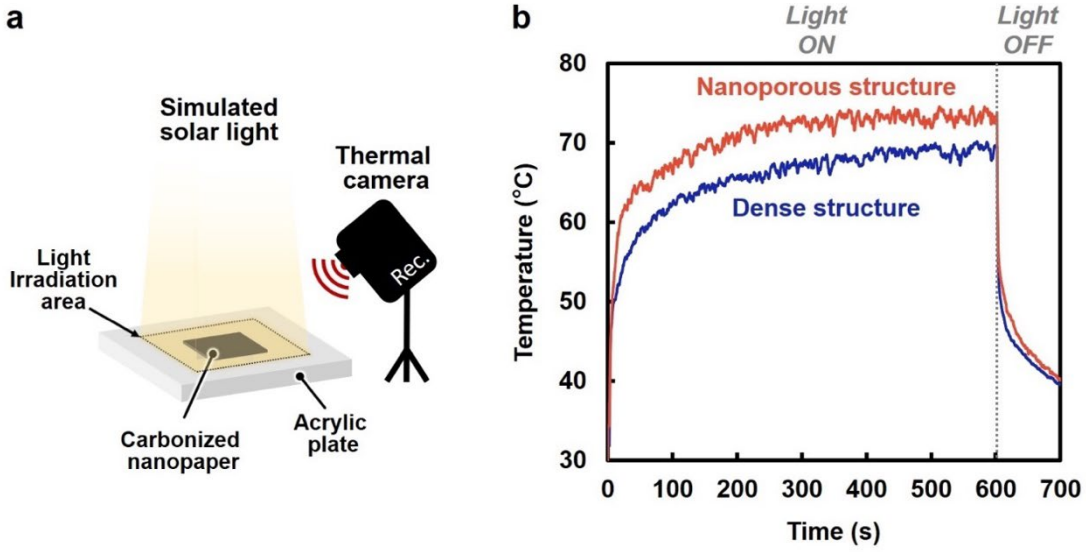

Fig. 1–3 Photothermal heating performances of cellulose nanopapers (approximately 1 cm × 1 cm) carbonized at 500 °C and exhibiting different porous structures. (a) Schematic illustration of experimental setup used to measure surface temperature during simulated solar light irradiation, and (b) surface temperature evolutions measured under 1 sun irradiation for carbonized cellulose nanopapers exhibiting dense or nanoporous structures.

Solar thermal heating performances of cellulose nanopapers carbonized at different temperatures.

Because the original nanopaper exhibiting nanoporous structures showed poor solar absorption and solar thermal heating (*e.g.*, the equilibrium surface temperature was only 37.9 °C for the nanopaper irradiated under 1 sun) **(Fig. 1–4)**, not only designing the subwavelength nanoporous structures but also carbonizing the nanopaper are the key to optimizing solar thermal heating. To elucidate the relationship between the nanopaper carbonization temperatures and the solar thermal heating performances, the nanopaper exhibiting nanoporous structures was carbonized in the temperature range of 300–1100 °C. The weight retention of the nanopaper was decreased from approximately 39.4 to 20.4% with increasing carbonization temperatures from 300 to 1100 °C, respectively **(Fig. 1–5)**. Then, the photothermal heating properties of the carbonized cellulose nanopapers were evaluated. As shown in **Fig. 1–6a**, the photothermal heating performance of the carbonized cellulose nanopaper (1 cm × 1 cm,

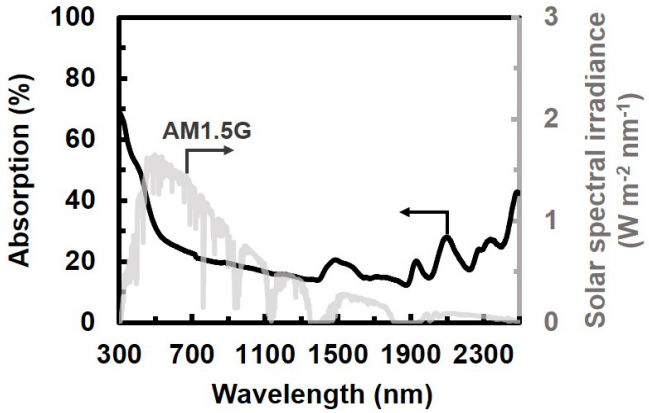

Fig. 1–4 UV–vis–NIR absorption spectrum of original cellulose nanopaper and corresponding solar spectral irradiance (AM1.5G).

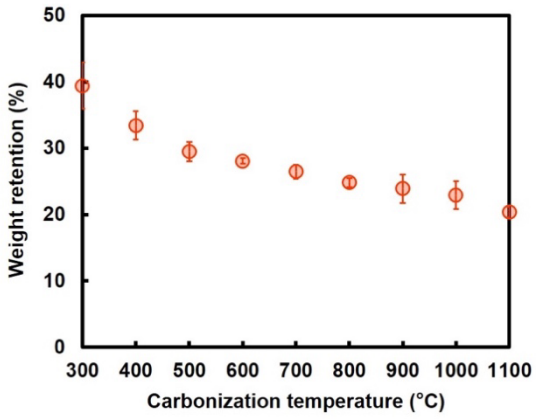

Fig. 1–5 Weight retention of cellulose nanopaper exhibiting nanoporous structures carbonized at different temperatures.

thickness = 160–200 μm) was dependent on carbonization temperature. Although the equilibrium surface temperature measured under 1 sun irradiation increased from 71.6 to 73.9 °C upon increasing carbonization temperature from 300 to 500 °C, respectively, it gradually decreased from 73.9 to 68.6 °C upon increasing carbonization temperature from 500 to 1100 °C, respectively. Thus, the cellulose nanopaper carbonized at 500 °C exhibited the best photothermal heating. According to the statistical analysis, the equilibrium surface temperature under 1 sun irradiation of the cellulose nanopaper carbonized at 500 °C was significantly different from those of the cellulose nanopapers carbonized at 300, 400, 600–1100 °C (p-value: ≤ 0.028).

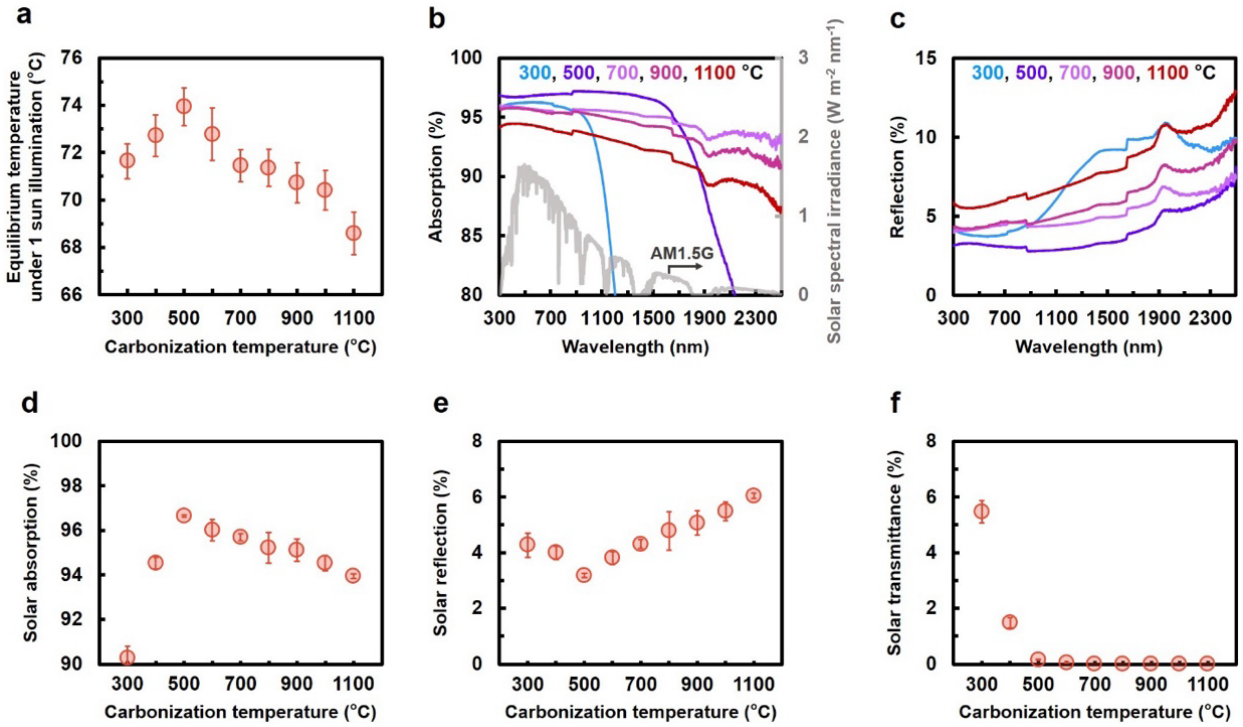

Fig. 1–6 Photothermal heating and light absorption of cellulose nanopaper exhibiting nanoporous structures carbonized at different temperatures. (a) Equilibrium surface temperature; (b) solar spectral irradiance (AM1.5G) and UV–vis–NIR absorption; (c) reflection spectra; solar light (d) absorption, (e) reflection, and (f) transmittance of cellulose nanopapers carbonized at different temperatures.

To elucidate why the cellulose nanopaper carbonized at 500 °C exhibited the best photothermal heating, the light absorption of the cellulose nanopapers carbonized at different temperatures were compared **(Fig. 1–6b)**. With increasing carbonization temperature, the light absorption range of the carbonized cellulose nanopaper extended toward the long-wavelength region. For instance, the cellulose nanopapers carbonized above 700 °C exhibited over 90% light absorption across a broad wavelength range. However, the cellulose nanopaper carbonized at 500 °C exhibited the highest light absorption (up to 97.2%) in the wavelength range 300–1700 nm, which accounts for most solar light energy. **Fig. 1–6c** shows the light reflection of the cellulose nanopapers carbonized at different temperatures. The cellulose nanopaper carbonized at 300 °C exhibited relatively strong light reflection in the long-wavelength region (>1300 nm), where it also exhibited low light absorption. Notably, the cellulose nanopaper carbonized at 500 °C exhibited the lowest light reflection in the entire examined wavelength range (300–2500 nm), while the nanopapers carbonized above 500 °C exhibited increased light reflection.

To compare the solar absorptions of the cellulose nanopapers carbonized at different temperatures more clearly, the solar absorption was calculated according the following equation:[36]

$$\bar{\alpha} = \frac{\int_{\lambda_{min}}^{\lambda_{max}} I_{solar}(\lambda) \cdot \alpha_{solar}(\lambda) d\lambda}{\int_{\lambda_{min}}^{\lambda_{max}} I_{solar}(\lambda) d\lambda} \quad (2)$$

where $\bar{\alpha}$ is the solar absorption (%), λ is the wavelength (nm), λ_{min} and λ_{max} are 300 and 2500 nm, respectively, $I_{solar}(\lambda)$ is the AM1.5G solar spectral irradiance at λ, and $\alpha_{solar}(\lambda)$ is the light absorption (%) at λ. Additionally, the solar reflection and transmittance were similarly calculated. **Fig. 1–6d–f** shows the as-calculated solar absorption, reflectance, and transmittance of the cellulose nanopapers carbonized at different temperatures. The cellulose nanopaper carbonized at 500 °C exhibited the highest solar absorption (96.7%) because it also exhibited the lowest solar reflectance (3.14%) and only a slight solar transmittance (0.16%). According to the statistical

analysis, the solar absorption of the cellulose nanopaper carbonized at 500 °C was significantly different from those of the cellulose nanopapers carbonized at 300, 400, 600–1100 °C (p-value: ≤ 0.038). The solar absorption of cellulose nanopaper carbonized at 500 °C (96.7%) was superior to those of various carbonized biomass materials, such as carbonized mushroom (96%),[12] carbonized corncob (95.7%),[37] and arched bamboo charcoal (94.1%).[38] Regardless of the carbonization temperature, the carbonized cellulose nanopapers exhibited almost no photoluminescence, indicating that most of the solar light absorbed by the carbonized cellulose nanopaper had been converted to heat **(Fig. 1–7)**. These results suggested that the cellulose nanopaper carbonized at 500 °C exhibited the best photothermal heating (*i.e.*, the equilibrium surface temperature was 73.9 °C for the nanopaper irradiated under 1 sun; **Fig. 1–6a**) because it exhibited excellent solar absorption by suppressing solar reflection.

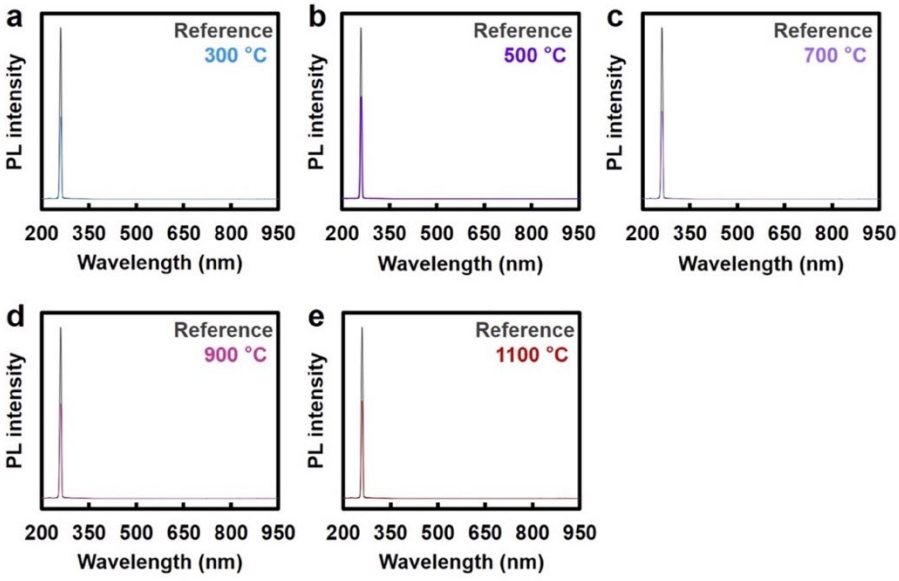

Fig. 1–7 Photoluminescence (PL) spectra of nanopaper exhibiting nanoporous structures carbonized at (a) 300, (b) 500, (c) 700, (d) 900, and (e) 1100 °C (Excitation wavelength: 260 nm).

Furthermore, the heat capacity and thermal conductivity of carbonized cellulose nanopapers were investigated. Although the original cellulose nanopaper specific heat capacity was ~1.39 J g^{-1} K^{-1}, that of the cellulose nanopaper carbonized at 1100 °C was ~1.21 J g^{-1} K^{-1}, suggesting that the carbonized cellulose nanopaper specific heat capacity had negligibly changed **(Fig. 1–8a)**. The carbonized cellulose nanopaper through-plane thermal conductivity gradually increased from 0.04 to 0.19 W m^{-1} K^{-1} as the carbonization temperature was increased from 300 to 1100 °C, respectively. Such gradual increase in through-plane thermal conductivity with increasing carbonization temperature would also cause the gradual decrease in the equilibrium surface temperature of the carbonized cellulose nanopaper under 1 sun irradiation. Thus, the high surface temperature of the cellulose nanopaper carbonized at 500 °C might attributed to the relatively low through-plane thermal conductivity (0.07 W m^{-1} K^{-1}) **(Fig. 1–8b)**.

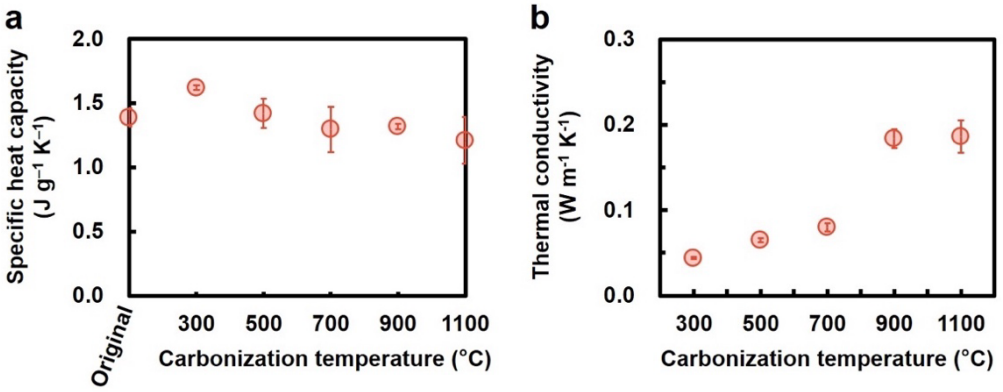

Fig. 1–8 Thermal properties of carbonized cellulose nanopapers. (a) Specific heat capacity and (b) through-plane thermal conductivity of cellulose nanopaper exhibiting nanoporous structures carbonized at different temperatures.

Impact of carbonized nanopaper chemical structures on solar thermal heating

Because the carbonized cellulose nanopaper nanoporous structures changed negligibly with the carbonization temperature **(Fig. 1–9)**, the carbonization-temperature-dependent solar absorption

and thermal heating properties of the carbonized cellulose nanopaper were attributed to the different cellulose nanofiber chemical structures formed at different carbonization temperatures.

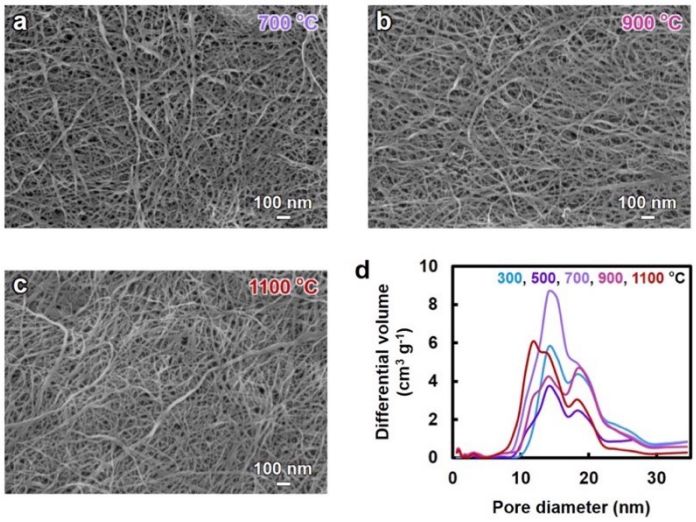

Fig. 1–9 Nanoporous structures of cellulose nanopapers carbonized at different temperatures. FE-SEM images of cellulose nanopaper exhibiting nanoporous structures carbonized at (a) 700, (b) 900, or (c) 1100 °C. (d) Pore size distribution curves of cellulose nanopapers carbonized at different temperatures.

To elucidate this point, during carbonization, the carbonized cellulose nanofiber chemical structures were analyzed using FT-IR spectroscopy, Raman spectroscopy, XRD analysis, and high-resolution transmission electron microscopy (HR-TEM). Although the original cellulose molecule consists of sp^3-hybridized carbon structures, the FT-IR spectra indicated that sp^2-hybridized carbon (C=C) and oxygen-containing functional groups such as C=O, C–O–C, and C–OH had formed in the samples carbonized up to 500 °C **(Fig. 1–10a)**. The C=O, C–O–C, and C–OH peaks weakened with increasing carbonization temperature. The C=C peak disappeared from the spectra for the samples carbonized at or above 900 °C, suggesting that the π-conjugated system had been extended because the sp^2-hybridized carbon domains had grown.[39] A G band appeared

in the Raman spectra of the samples carbonized at or above 500 °C, indicating that sp^2-hybridized graphitic carbon domains had formed **(Fig. 1–10b)**.[40] A D band also appeared, suggesting that the disordered graphitic carbon structures (*e.g.*, at the edge of the graphitic domains and in-plane imperfections)[40] remained even in the sample carbonized at 1100 °C.

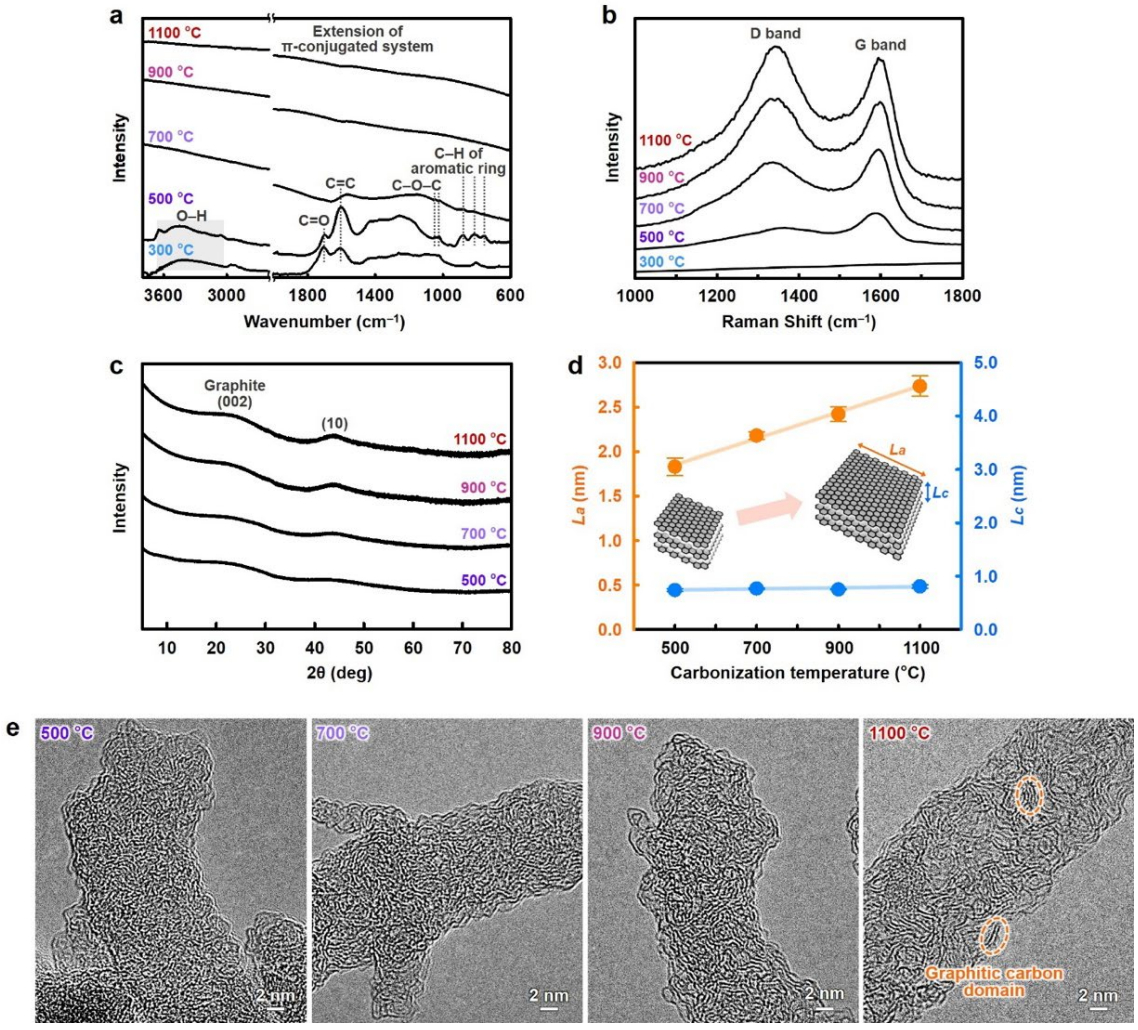

Fig. 1–10 Chemical structural evolution of cellulose nanofibers during carbonization. (a) FT-IR, (b) Raman, and (c) XRD spectra; (d) graphitic carbon fragment crystallite sizes in in-plane (L_a) and stacking (L_c) directions; and (e) HR-TEM images of cellulose nanofiber carbonized at different temperatures.

XRD was used to further analyze the sp^2-hybridized graphitic carbon domain growth during carbonization. As shown in **Fig. 1–10c**, two broad peaks associated with the crystalline reflections (002) and the two-dimensional reflections (10) of graphite appeared at approximately 22° and 44°, corresponding to interplanar distances (d_c and d_a) of ~0.4 and ~0.2 nm, respectively.[31] These peaks intensified with increasing carbonization temperature. The graphite crystallite sizes in the stacking and in-plane directions (L_c and L_a, respectively) were estimated using these peaks and Scherrer's formula **(Fig. 1–10d)**.[31] Although L_c remained constant at ~1.0 nm, L_a gradually increased from ~1.8 to 2.7 nm upon increasing carbonization temperature from 500 to 1100 °C, suggesting that the graphitic carbon domains gradually grew in the in-plane rather than the stacking direction. These trends were consistently observed in the corresponding HR-TEM images **(Fig. 1–10e)**. Notably, numerous randomly oriented graphitic carbon domains exhibiting layer structures with the width and thickness of a few nanometers more prominently appeared at higher carbonization temperatures, which confirmed that graphitic carbon domains had progressively grown in the carbonized cellulose nanofiber with increasing carbonization temperature. Furthermore, the in-plane growth graphite crystallite sizes were found to be correlated to the electrical properties of carbonized cellulose nanopaper. As a result, the original cellulose nanopaper demonstrated highly insulating electrical properties characterized by an electrical resistivity at ca. 10^{11} Ω cm. This high resistivity was attributed to the presence of sp^3-hybridized carbons in cellulose. However, through I_2-treated and high-temperature carbonization, the electrical resistivity was significantly modulated within the range of 10^{11} to 10^{-1} Ω cm, thereby altering the electrical behavior of the material **(Fig. 1–11)**.

Such progressive graphitic carbon domain growth governed the carbonization-temperature-dependent solar absorption and thermal heating of the carbonized cellulose nanopaper as follows.

The original cellulose nanopaper exhibited poor solar absorption **(Fig. 1–4)** owing to the wide σ–σ^* energy gap of the sp^3-hybridized carbons in the cellulose molecule. The cellulose nanopaper carbonized at 300 °C exhibited sp^2-hybridized carbon domains (*i.e.*, π-orbitals), wherein the π–π^* energy gap is within the σ–σ* one[41] and promotes light absorption at lower energies (*i.e.*, longer wavelengths) than the original nanopaper. In the cellulose nanopapers carbonized at temperatures of 500 °C or above, the light-absorption wavelength range can be further extended to longer wavelengths by growing graphitic sp^2-hybridized carbon domains **(Fig. 1–6b)** because the π–π^* energy gap decreases with the growth of these domains.[41] However, excess sp^2-hybridized graphitic carbon domain growth increases light reflection across a broad wavelength range **(Fig. 1–6c)**. The observed light reflection is attributed to the metallic luster induced by graphitic carbon domains, which is closely associated with the delocalization of free electrons within π-conjugated systems. This correlation could be confirmed through the decrease in electrical resistivity[42,43] **(Fig. 1-11)** and similar phenomenon have been previously reported in studies on graphite films,[44] graphene nanosheets[45], and graphene papers[46].

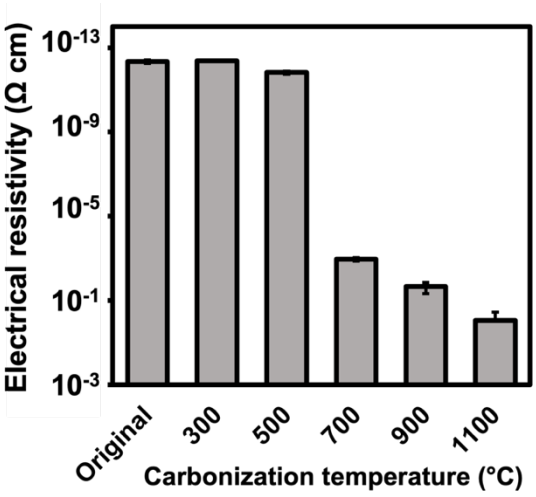

Fig. 1–11 Electrical resistivity of the cellulose nanopaper carbonized at different temperatures.

To effectively absorb solar irradiation, therefore, the graphitic carbon domain growth should be tailored to extend the light-absorption wavelength range while suppressing the light reflection. In this chapter, the cellulose nanopaper carbonized at 500 °C exhibited this optimal balance; the graphitic carbon domains therein exhibited an L_c and L_a of ~0.74 and 1.83 nm, respectively **(Fig. 1–10d).** Such semicarbonized cellulose chemical structures provided the highest solar absorption (96.7%) and the lowest solar reflectance (3.14%) **(Fig. 1–6d,e)**; therefore, the cellulose nanopaper carbonized at 500 °C exhibited the best solar thermal heating **(Fig. 1–6a)**. Furthermore, the low through-plane thermal conductivity of the semicarbonized cellulose nanopaper (0.07 W m^{-1} K^{-1}) **(Fig. 1–8b)** can be beneficial for localized heating,[47] providing a higher surface temperature for the cellulose nanopaper irradiated under 1 sun than even state-of-the-art nanocarbon materials, such as a carbon nanotube black body, graphene paper, and graphene oxide film **(Table. 1–1)**. Such higher surface temperature can contribute to the effective use of renewable solar energy such as solar-driven thermoelectric power generation. For example, Komatsu et al. has recently reported the macroscopic weavable fibers of carbon nanotubes with giant thermoelectric power factor (14 mW m^{-1} K^{-2}),[48] indicating that even a 1 K temperature difference can produce mW levels of energy.

Moreover, to demonstrate the importance of solar thermal heating, the cellulose nanopaper carbonized at 500 °C was applied to thermoelectric power generation. As shown in **Fig. 1–12**, three pieces (3.5 cm × 3.5 cm) of the cellulose nanopaper carbonized at 500 °C were adhered to a commercial thermoelectric power generator to fabricate a thermoelectric power generation module. On a sunny day, natural sunlight was irradiated on one side of the carbonized cellulose nanopaper, and this module generated enough electricity to run the propeller motor (working voltage: 0.4–1.5 V, working current: 16–20 mA). Thus, the cellulose nanopaper carbonized at

500 °C exhibited excellent solar thermal heating and was applied to solar-driven thermoelectric power generation. Thus, the excellent solar thermal heating performance of the semicarbonized cellulose nanopaper exhibiting nanoporous structures can be significant toward the effective use of renewable solar energy.

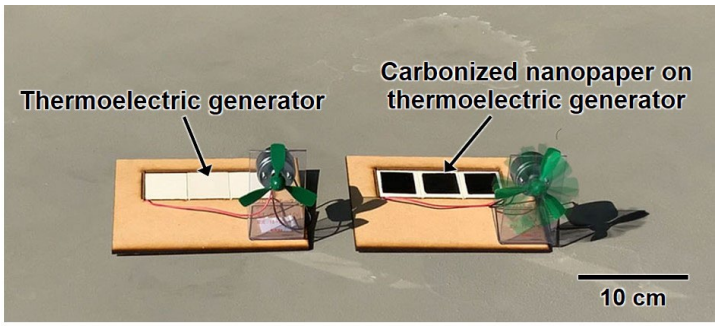

Fig. 1–12 Solar-driven thermoelectric power generation using cellulose nanopaper carbonized at 500 °C.

Table. 1–1 Photothermal heating performances of cellulose nanopaper semicarbonized at 500 °C and various conventional carbon materials irradiated under 1 sun.

Carbon material	Surface temperature (°C)
CNT† black body	55.0 ± 0.28
Graphite sheet	64.5 ± 1.98
Graphene paper	65.2 ± 1.46
Graphene oxide film	69.4 ± 1.53
Semicarbonized cellulose nanopaper exhibiting nanoporous structures	73.9 ± 0.80

†CNT, carbon nanotube.

1.4 Conclusions

In summary, a semicarbonized cellulose nanofiber paper was tailored with subwavelength nanoporous structures and adequately grown graphitic carbon domains for application to solar thermal heating. The tailored subwavelength nanoporous structures enhanced the solar absorption by suppressing the light reflection. The graphitic carbon domains grown by semicarbonization at 500 °C balanced the tradeoff between extending the light-absorption wavelength range and suppressing the light reflection. Thus, the semicarbonized subwavelength-nanopore-structured cellulose nanopaper exhibited high solar absorption, and therefore, effective solar thermal heating, which enabled the cellulose nanopaper to be applied to thermoelectric power generation. While a further challenge remains to make the tailoring process of the nanoporous structures greener, the study findings can provide a guideline for structurally designing biomass-derived carbon materials for application to solar absorption and thermal heating. Furthermore, the concept for tailoring the carbonized cellulose nanofiber nanoporous and chemical structures can be applied to various carbonized bionanomaterials, opening a pathway to develop structurally and functionally designable carbonized bionanomaterials for diverse applications.

1.5 References

1 B. Szczęśniak, J. Phuriragpitikhon, J. Choma and M. Jaroniec, *J. Mater. Chem. A*, 2020, **8**, 18464–18491.

2 Y. Wang, M. Zhang, X. Shen, H. Wang, H. Wang, K. Xia, Z. Yin and Y. Zhang, *Small*, 2021, **17**, 2008079.

3 G.-J. Jiao, J. Ma, Y. Li, D. Jin, Z. Ali, J. Zhou and R. Sun, *Chemosphere*, 2021, **278**, 130377.

4 L. J. Konwar, J. Boro and D. Deka, *Renew. Sustain. Energy Rev.*, 2014, **29**, 546–564.

5 C. Wang, K. Xia, H. Wang, X. Liang, Z. Yin and Y. Zhang, *Adv. Mater.*, 2019, **31**, 1801072.

6 L. Zhu, Y. Huang, Y. Morishita, K. Uetani, M. Nogi and H. Koga, *J. Mater. Chem. C*, 2021, **9**, 4444–4452.

7 J. Deng, M. Li and Y. Wang, *Green Chem.*, 2016, **18**, 4824–4854.

8 L. Zhu, K. Uetani, M. Nogi and H. Koga, *Nanomaterials*, 2021, **11**, 3249.

9 C. Zhang, H. Liang, Z. Xu and Z. Wang, *Adv. Sci.*, 2019, **6**, 1900883.

10 H. Liu, C. Chen, G. Chen, Y. Kuang, X. Zhao, J. Song, C. Jia, X. Xu, E. Hitz, H. Xie, S. Wang, F. Jiang, T. Li, Y. Li, A. Gong, R. Yang, S. Das and L. Hu, *Adv. Energy Mater.*, 2018, **8**, 1701616.

11 X. Wu, L. Wu, J. Tan, G. Y. Chen, G. Owens and H. Xu, *J. Mater. Chem. A*, 2018, **6**, 12267–12274.

12 N. Xu, X. Hu, W. Xu, X. Li, L. Zhou, S. Zhu and J. Zhu, *Adv. Mater.*, 2017, **29**, 1606762.

13 J. Liu, Q. Liu, D. Ma, Y. Yuan, J. Yao, W. Zhang, H. Su, Y. Su, J. Gu and D. Zhang, *J. Mater. Chem. A*, 2019, **7**, 9034–9039.

14 M. Zhu, J. Yu, C. Ma, C. Zhang, D. Wu and H. Zhu, *Sol. Energy Mater. Sol. Cells*, 2019, **191**, 83–90.

15 E. G. Villabona-Leal, A. G. Escobar-Villanueva, E. B. Pérez-Pérez, H. Martínez-Gutiérrez and V. M. Ovando-Medina, *Int. J. Energy Res.*, 2021, **45**, 19521–19534.

16 M. Gao, L. Zhu, C. K. Peh and G. W. Ho, *Energy Environ. Sci.*, 2019, **12**, 841–864.

17 ASTM G173-03., *Standard Tables for Reference Solar Spectral Irradiances: Direct Normal and Hemispherical on 37° Tilted Surface*, ASTM International: West Conshohocken, PA, 2012.

18 X. Zheng and L. Zhang, *Energy Environ. Sci.*, 2016, **9**, 2511–2532.

19 G. Feng, G.-Q. Zhang and D. Ding, *Chem. Soc. Rev.*, 2020, **49**, 8179–8234.

20 B. Thomas, M. C. Raj, K. B. Athira, M. H. Rubiyah, J. Joy, A. Moores, G. L. Drisko and C. Sanchez, *Chem. Rev.*, 2018, **118**, 11575–11625.

21 A. Isogai, T. Saito and H. Fukuzumi, *Nanoscale*, 2011, **3**, 71–85.

22 R. J. Moon, A. Martini, J. Nairn, J. Simonsen and J. Youngblood, *Chem. Soc. Rev.*, 2011, **40**, 3941.

23 Nanocellulose Market by Type (MFC & NFC, CNC/NCC), Raw Material (Wood, Non-Wood), Application (Pulp & Paper, Composites, Biomedical & Pharmaceuticals, Electronics & Sensors), Andregion(North America, APAC, Europe, Row) - Global Forecast to 2026, https://www.marketsandmarkets.com/Market-Reports/nano-cellulose-market-56392090.html, (accessed March 14, 2022).

24 D. Klemm, B. Heublein, H.-P. Fink and A. Bohn, *Angew. Chem. Int. Ed.*, 2005, **44**, 3358-3393.

25 H. Koga, K. Nagashima, K. Suematsu, T. Takahashi, L. Zhu, D. Fukushima, Y. Huang, R. Nakagawa, J. Liu, K. Uetani, M. Nogi, T. Yanagida and Y. Nishina, *ACS Nano*, 2022, **16**, 8630–8640.

26 H.-W. Liang, Q.-F. Guan, Z.- Zhu, L.-T. Song, H.-B. Yao, X. Lei and S.-H. Yu, *NPG Asia Mater.*, 2012, **4**, e19–e19.

27 Z.-Y. Wu, H.-W. Liang, L.-F. Chen, B.-C. Hu and S.-H. Yu, *Acc. Chem. Res.*, 2016, **49**, 96–105.

28 S.-C. Li, B.-C. Hu, Y.-W. Ding, H.-W. Liang, C. Li, Z.-Y. Yu, Z.-Y. Wu, W.-S. Chen and S.-H. Yu, *Angew. Chem. Int. Ed.*, 2018, **57**, 7085–7090.

29 E. Jazaeri and T. Tsuzuki, *Cellulose*, 2013, **20**, 707–716.

30 Y. Huang, Y. Morishita, K. Uetani, M. Nogi and H. Koga, *Nanoscale Adv.*, 2020, **2**, 2339–2346.

31 J. Biscoe and B. E. Warren, *J. Appl. Phys,* 1942, **13**, 364–371

32 X. Meng, H. Pan, C. Zhu, Z. Chen, T. Lu, D. Xu, Y. Li and S. Zhu, *ACS Appl. Mater. Interfaces*, 2018, **10**, 22611–22622.

33 J. J. Jasper, *J. Phys. Chem. Ref. Data*, 1972, **1**, 841–1010.

34 M. Kyotani, S. Matsushita, T. Nagai, Y. Matsui, M. Shimomura, A. Kaito and K. Akagi, *J. Am. Chem. Soc.*, 2008, **130**, 10880–10881.

35 J. Wang, J. Zhao, Y. Li, M. Yang, Y. Q. Chang, J. P. Zhang, Z. Sun and Y. Wang, *ACS Macro Lett.*, 2015, **4**, 392–397.

36 J. Mandal, D. Wang, A. C. Overvig, N. N. Shi, D. Paley, A. Zangiabadi, Q. Cheng, K. Barmak, N. Yu and Y. Yang, *Adv. Mater.*, 2017, **29**, 1702156.

37 Y. Sun, Z. Zhao, G. Zhao, L. Wang, D. Jia, Y. Yang, X. Liu, X. Wang and J. Qiu, *Carbon*, 2021, **179**, 337–347.

38 Z. Li, C. Wang, T. Lei, H. Ma, J. Su, S. Ling and W. Wang, *Adv. Sustain. Syst.*, 2019, **3**, 1800144.

39 J. Ning, L. Hao, M. Jin, X. Qiu, Y. Shen, J. Liang, X. Zhang, B. Wang, X. Li and L. Zhi, *Adv. Mater.*, 2017, **29**, 1605028.

40 M. S. Dresselhaus, A. Jorio, A. G. Souza Filho and R. Saito, *Philos. Trans. R. Soc. Math. Phys. Eng. Sci.*, 2010, **368**, 5355–5377.

41 C. Mathioudakis, G. Kopidakis, P. C. Kelires, P. Patsalas, M. Gioti and S. Logothetidis, *Thin Solid Films*, 2005, **482**, 151–155.

42 G. Qi, L. Huang and H. Wang, *Chem. Commun.*, 2012, **48**, 8246.

43 H.-P. Cong, X.-C. Ren, P. Wang and S.-H. Yu, *Energy Environ. Sci.*, 2013, **6**, 1185.

44 M. Isayama, K. Nomiyama and T. Kunitake, *Adv. Mater.*, 1996, **8**, 641–644.

45 D. Li, M. B. Müller, S. Gilje, R. B. Kaner and G. G. Wallace, *Nat. Nanotechnol.*, 2008, **3**, 101–105.

46 H. Chen, M. B. Müller, K. J. Gilmore, G. G. Wallace and D. Li, *Adv. Mater.*, 2008, **20**, 3557–3561.

47 Y. Yang, X. Yang, L. Fu, M. Zou, A. Cao, Y. Du, Q. Yuan and C.-H. Yan, *ACS Energy Lett.*, 2018, **3**, 1165–1171.

48 N. Komatsu, Y. Ichinose, O. S. Dewey, L. W. Taylor, M. A. Trafford, Y. Yomogida, G. Wehmeyer, M. Pasquali, K. Yanagi and J. Kono, *Nat. Commun.*, 2021, **12**, 4931.

Chapter 2

Chitin-Derived Nitrogen-Doped Carbon Nanopaper with Subwavelength Nanoporous Structures for Solar Thermal Heating

2.1 Introduction

Solar thermal heating has been receiving increasing attention from researchers as a promising process for using solar light as thermal energy. Solar thermal heating requires photothermal materials, which absorb light and convert it into heat.[1,2] Examples of photothermal materials include plasmonic metal nanoparticles, metal oxide semiconductors, carbon materials,[2] and plasmonic metamaterials.[3,4] Among these, carbon materials exhibit a broad light absorption range,[5] which covers the wavelength range of solar light (300–2500 nm, ASTM G173-03, Air Mass 1.5 Global spectrum (AM1.5G)).[6] Biomass-derived carbons have been used as sustainable photothermal materials for various solar thermal heating applications such as solar steam generation,[7] desalination, wastewater purification,[8,9] and photothermal catalysis.[10]

The rational structural design of biomass-derived carbons is desirable for further enhancing their solar thermal heating performance.[2] For example, carbon-based chemical structures, including *sp2*-hybridized carbon and heteroatom-doped carbon structures with a customized distribution of the highest occupied molecular orbital and lowest unoccupied molecular orbital, should be designed. The design of such carbon-based chemical structures can influence not only light absorption but also the conversion of the absorbed light to heat by vibration relaxation.[11,12] Furthermore, subwavelength nanoporous structures should be designed to suppress light reflection and facilitate light absorption via light confinement, as reported for plasmonic metal nanoparticles and metal oxide semiconductors.[13]

Chapter 1 reported that the carbon material derived from wood cellulose nanofiber paper, referred to as cellulose nanopaper, whose chemical and subwavelength nanoporous structures can be customized, acts as a photothermal material for solar thermal heating.[14] The carbon-based chemical structures of cellulose nanopaper were customized by controlling the carbonization temperatures; the *sp2*-hybridized carbon structures formed by semicarbonization at 500 °C afforded high solar-light absorption by adequately balancing solar-light absorption and reflection. Subwavelength nanoporous structures have also been constructed within cellulose nanopaper-derived carbon by expanding the pore spaces between cellulose nanofibers via treatment with low-surface-tension *tert*-butyl alcohol (*t*-BuOH),[15] thereby suppressing solar-light reflection. The resulting cellulose nanopaper-derived carbon with customized chemical and subwavelength nanoporous structures exhibited effective solar thermal heating performance, which was higher than those of previously reported biomass-derived carbons and conventional nanocarbon materials, including graphene and carbon nanotube films.[14] However, cellulose nanopaper requires iodine gas pretreatment (100 °C) for a long duration (24 h) to retain its customized subwavelength nanoporous structures after carbonization because the original morphology of cellulose nanofibers collapses after high-temperature treatment.[16] Hence, discovering alternative biomass nanofibers that can retain their original morphology without pretreatment, even after carbonization, with adequate carbon-based chemical structures for excellent solar thermal heating is desirable.

Chitin (β-(1→4)-linked N-acetyl anhydroglucosamine) is among the most abundant and renewable biomass materials on earth. Its chemical structure is similar to that of cellulose, except for the presence of an acetyl-amino group instead of a hydroxyl group on C-2 position of cellulose. Chitin can be extracted as nanofibers from the exoskeletons of crustacean wastes such as crabs, squid pens, and prawns[17–20]. Chitin nanofibers intrinsically contain nitrogen derived from their

acetyl-amino group, providing an opportunity to prepare N-doped carbon structures by carbonization.[21,22] N-doped carbon structures have demonstrated enhanced functionality in various applications such as energy storage,[21,23,24] adsorption and catalysis,[22] photosensing,[24] and microwave absorption.[25] Furthermore, chitin nanofibers exhibit higher thermal stability than do cellulose nanofibers against the collapse of their original morphology during carbonization.[26] Thus, carbonized chitin nanofibers could be a superior alternative to carbonized cellulose nanofibers as high-performance photothermal materials. However, to the best of our knowledge, the photothermal heating properties of carbonized chitin nanofiber materials have not yet been explored.

In this chapter, chitin-nanofiber-derived N-doped carbon was fabricated and evaluated as a photothermal material for solar thermal heating. Chitin nanofibers were transformed into a nanopaper with subwavelength nanoporous structures by expanding the pore spaces between the nanofibers via *t*-BuOH treatment. Subsequently, carbonization was performed without pretreatment at controlled temperatures to customize the carbon-based chemical structures. Moreover, to elucidate the significance of the carbonized chitin nanopaper, its solar thermal heating performance was compared with that of a carbonized cellulose nanopaper.

2.2 Experimental Section

Materials

Aqueous dispersions of chitin nanofibers (2 wt%, SFo-20002) and cellulose nanofibers (2 wt%, WFo-10002) were obtained from Sugino Machine Ltd., Namerikawa, Japan. *t*-BuOH (>99.0% purity) was obtained from Nacalai Tesque Inc., Kyoto, Japan.

Preparation and carbonization of cellulose and chitin nanopapers

A water dispersion of chitin or cellulose nanofibers (0.2 wt%, 200 mL) was vacuum filtered on a hydrophilic polytetrafluorethylene membrane (pore diameter: 0.2 μm, H020A090C, Advantec Toyo Kaisha, Ltd., Tokyo, Japan). The nanofibers on the membrane were then treated by gently pouring *t*-BuOH onto it while vacuum filtering. The resulting wet nanopaper was peeled from the membrane, stored in a refrigerator (SJ-23T-S, Sharp, Corp., Osaka, Japan) at −18 °C for 30 min, and then freeze-dried overnight (FDU-2200, Tokyo Rikakikai Co., Ltd, Tokyo, Japan). Subsequently, the as-prepared nanopaper with a thickness of ~300 μm was cut into a square sheet with an area of 1.5 × 1.5 cm^2. A molybdenum block (area: 1.5 × 1.5 cm^2, thickness: ~1.0 cm, weight: ~20 g, MO-293771, The Nilaco Corp., Tokyo, Japan) was placed on it. Then, carbonization was performed in a furnace (KDF-75, DENKEN-HIGHDENTAL Co., Ltd., Kyoto, Japan) under a N_2 gas flow at a flow rate of ~500 mL min^{-1} in three stages:[14] (1) the temperature was increased from room temperature to 240 °C at 2 °C min^{-1} and maintained for 17 h; (2) the temperature was increased from 240 °C to the target temperature (300–1100 °C) at 2 °C min^{-1} and maintained for 1 h; and (3) the temperature was decreased to room temperature at 2 °C min^{-1}.

Solar thermal heating performances evaluation

Following our previous study,[14] we evaluated the solar thermal heating performances of the original and carbonized nanopapers by measuring the changes in their surface temperatures during solar-light irradiation. Prior to the evaluation, the emissivity of each nanopaper was evaluated using a commercial black tape (emissivity: 0.95, HB-250, OPTEX Co., Ltd., Shiga, Japan) as a reference. Briefly, black tape and a carbonized nanopaper were heated to 75 °C on a thermo-controller (SBX-303, Sakaguchi E.H VOC Corp., Tokyo, Japan). The emissivity of each

nanopaper was estimated using a thermal imaging camera (FLIR ETS320, FLIR Systems. Inc., Wilsonville, USA) by adjusting the temperature according to the reference temperature of black tape. Subsequently, surface temperature measurements were performed using a solar simulator (HAL-320W, Asahi Spectra Co., Ltd., Tokyo, Japan) as the light source. The nanopaper with an area of less than 1.5 × 1.5 cm^2 was placed on an acrylic plate (3 × 3 cm^2) with a rectangular hole (0.7 × 0.7 cm^2). Thereafter, it was irradiated by simulated solar light (AM1.5G, light intensity: 1.0 kW m^{-2} (1 sun)) such that the area of light illumination was larger than that of the nanopaper. The surface temperature of the nanopaper was recorded using a thermal imaging camera, and its equilibrium surface temperature was evaluated from the average temperature during a solar illumination time of 500–600 s (~850 plots). More than five samples were prepared and evaluated under each condition. The surface temperature measurements were conducted at 25 °C and 65% relative humidity.

Optical properties evaluation

The light absorption, transmittance, and reflection of the carbonized chitin and cellulose nanopapers were evaluated using an ultraviolet−visible−near-infrared (UV–vis–NIR) spectrometer (UV-3600i Plus, Shimadzu Corp., Kyoto, Japan) with an integrating sphere attachment (ISR-603, Shimadzu Corp., Kyoto, Japan). More than five samples were prepared and evaluated under each condition. Light absorption was calculated from the total light transmittance and reflection spectra. Solar absorption was calculated using Equation (1),[27] as follows:

$$\bar{\alpha} = \frac{\int_{\lambda_{min}}^{\lambda_{max}} I_{solar}(\lambda) \cdot \alpha_{solar}(\lambda) d\lambda}{\int_{\lambda_{min}}^{\lambda_{max}} I_{solar}(\lambda) d\lambda} \quad (1)$$

where $\bar{\alpha}$ is the solar absorption (%); λ is the wavelength (nm); λmin and λmax are 300 and 2500 nm, respectively; $Isolar(\lambda)$ is the AM1.5G solar spectral irradiance at λ; and $\alpha solar(\lambda)$ is the light

absorption (%) at λ. The optical bandgap values were also calculated from the UV–vis–NIR absorption spectra according to a previously reported method and Tauc's equation (Equation 2):

$$(\alpha hv)^{1/n} = A(hv - Eg) \quad (2)$$

where α, hv, A, and Eg are the absorbance, photon energy, constant, and optical band gap, respectively. The optical bandgap was estimated by plotting $(\alpha hv)^{1/n}$ vs. photon energy (hv) and extrapolating the linear region of the curve to the X-axis. The parameter n was set to 2 for the indirect transition of the carbonized nanopapers because of their amorphous carbon structures.

Chemical structures evaluation

Laser Raman spectroscopic analyses were performed by a RAMAN-touch VISNIR-OUN apparatus (Nanophoton Corp., Osaka, Japan) with an incident laser wavelength of 532 nm. Elemental analyses were performed by a 2400II instrument (PerkinElmer Japan Co. Ltd., Kanagawa, Japan). X-ray photoelectron spectroscopy (XPS) profiles were recorded by a JPS-9010 photoelectron spectrometer with a monochromatic Al Kα X-ray source (1486.6 eV) (JEOL, Ltd., Tokyo, Japan) at 15 kV voltage and 20 mA current.

Nanoporous structures evaluation

Surface structures of the original and carbonized chitin and cellulose nanopapers were observed by field-emission scanning electron microscopy (FE-SEM) (SU-8020, Hitachi High-Tech Science Corp., Tokyo, Japan) at an accelerating voltage of 2 kV. Prior to FE-SEM, platinum sputtering of the samples was conducted using an E-1045 Ion Sputter (Hitachi High-Tech Science Corp., Tokyo, Japan) at a current of 20 mA for 10 s. Pore-size distribution curves were obtained by nitrogen

adsorption analysis at −196 °C based on the Brunauer−Emmett−Teller and density functional theory models (NOVA 4200e, Quantachrome Instruments, Kanagawa, Japan).

2.3 Results and Discussion

Preparation of chitin-derived nitrogen-doped carbon nanopaper for solar thermal heating

The fabrication of the carbonized chitin nanopaper is schematically illustrated in **Fig. 2–1a**. A water dispersion of crab-shell-derived chitin nanofibers (0.2 wt%, 200 mL) was suction filtered. Then, it was treated by gently pouring *t*-BuOH (200 mL) onto the resulting wet sheet and vacuum filtered. Next, it was freeze-dried overnight and carbonized at 400 °C under a N_2 atmosphere without any pretreatment. The color of the chitin nanopaper changed from white to black after carbonization. Similarly, a carbonized cellulose nanopaper was fabricated using a water dispersion of wood-derived cellulose nanofibers (0.2 wt%, 200 mL). Although the chitin and cellulose nanopapers became somewhat brittle after carbonization, they were freestanding and allowed easy handling for characterization and evaluation. The solar thermal heating properties of the carbonized chitin and cellulose nanopapers were evaluated and compared. As shown in **Fig. 2–1b**, the change in the surface temperature of the carbonized chitin or cellulose nanopaper under simulated solar illumination (AM1.5G, light intensity: 1 sun) was monitored using a thermal imaging camera. The surface temperatures of the carbonized chitin and cellulose nanopapers rapidly increase upon 1-sun illumination and are saturated within 600 s **(Fig. 2–1c)**. The equilibrium surface temperatures of the original chitin and cellulose nanopapers (before carbonization) are 37.7 ± 0.40 and 37.1 ± 1.40 °C, respectively, while those of the carbonized chitin and cellulose nanopapers are 75.9 ± 1.27 and 66.9 ± 1.40 °C, respectively **(Fig. 2–1d)**, suggesting that the carbonized chitin nanopaper exhibits a higher solar thermal heating performance than the carbonized cellulose nanopaper.

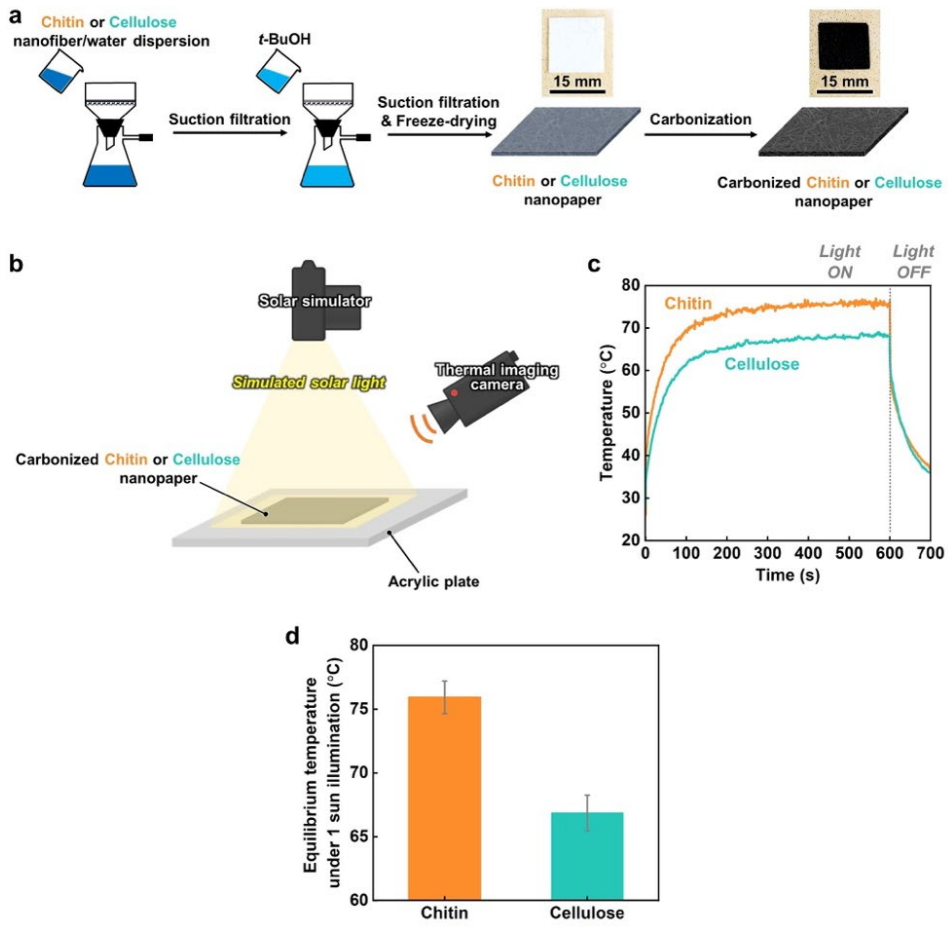

Fig. 2–1 Preparation and solar thermal heating performance of carbonized chitin and cellulose nanopapers. (a) Schematic of the preparation of the original and carbonized chitin or cellulose nanopaper and optical images of the original and carbonized chitin nanopaper; (b) schematic of the experimental setup for the measurement of the surface temperature during simulated solar light illumination; (c) surface temperature evolution and (d) equilibrium surface temperature of carbonized chitin and cellulose nanopapers under 1-sun illumination. Carbonization temperature: 400 °C.

Solar thermal heating by photothermal materials depends on their ability to absorb solar light and convert it into heat.[1,2] Therefore, to observe the difference in the solar thermal heating properties of the carbonized chitin and cellulose nanopapers, their light absorption properties were

compared. As shown in **Fig. 2–2a**, the carbonized chitin nanopaper exhibits a higher light absorption than the carbonized cellulose nanopaper in the wavelength range of solar light (AM1.5G, 300–2500 nm).[6] The higher light absorption of the carbonized chitin nanopaper is attributed to (1) the light transmission (transmittance: ~0%) wavelength being extended to a longer wavelength region **(Fig. 2–2b)** and (2) light reflection being suppressed in the entire solar wavelength region (300−2500 nm) **(Fig. 2–2c).** Furthermore, for a clearer comparison of the carbonized chitin and cellulose nanopapers, their solar absorptions, transmittances, and reflections were calculated from UV−vis−NIR absorption, transmittance, and reflection spectra, respectively, and the AM1.5G solar spectral irradiance, according to a previously reported method.[27] As shown in **Fig. 2–2d–f**, the carbonized chitin nanopaper provides a higher solar absorption (97.0 ± 0.19%) than the carbonized cellulose nanopaper (90.9 ± 0.43%) owing to the slight suppression of solar transmittance and large suppression of reflection. Thus, the carbonized chitin nanopaper exhibits a higher solar thermal heating performance than the carbonized cellulose nanopaper owing to higher solar absorption.

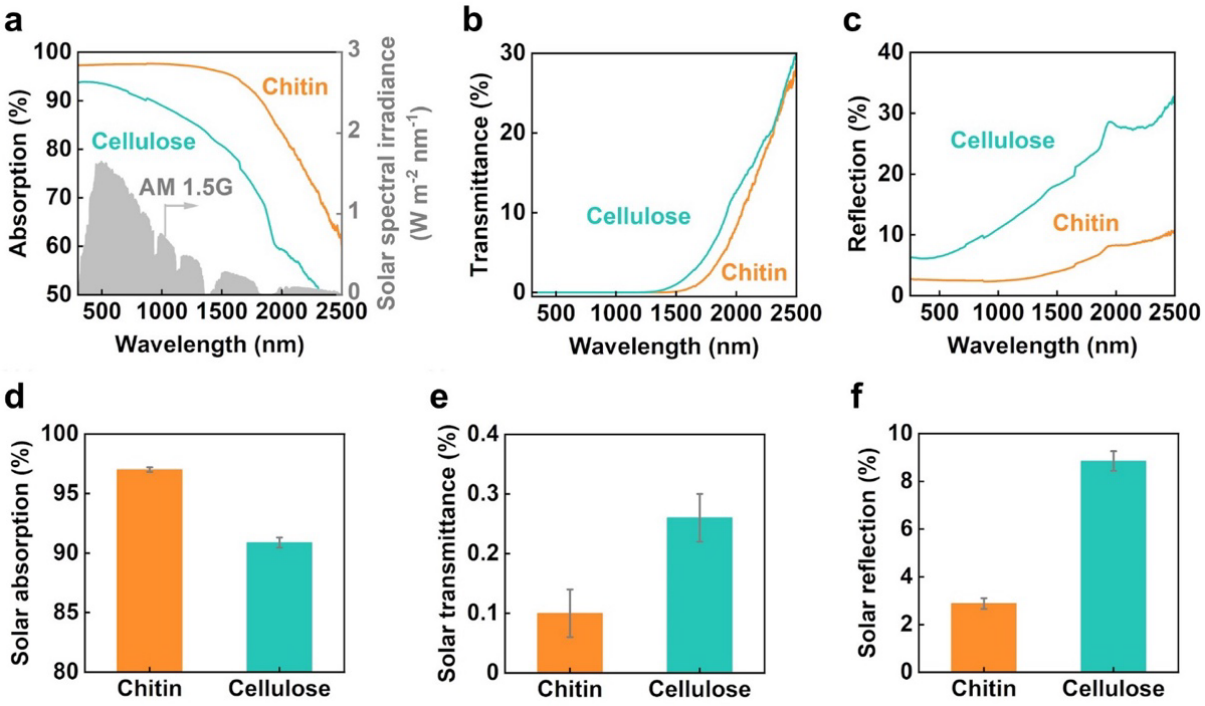

Fig. 2–2 Light absorption properties of the carbonized chitin and cellulose nanopapers. (a) AM1.5G solar spectral irradiance and UV−vis−NIR absorption, (b) transmittance, and (c) reflection spectra; solar light (d) absorption, (e) transmittance, and (f) reflection. Carbonization temperature: 400 °C.

The UV–vis–NIR absorption and transmission spectra of the carbonized chitin nanopaper exhibit light absorption over longer wavelength regions compared to those of the carbonized cellulose nanopaper **(Fig. 2–2a,b)**. This characteristic of the carbonized chitin nanopaper is beneficial for the suppression of light transmission and reflection in the longer wavelength region. We attributed this phenomenon to the lower optical bandgap of the carbonized chitin nanopaper (0.74 eV) compared with that of the carbonized cellulose nanopaper (1.01 eV) **(Fig. 2–3)**. A lower bandgap can facilitate light absorption at lower energies (longer wavelengths).

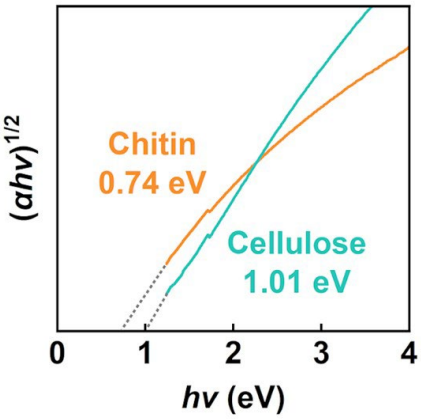

Fig. 2–3 Tauc plots and estimated optical bandgap values of the carbonized chitin and cellulose nanopapers. Carbonization temperature: 400 °C.

Impact of chemical structure and nitrogen-doped to the solar thermal heating performance

To confirm that the carbonized chitin nanopaper exhibited a lower optical bandgap, its chemical structures were analyzed and compared with those of the carbonized cellulose nanopaper**.** The original chitin and cellulose nanopapers before carbonization have the wide $\sigma-\sigma^*$ bandgap due to their *sp3*-hybridized carbon structures, resulting in low light absorption (i.e., high light transmission and reflection) **(Fig. 2–4)**.

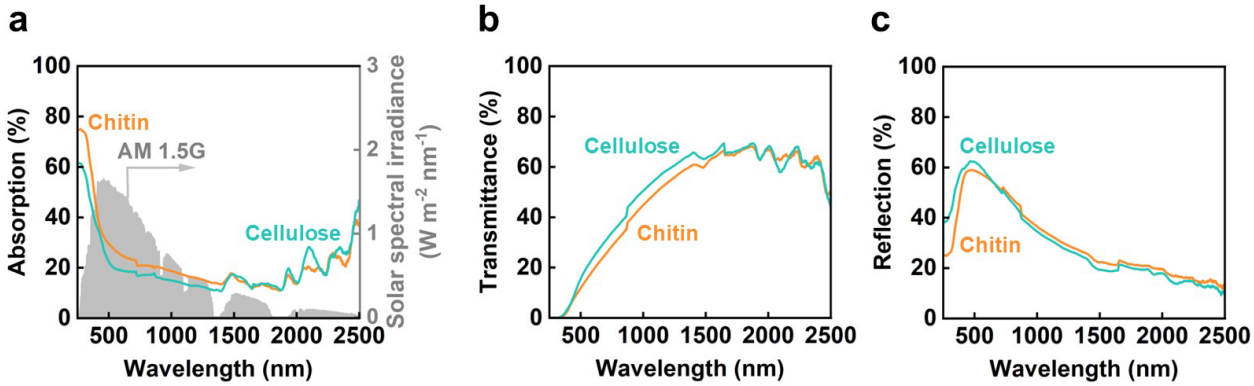

Fig. 2–4 Light absorption properties of the original chitin and cellulose nanopapers before carbonization. (a) Solar spectral irradiance (AM1.5G) and UV−vis−NIR absorption, (b) transmittance, and (c) reflection spectra.

The Raman spectra of the carbonized chitin and cellulose nanopapers display G and D bands **(Fig. 2–5a)**, which are associated with graphitic sp^2-hybridized carbon domains and defective carbon structures,[28] respectively, indicating that both chitin and cellulose nanopapers formed graphitic and defective carbon structures after carbonization at 400 °C. Owing to the graphitic carbon structures (i.e., π-orbital), the carbonized chitin and cellulose nanopapers had the $\pi-\pi^*$ bandgap, which lies within the $\sigma-\sigma^*$ bandgap. Hence, the carbonized nanopapers could promote light absorption as compared with the original nanopapers, while suppressing light transmission and reflection **(Fig. 2–2a–c, and 2–4)**. Elemental analyses show that the carbonized chitin nanopaper contains C (69.9%), O (17.8%), H (3.90%), and N (8.40%) and that the carbonized cellulose nanopaper contains C (75.5%), O (20.3%), and H (4.20%) **(Fig. 2–5b)**. The presence of N in the carbonized chitin nanopaper was verified by XPS **(Fig. 2–5c)**. The C 1s spectrum of the carbonized chitin nanopaper can be deconvoluted into five peaks: C–C or C=C (284.6 eV), C=N (285.8 eV), C-O (286.1 eV), C-N (287.4 eV), and C=O (287.8 eV),[29,30] whereas that of the carbonized cellulose nanopaper shows three peaks: C–C or C=C, C-O, and C=O **(Fig. 2-5d)**. The N 1s spectrum of the carbonized chitin nanopaper suggests the formation of pyridinic N (398.4 eV), pyrrolic N (399.9 eV), and graphitic N (401.0 eV) **(Fig. 2–5e)**.[31] These results indicate that the carbonized cellulose nanopaper possessed O-doped defective carbon structures, whereas the carbonized chitin nanopaper possessed N- and O-doped defective carbon structures. The carbonized cellulose nanopaper had graphitic sp^2-hybridized carbon domains (π-orbital) and defective regions such as O-containing functional groups (*n-orbital*), in which the n energy level lies within the $\pi-\pi^*$ energy gaps and reduces the optical bandgap.[32] The carbonized chitin nanopaper had additional N-containing functional groups (*n*-orbital) in the defective regions, which could further reduce the optical bandgap. Thus, the N- and O-doped defective carbon structures of the carbonized chitin

nanopaper result in a decreased optical bandgap, facilitating light absorption at lower energies (longer wavelengths) and consequently enhancing its solar absorption performance.

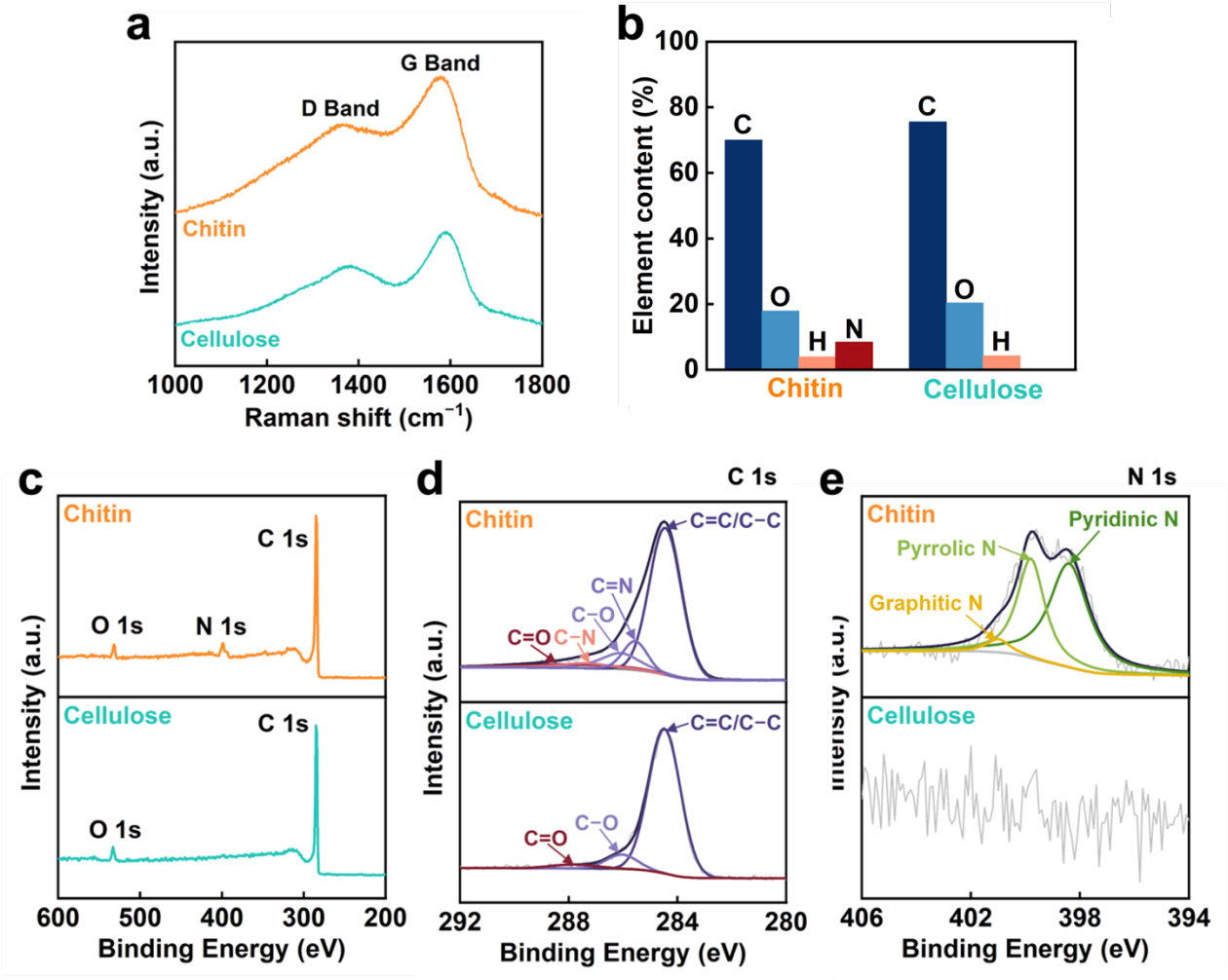

Fig. 2–5 Chemical structures of the carbonized chitin and cellulose nanopapers. (a) Raman spectra, (b) element contents, (c) wide XPS profiles, (d) C 1s XPS, and (e) N 1s XPS. Carbonization temperature: 400 °C.

Impact of subwavelength nanoporous structure to the solar thermal heating

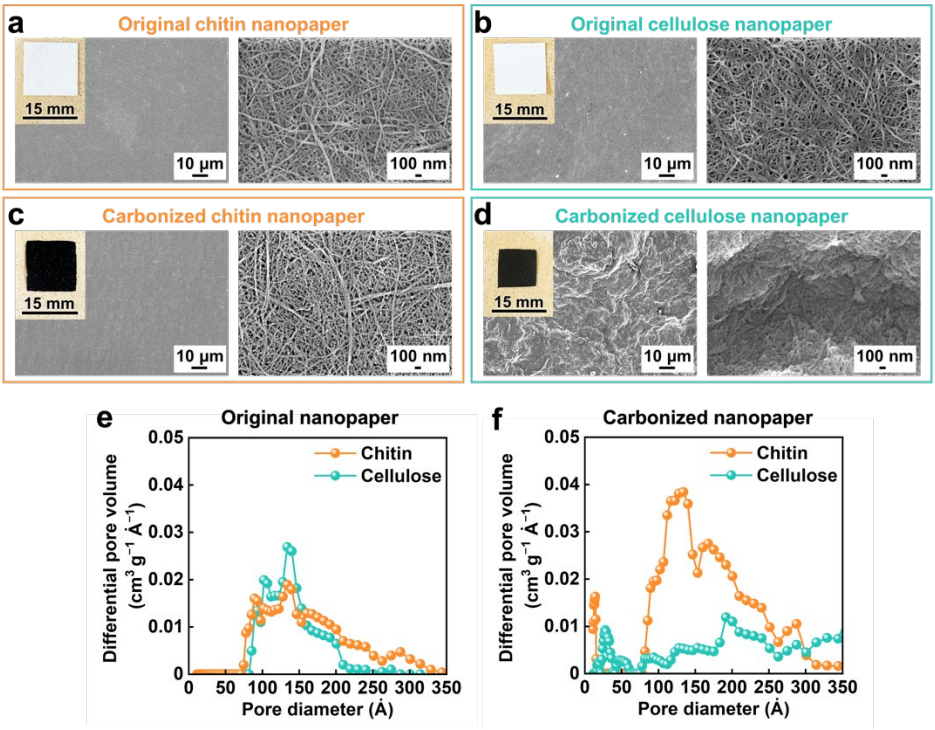

Fig. 2–6 Morphologies of the carbonized chitin and cellulose nanopapers. Optical and field-emission scanning electron microscopy images of the original (a) chitin and (b) cellulose nanopapers and the carbonized (c) chitin and (d) cellulose nanopapers; pore size distribution curves of the (e) original and (f) carbonized chitin and cellulose nanopapers. Carbonization temperature: 400 °C.

Unlike the carbonized cellulose nanopaper, the carbonized chitin nanopaper suppresses light reflection over the entire solar wavelength region **(Fig. 2–2c)**, demonstrating excellent solar absorption. To determine the reason for this suppressed light reflection, the morphologies of the carbonized chitin and cellulose nanopapers were analyzed and compared. The original chitin and cellulose nanopapers prepared in this chapter constitute subwavelength nanoporous structures that can suppress light reflection via the light confinement effect.[13] The subwavelength nanoporous structures of both nanopapers have similar pore size distributions **(Fig. 2–6a,b,e)**. However, the

cellulose nanopaper shrinks considerably after carbonization, closing its nanopores and forming microscale wrinkles on its surface **(Fig. 2–6d)**. The resulting dense and microscale structures cause light reflection.[14] By contrast, the shrinkage in chitin nanopaper after carbonization is lower than that in the cellulose nanopaper, which helps maintain the nanoporous structure and prevents the formation of microscale wrinkles in chitin nanopaper **(Fig. 2–6c,f)**.

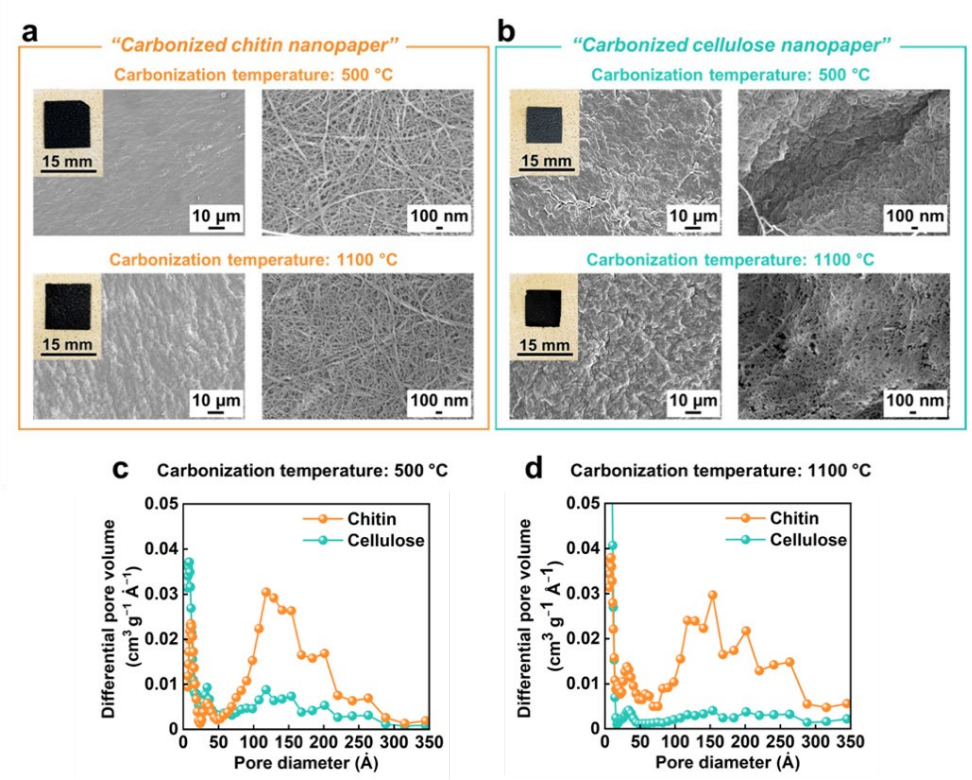

Fig. 2–7 Morphologies of the carbonized chitin and cellulose nanopapers. Optical and field-emission scanning electron microscopy images of the carbonized (a) chitin and (b) cellulose nanopapers, and pore size distribution curves of the chitin and cellulose nanopapers carbonized at (c) 500 and (d) 1100 °C. Carbonization temperature: 500 or 1100 °C.

Furthermore, the carbonized chitin nanopaper could retain the subwavelength nanoporous structures even at 1100 °C, while microscale wrinkles were gradually formed on its surfaces with increasing carbonization temperatures **(Fig. 2–7)**. The morphological stability of the chitin

nanopaper against carbonization could be attributed to the acetyl-amino group of chitin.[33] Hence, the carbonized chitin nanopaper demonstrated the light confinement effect owing to its subwavelength nanoporous structures, which suppress light reflection, thereby facilitating solar absorption. Finally, the morphologies and solar thermal heating properties of the carbonized chitin and cellulose nanopapers were compared at different carbonization temperatures. At the carbonization temperatures of 300–1100 °C, the chitin nanopaper retains more area and volume than the cellulose nanopaper **(Fig. 2–8a,b)**.

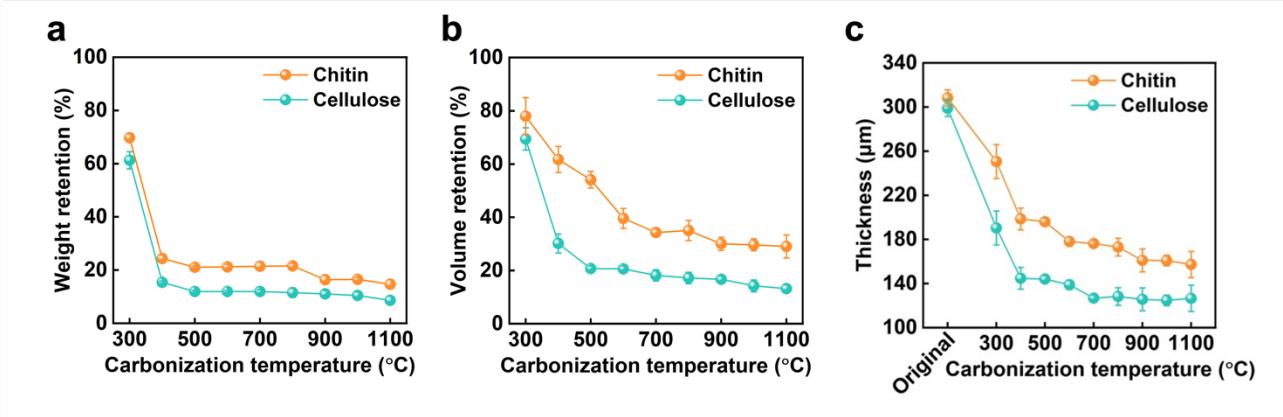

Fig. 2–8 Morphology retention of the chitin and cellulose nanopapers carbonized at different temperatures. (a) Area and (b) volume retention and (c) thickness. Carbonization temperature: 300−1100 °C.

The carbonized chitin nanopaper suppresses solar reflection and demonstrates higher solar absorption than does the carbonized cellulose nanopaper at all carbonization temperatures (300−1100 °C) **(Fig. 2–9a–c)**. Although the thicknesses of the carbonized chitin and cellulose nanopapers were gradually decreased with increasing carbonization temperatures **(Fig. 2–8c)**, the carbonized nanopapers exhibited very low solar transmittance, regardless of their carbonization temperatures **(Fig. 2–9b)**. These results suggested that the thickness of the carbonized nanopapers investigated in this study is not a dominant factor for their solar absorption properties.

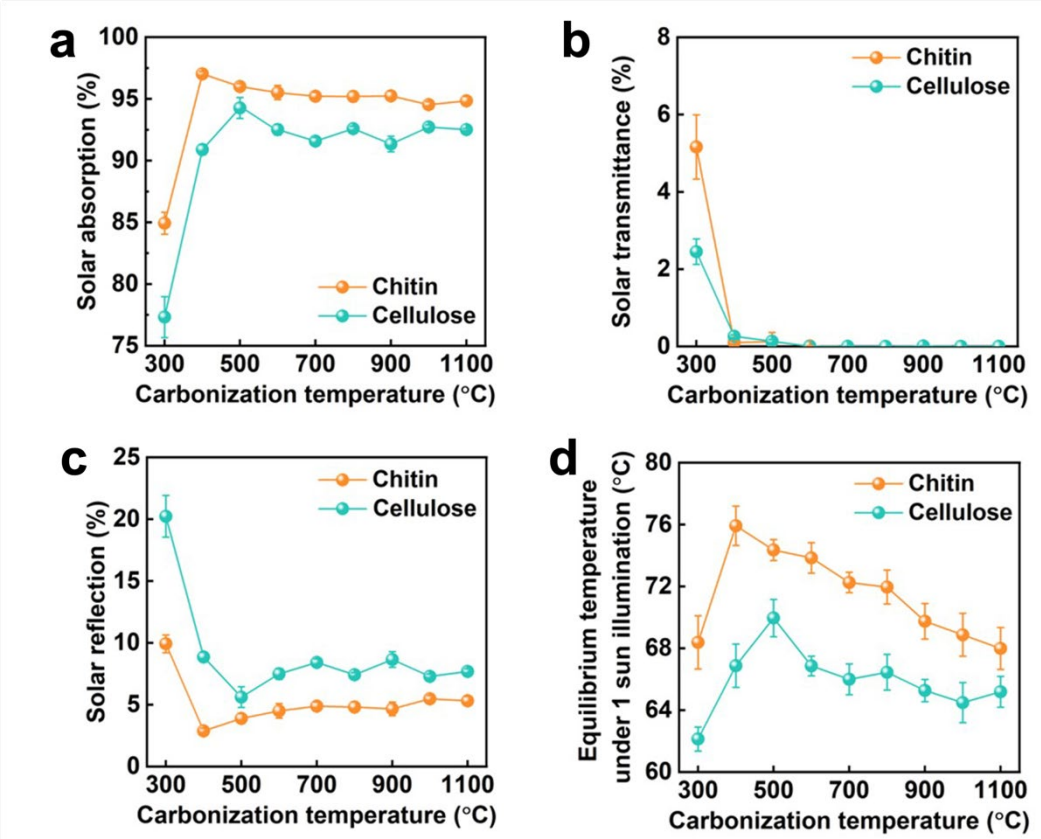

Fig. 2–9 Solar absorption properties, and solar thermal heating performances of the chitin and cellulose nanopapers carbonized at different temperatures. Solar (a) absorption, (b) transmittance, and (c) reflection; and (d) equilibrium surface temperature under 1-sun illumination. Carbonization temperature: 300−1100 °C.

Notably, the chitin nanopaper carbonized at 400 °C exhibits the highest solar absorption and the highest equilibrium surface temperature under 1-sun illumination **(Fig. 2–9a,d)**. The solar absorption and surface temperature under 1-sun illumination of the carbonized chitin nanopaper gradually decrease with increasing carbonization temperature above 400 °C. The lower solar absorption at higher carbonization temperatures **(Fig. 2–9a)** is attributed to higher light reflection **(Fig. 2–9c)**; the light reflection increases with increasing carbonization temperatures, possibly due to the gradual growth of graphitic sp^2-hybridized carbon domains by removing N and O.[24,25]

Moreover, the correlation upon light reflection and the electrical resistivity of the chitin and cellulose nanopapers were observed. The electrical resistivity underwent a dramatic change upon carbonization. The original chitin and cellulose nanopapers exhibited very high electrical resistivity, approximately 2.36×10^{12} and 3.07×10^{12} Ω cm, respectively. As the carbonization temperature increased, the electrical resistivity of both materials gradually decreased from approximately 10^{12} to 10^{-1} Ω cm. This gradual decrease in resistivity could be attributed to the growth of electrically conductive graphitic carbon structures (sp^2-hybridized carbon domains)[34,35] within the carbonized chitin and cellulose nanopaper **(Fig. 2–10)**. These structures facilitate free electron delocalization within π-conjugated systems, resulting in a metallic luster, as previously reported for graphite films,[36] and graphene papers.[37]

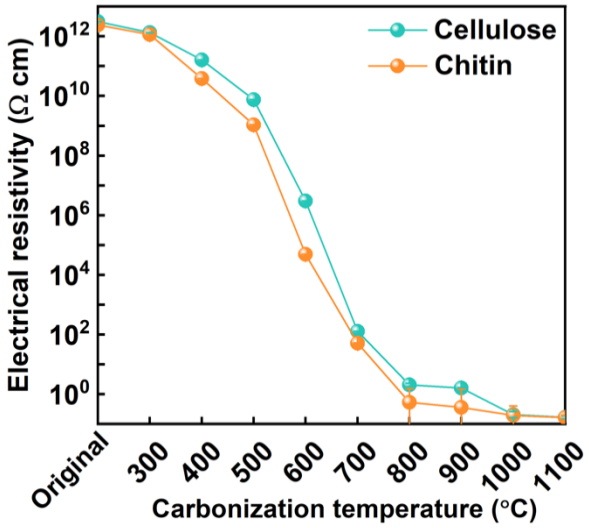

Fig. 2–10 Electrical resistivity of the chitin and cellulose nanopaper carbonized at different temperatures.

Furthermore, the gradual formation of microscale wrinkles on the surfaces of the carbonized chitin nanopaper with increasing carbonization temperatures **(Fig. 2–7a,b)** could also increase its light reflection. The lower surface temperature under 1-sun illumination at higher carbonization

temperatures could be attributed to the increased through-plane thermal conductivity resulting from the growth of the graphitic sp^2-hybridized carbon domain[14] in addition to the decreased solar absorption. The optimal carbonization temperature for solar absorption and surface temperature under 1-sun illumination are slightly different for the chitin (400 °C) and cellulose nanopapers (500 °C) **(Fig. 2–9a,d)**, which could be ascribed to the balance of their carbon-based chemical structures and morphologies. Moreover, the chitin nanopaper exhibits the best solar thermal heating performance at a lower carbonization temperature of 400 °C than that of the cellulose nanopaper (500 °C). Furthermore, the carbonized chitin nanopaper exhibits a higher solar thermal heating performance than the carbonized cellulose nanopaper regardless of the carbonization temperature. The solar thermal heating performance (surface temperature under 1-sun illumination: 75.9 ± 1.27 °C) of the chitin nanopaper carbonized at 400 °C is superior to those of commercial nanocarbon materials, such as carbon nanotube black body (55.0 °C), graphite sheet (64.5 °C), graphene paper (65.2 °C), and graphene oxide film (69.4 °C).[14]

2.4 Conclusions

In summary, the excellent solar thermal heating properties of the carbonized chitin nanopaper were demonstrated. N-doped carbon structures and subwavelength nanoporous structures were customized within the carbonized chitin nanopaper, facilitating its effective solar thermal heating. The appropriate carbonization temperature for the chitin nanopaper was verified as 400 °C to optimize its solar thermal heating performances by balancing its carbon-based chemical structures and nano/microscale morphologies. Notably, the optimized solar thermal heating performance of the carbonized chitin nanopaper (solar absorption: 97.0 ± 0.19%, surface temperature under 1 sun illumination: 75.9 ± 1.27 °C) was much higher than that of the carbonized cellulose nanopaper (solar absorption: 94.3 ± 0.85%, surface temperature under 1 sun illumination: 69.9 ± 1.20 °C). This result was because the carbonized chitin nanopaper provided higher solar absorption, by its lower optical bandgap derived from its N-doped carbon structures and by its higher morphological stability against carbonization to maintain its subwavelength nanoporous structures without any pretreatment. Thus, the carbonized chitin nanopaper is expected as a promising photothermal material for further effective use of renewable solar energy. This study can also guide the functionalization of carbonized bionanofiber materials as heteroatom-doped and nanostructured carbons for further applications.

2.5 References

1 M. S. Guney, *Renew. Sustain. Energy Rev.*, 2016, **57**, 776–785.

2 M. Gao, L. Zhu, C. K. Peh and G. W. Ho, *Energy Environ. Sci.*, 2019, **12**, 841–864.

3 Y. Liang, K. Koshelev, F. Zhang, H. Lin, S. Lin, J. Wu, B. Jia and Y. Kivshar, *Nano Lett.*, 2020, **20**, 6351–6356.

4 J. Y. Y. Loh, M. Safari, C. Mao, C. J. Viasus, G. V. Eleftheriades, G. A. Ozin and N. P. Kherani, *Nano Lett.*, 2021, **21**, 9124–9130.

5 B. Han, Y.-L. Zhang, Q.-D. Chen and H.-B. Sun, *Adv. Funct. Mater.*, 2018, **28**, 1802235.

6 ASTM G173-03., *Standard Tables for Reference Solar Spectral Irradiances: Direct Normal and Hemispherical on 37° Tilted Surface*, ASTM International: West Conshohocken, PA, 2012.

7 R. Fillet, V. Nicolas, V. Fierro and A. Celzard, *Sol. Energy Mater. Sol. Cells*, 2021, **219**, 110814.

8 W. Guan, Y. Guo and G. Yu, *Small*, 2021, **17**, 2007176.

9 A. M. Saleque, N. Nowshin, Md. N. A. S. Ivan, S. Ahmed and Y. H. Tsang, *Sol. RRL*, 2022, **6**, 2100986.

10 S. Zhou, L. Zhou, Y. Zhang, J. Sun, J. Wen and Y. Yuan, *J. Mater. Chem. A*, 2019, **7**, 4217–4229.

11 G. Feng, G.-Q. Zhang and D. Ding, *Chem. Soc. Rev.*, 2020, **49**, 8179–8234.

12 P. Tao, G. Ni, C. Song, W. Shang, J. Wu, J. Zhu, G. Chen and T. Deng, *Nat. Energy*, 2018, **3**, 1031–1041.

13 X. Zheng and L. Zhang, *Energy Environ. Sci.*, 2016, **9**, 2511–2532.

14 T. Yeamsuksawat, Y. Morishita, J. Shirahama, Y. Huang, T. Kasuga, M. Nogi and H. Koga, *Chem. Mater.*, 2022, **34**, 7379–7388.

15 J. J. Jasper, *J. Phys. Chem. Ref. Data*, 1972, **1**, 841–1010.

16 H. Koga, K. Nagashima, K. Suematsu, T. Takahashi, L. Zhu, D. Fukushima, Y. Huang, R. Nakagawa, J. Liu, K. Uetani, M. Nogi, T. Yanagida and Y. Nishina, *ACS Nano*, 2022, **16**, 8630–8640.

17 J. L. Shamshina, P. Berton and R. D. Rogers, *ACS Sustain. Chem. Eng.*, 2019, **7**, 6444–6457.

18 S. Ifuku and H. Saimoto, *Nanoscale*, 2012, **4**, 3308–3318.

19 Y. Fan, T. Saito and A. Isogai, *Biomacromolecules*, 2008, **9**, 1919–1923.

20 S. Ifuku, M. Nogi, K. Abe, M. Yoshioka, M. Morimoto, H. Saimoto and H. Yano, *Biomacromolecules*, 2009, **10**, 1584–1588.

21 T.-D. Nguyen, K. E. Shopsowitz and M. J. MacLachlan, *J. Mater. Chem. A*, 2014, **2**, 5915.

22 Y. Gao, X. Chen, J. Zhang and N. Yan, *ChemPlusChem*, 2015, **80**, 1556–1564.

23 B. Ding, S. Huang, K. Pang, Y. Duan and J. Zhang, *ACS Sustain. Chem. Eng.*, 2018, **6**, 177–185.

24 L. Zhu, Y. Huang, Y. Morishita, K. Uetani, M. Nogi and H. Koga, *J. Mater. Chem. C*, 2021, **9**, 4444–4452.

25 X. Li, L. Zhu, T. Kasuga, M. Nogi and H. Koga, *Chem. Eng. J.*, 2022, **450**, 137943.

26 M. Nogi, F. Kurosaki, H. Yano and M. Takano, *Carbohydr. Polym.*, 2010, **81**, 919–924.

27 J. Mandal, D. Wang, A. C. Overvig, N. N. Shi, D. Paley, A. Zangiabadi, Q. Cheng, K. Barmak, N. Yu and Y. Yang, *Adv. Mater.*, 2017, **29**, 1702156.

28 M. S. Dresselhaus, A. Jorio, A. G. Souza Filho and R. Saito, *Philos. Trans. R. Soc. Math. Phys. Eng. Sci.*, 2010, **368**, 5355–5377.

29 H. Yu, L. Shang, T. Bian, R. Shi, G. I. N. Waterhouse, Y. Zhao, C. Zhou, L.-Z. Wu, C.-H. Tung and T. Zhang, *Adv. Mater.*, 2016, **28**, 5080–5086.

30 Z.-H. Sheng, L. Shao, J.-J. Chen, W.-J. Bao, F.-B. Wang and X.-H. Xia, *ACS Nano*, 2011, **5**, 4350–4358.

31 H. B. Yang, J. Miao, S.-F. Hung, J. Chen, H. B. Tao, X. Wang, L. Zhang, R. Chen, J. Gao, H. M. Chen, L. Dai and B. Liu, *Sci. Adv.*, 2016, **2**, e1501122.

32 M. Li, S. K. Cushing, X. Zhou, S. Guo and N. Wu, *J. Mater. Chem.*, 2012, **22**, 23374.

33 T. A. Khan, A. S. Saud, S. S. Jamari, M. H. A. Rahim, J. W. Park and H. J. Kim, *Biomass Bioenergy*, 2019, **130**, 105384.

34 H.-P. Cong, X.-C. Ren, P. Wang and S.-H. Yu, *Energy Environ. Sci.*, 2013, **6**, 1185.

35 G. Qi, L. Huang and H. Wang, *Chem. Commun.*, 2012, **48**, 8246.

36 M. Isayama, K. Nomiyama and T. Kunitake, *Adv. Mater.*, 1996, **8**, 641–644.

37 H. Chen, M. B. Müller, K. J. Gilmore, G. G. Wallace and D. Li, *Adv. Mater.*, 2008, **20**, 3557–3561.

Chapter 3

CO_2-Laser-Induced Carbonization of Calcium Chloride-Treated Chitin Nanopaper for Applications in Solar Thermal Heating Materials

3.1 Introduction

Carbonized biomass materials have garnered increasing attention owing to their light weight, large specific surface areas, unique electrical properties, high thermal stability, and sustainable nature.[1] Functional design of carbonized biomass materials has been actively investigated for various applications, such as adsorption/separation,[2,3] sensing,[4] energy generation,[4] and storage.[5–7] Among various biomass materials, chitin (β-(1→4)-linked N-acetyl anhydroglucosamine), which is mainly derived from marine creatures such as crabs and shrimps, has been regarded as a promising one for the functional design by carbonization. For instance, carbonized chitin nanofiber materials can provide multiple functions, including sensing,[8,9] energy storage for supercapacitors,[8–10] and microwave absorption[11] by tailoring their N- and O-doped carbon structures, as well as their porous nano/microstructures.

One of the emerging applications of carbonized biomass materials is solar thermal heating.[12–16] Solar thermal heating is a phenomenon to absorb and convert solar light into thermal energy, which can be achieved using photothermal materials. Carbonized biomass materials afford broadband light absorption, which is beneficial for absorbing solar light in the wavelength range of 300–2500 nm (ASTM G173-03, Air Mass 1.5 Global spectrum (AM1.5G)).[17] The absorption-wavelength range is wider than those of other photothermal materials, such as plasmonic nanomaterials (approximately 300–1000 nm) and oxide semiconductors (approximately 300–1500 nm).[18] Accordingly, carbonized biomass materials are expected to be sustainable and high-performance

photothermal materials. Thus, solar thermal heating by carbonized biomass materials has become a major center of attraction toward the effective use of renewable solar energy and is used in various applications, including photothermal catalysis,[19] solar steam generation,[20] wastewater purification,[21] desalination,[22] and thermoelectric generation.[15]

Carbonization is essential for the fabrication of carbonized biomass materials. Biomass materials have been traditionally carbonized by acid,[23,24] hydrothermal,[3,5,25,26] and high-temperature treatments.[2–16] Although these traditional carbonization treatments require harmful reagents[23,24] or time-consuming processes,[2–16,25,26] CO_2 laser irradiation treatment has been progressing as a facile and second-scale fast carbonization process.[27–32] The CO_2-laser-induced carbonization has been first reported for polyimide,[27] and thereafter actively applied for various organic polymer materials including biomass materials.[28–32] Upon CO_2 laser irradiation, the organic polymer materials reach a high temperature, causing their chemical bonds such as C–O and C=O to break and rearrange to form a graphitic carbon structure.[27] Recently, the CO_2-laser-induced carbonization has been applied to a synthetic polybenzoxazine resin film to fabricate a graphitic carbon with forest-like morphologies, providing excellent solar thermal heating properties.[33] To the best of our knowledge, however, the CO_2-laser-induced carbonization of biomass materials for solar thermal heating applications has been unexplored.

In chapter 2, the high solar-thermal heating performance of a high-temperature (400 °C) carbonized chitin nanofiber paper (denoted as chitin nanopaper) was reported.[16] Here, this chapter showed the CO_2-laser-induced carbonization of chitin nanopaper and further evaluated the CO_2-laser-carbonized chitin nanopaper as a photothermal material for solar thermal heating. The chitin nanopaper inevitably burned out during CO_2 laser irradiation, indicating the difficulty of its CO_2-laser-induced carbonization. To inhibit combustion, the chitin nanopaper was pretreated with

calcium chloride ($CaCl_2$). $CaCl_2$-treated chitin nanopaper was successfully carbonized using seconds-scale CO_2 laser irradiation process. Excellent solar thermal heating performance of the CO_2-laser-carbonized chitin nanopaper was also demonstrated.

3.2 Experimental Section

Materials

A chitin nanofiber/water dispersion (2 wt%, SFo-20002) was supplied by Sugino Machine, Ltd. (Namerikawa, Japan). $CaCl_2$ (>95.0% purity) and ethanol (>99.5% purity) were obtained from Nacalai Tesque, Inc. (Kyoto, Japan).

Preparation of chitin nanopaper

A chitin nanofiber/water dispersion (0.2 wt%, 200 mL) was dewatered by suction filtration through a hydrophilic polytetrafluoroethylene membrane with a pore diameter of 0.2 μm (H020A090C, Advantec Toyo Kaisha, Ltd., Tokyo, Japan). The wet sheet obtained was peeled from the membrane, placed on a hydrophobic glass plate, covered with a #400 stainless-steel wire mesh (CLV-SUS304M-48, Kurubaa Co., Ltd., Toyohashi, Japan), and sandwiched between paper towels (Kimtowel White, Nippon Paper Crecia Co., Ltd., Tokyo, Japan). Finally, the resulting assembly was dried by hot pressing at 110 °C and 0.35 MPa for 25 min (AYSR-5, Shinto Metal Industries, Ltd., Osaka, Japan) to prepare chitin nanopaper with a diameter and thickness of approximately 70 mm and 100 μm, respectively.

Treatment of chitin nanopaper with $CaCl_2$

Prior to the $CaCl_2$ treatment, the as-prepared chitin nanopaper was fixed on a glass plate. Subsequently, a $CaCl_2$/ethanol solution ($CaCl_2$ content: approximately 25 wt%) was sprayed onto the surface of the chitin nanopaper for 5, 10, or 20 s using a spray machine (Handheld Nano Spray K5, Shenzhen NOYAFA Electronic Co., Ltd., Shenzhen, China). The distance between the spray jet and chitin nanopaper was set to approximately 10 cm while the spray jet was held at a 45° to the chitin nanopaper. The as-sprayed chitin nanopaper was stored in a fume hood under ambient conditions for at least 2 h. The $CaCl_2$ content of the resulting chitin nanopaper was calculated by subtracting the dry weight of the $CaCl_2$-treated chitin nanopaper from that of the chitin nanopaper.

CO_2-laser-induced carbonization of the $CaCl_2$-treated chitin nanopaper

The $CaCl_2$-treated chitin nanopaper on a glass plate was irradiated using a CO_2 laser with a wavelength of 10.2 μm and a laser spot diameter of 300 μm (CO_2-MK-kit, Kokyo, Inc., Kyoto, Japan) under a nitrogen atmosphere to prepare the CO_2-laser-carbonized chitin nanopaper. The focal distance was 160 mm. A computer-controlled laser program was used to control the laser pattern (square shape: 1.5 cm × 1.5 cm), scan speed (100 mm s^{-1}), pulsed laser frequency (25 kHz), and laser power (1.5, 3.0, 4.5, or 6.0 W) for a single irradiation loop.

Solar thermal heating performance testing

Solar thermal heating performances were measured in a dark room, according to our previous studies.[15,16,34] The emissivity of each sample was first measured using a black tape with a known emissivity of 0.95 (HB250, OPTEX Co., Ltd., Otsu, Japan) as a reference. In brief, the sample and black tape were heated to 75 °C by an SBX-303 temperature-controller (Sakaguchi E.H. VOC

Corp., Tokyo, Japan). The emissivity of the sample was evaluated using an FLIR ETS320 thermal imaging camera (FLIR Systems. Inc., Wilsonville, USA) by adjusting the temperature based on the reference temperature of black tape. After emissivity calibration, the solar thermal heating performance of each sample was evaluated by measuring its surface temperature under 1 sun irradiation as follows: The 2.5 cm × 2.5 cm of chitin nanopaper, $CaCl_2$-treated chitin nanopaper, or CO_2-laser-carbonized chitin nanopaper (carbonized area: 1.5 cm × 1.5 cm) was placed on an acrylic plate (3 cm × 3 cm) with a central hole (0.7 cm × 0.7 cm). The change in surface temperature during simulated solar light irradiation (AM1.5G, light intensity: 1 sun, HAL-320W, Asahi Spectra Co., Ltd., Tokyo, Japan) was recorded by a thermal imaging camera. The solar light irradiation area was larger than that of the samples. The equilibrium surface temperature of the samples was estimated as the average surface temperature of approximately 850 plots during solar irradiation times of 500–600 s. This experiment was performed at approximately 25 °C and 50% relative humidity.

Characterization

Chemical structures were analyzed by laser Raman spectroscopy (laser wavelength: 532 nm, RAMAN-touch VISNIR-OUN, Nanophoton Corp., Osaka, Japan), FT-IR/attenuated total reflection spectroscopy (KJP-05120S, PerkinElmer Japan Co., Ltd., Kanagawa, Japan), and XPS (JPS-9010, JEOL, Ltd., Tokyo, Japan) with a monochromatic AlKα X-ray source (1486.6 eV) at 15 kV and 20 mA. For FT-IR analysis of the CO_2-laser-carbonized chitin nanopaper, the carbonized layer was scratched, recovered, and analyzed. The morphologies were observed by FE-SEM at an accelerating voltage of 2 kV (SU-8020, Hitachi High-Tech Science Corp., Tokyo, Japan). Prior to observation, platinum was sputtered onto the sample surfaces (E-1045 Ion Sputter,

Hitachi High-Tech Science Corp., Tokyo, Japan). Optical absorption, reflection, and transmittance were measured using a UV-3600i Plus spectrometer with an ISR-603 integrating sphere attachment (Shimadzu Corp., Kyoto, Japan). The absorption (%A) was calculated from the transmittance (%T) and reflectance (%R) according to the following equation: %A = 100–(%T + %R). The optical bandgap values of the original chitin nanopaper, $CaCl_2$-treated chitin nanopaper, and CO_2-laser-carbonized chitin nanopaper were estimated from the UV-vis-NIR absorbance spectra of their water dispersions, according to a previous study[4] and Tauc's equation:[35] $(\alpha h\nu)^{1/n} = A(h\nu - E_g)$, where α denotes the absorbance, $h\nu$ denotes the photon energy, A is a constant, and E_g denotes the optical bandgap. The parameter n is 1/2 and 2 for direct and indirect transitions, respectively. To estimate the optical bandgap, $(\alpha h\nu)^{1/n}$ was plotted against the photon energy ($h\nu$), and the linear region of the curve was extrapolated to the x-axis. The optical bandgap values of the chitin nanopaper and $CaCl_2$-treated chitin nanopaper were estimated to be n = 1/2, whereas that of the CO_2-laser-carbonized chitin nanopaper was estimated to be n = 2 because of its amorphous carbon structure.

3.3 Results and Discussion

$CaCl_2$ treatment of chitin nanopaper for CO_2-laser-induced carbonization

CO_2-laser-induced carbonization of the chitin nanopaper was performed according to the workflow shown in **Fig. 3–1a**. Chitin nanopapers were prepared from a crab-shell-derived chitin nanofiber/water dispersion by suction filtration and subsequent hot-press drying. When the CO_2 laser was irradiated with the chitin nanopaper without any pretreatment, it completely burned out, even under an inert nitrogen atmosphere **(Fig. 3–1b, left)**, indicating that the chitin nanopaper was difficult to carbonize by CO_2 laser irradiation. Such difficulties have been frequently observed for

various biomass materials owing to their low thermal stability; they have been subjected to fire-retardant treatments such as additive mixing[28,31,32] and chemical modification.[29,30] To overcome this problem, in this chapter, $CaCl_2$, which has been used as a combustion inhibitor,[36–39] was introduced into chitin nanopaper. As depicted in **Fig. 3–1a**, chitin nanopaper (approximately 400 mg) with a diameter and thickness of approximately 70 mm and 100 μm, respectively, was sprayed with an approximately 25 wt% $CaCl_2$/ethanol solution for 10 s. After drying, the $CaCl_2$ content of the chitin nanopaper was approximately 78 mg. The $CaCl_2$-treated chitin nanopaper with a thickness of approximately 105 μm was thereafter irradiated with a CO_2 laser at a power and speed of 4.5 W and 100 mm s^{-1}, respectively. The CO_2-laser-irradiated area on the $CaCl_2$-treated chitin nanopaper turned black **(Fig. 3–1b, right)**. In the Raman spectra, three characteristic peaks, namely, the D band (approximately 1350 cm^{-1}),[40] G band (approximately 1600 cm^{-1}),[40] and 2D band (approximately 2680 cm^{-1})[41] were confirmed in the CO_2-laser-irradiated area, whereas these peaks were not observed in the original and $CaCl_2$-treated chitin nanopapers before CO_2 laser irradiation **(Fig. 3–1c)**. The D, G, and 2D bands are reportedly ascribed to defective carbon structures,[40] graphitic sp^2-hybridized carbon structures,[40] and stacking of graphitic carbon structures,[41] respectively. These results indicated that the CO_2-laser-induced carbonization of the chitin nanopaper was successfully achieved by $CaCl_2$ pretreatment. The CO_2-laser-induced carbonization process of the $CaCl_2$-treated chitin nanopaper (carbonization area: 1.5 cm × 1.5 cm) was completed in approximately 32 s, which was much faster than the conventional hours-scale carbonization processes of chitin materials such as hydrothermal[25] and high-temperature treatments.[7–11,16]

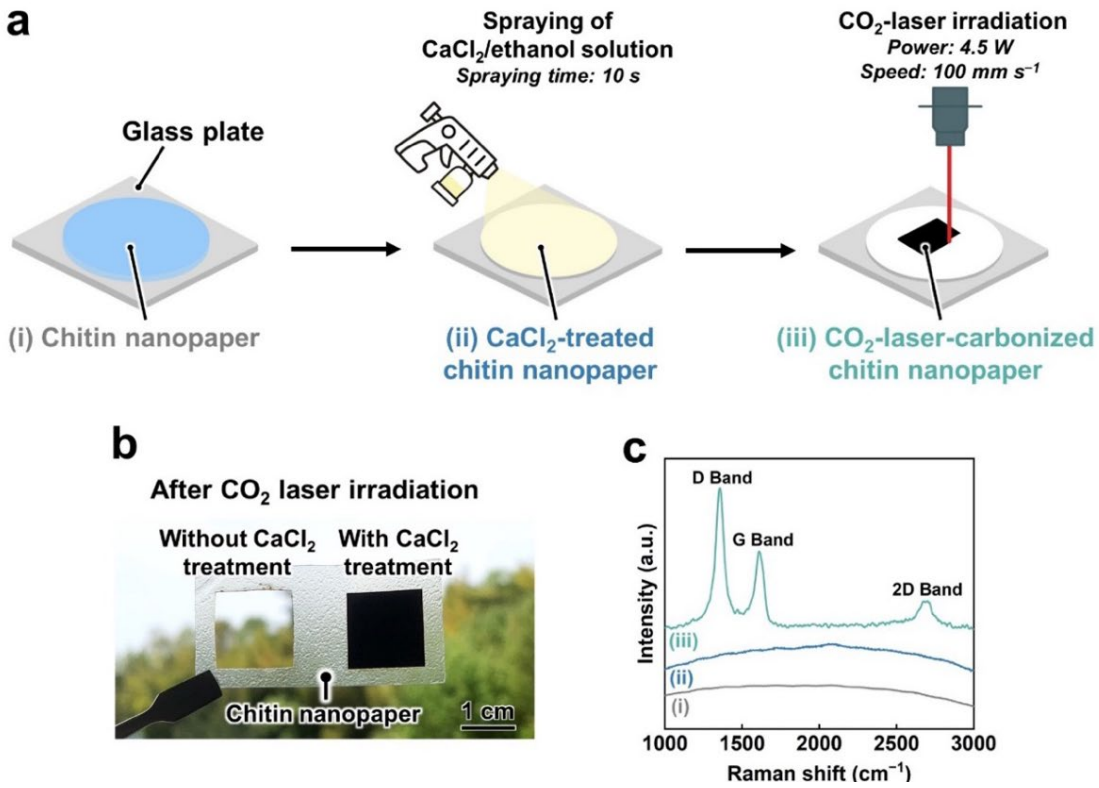

Fig. 3–1 $CaCl_2$ treatment and CO_2-laser-induced carbonization of chitin nanopaper. (a) Procedure schematic, (b) optical image of chitin nanopaper with or without the $CaCl_2$ treatment after CO_2 laser irradiation, and (c) Raman spectra of the (i) original chitin nanopaper, (ii) $CaCl_2$-treated chitin nanopaper, and (iii) CO_2-laser-carbonized chitin nanopaper.

Chemical structures of CO_2-laser-carbonized chitin nanopaper

The chemical structures of the CO_2-laser-carbonized chitin nanopaper were further analyzed by Fourier-transform infrared (FT-IR) spectroscopy and X-ray photoelectron spectroscopy (XPS) **(Fig. 3–2)**. In the FT-IR spectra **(Fig. 3–2a)**, the original chitin nanopaper exhibited characteristic peaks corresponding to the O–H groups (3450 cm^{-1}),[42] N–H groups (3260 cm^{-1}),[42] amide I region (1660 and 1620 cm^{-1}),[43] and amide II region (1560 cm^{-1}),[43] which are derived from α-chitin.[43] The $CaCl_2$-treated chitin nanopaper exhibited similar spectra with the original chitin nanopaper, indicating that the original chemical structure of chitin nanopaper remained unchanged after the

$CaCl_2$ treatment. The original chemical structure changed significantly after CO_2 laser irradiation. The CO_2-laser-carbonized chitin nanopaper exhibited the formation of C=C and C=N (1580 cm^{-1}),[44] and C=O groups (1700 cm^{-1}),[44] while retaining the C=O groups of the acetyl unit on amide I (1620 cm^{-1}),[45] and O–H and N–H groups. Notably, the characteristic peak of carbonate (CO_3^{2-}) appeared at 875 cm^{-1}, suggesting the formation of calcium carbonate ($CaCO_3$)[46] after the CO_2 laser carbonization. The wide XPS spectrum of the CO_2-laser-carbonized chitin nanopaper indicated the presence of C, O, N, Ca, and Cl **(Fig. 3–2b)**. The C 1s XPS spectrum of the CO_2-laser-carbonized chitin nanopaper could be divided into six peaks at 284.6, 285.8, 286.1, 287.4, 287.8, and 290.0 eV, which are attributed to C–C or C=C, C=N, C–O, C–N, C=O, and CO_3^{2-}, respectively **(Fig. 3–2c)**.[47–50] From the results of Raman, FT-IR, and XPS analyses **(Fig. 3–1c and 3–2)**, it was indicated that the CO_2-laser-carbonized chitin nanopaper has N- and O-doped defective carbon structures, as reported for the high-temperature-carbonized chitin nanopaper.[16] While the Ca 2p XPS spectrum of the $CaCl_2$-treated chitin nanopaper exhibited characteristic peaks at 348.3 eV for $2p_{3/2}$ and 351.8 eV for $2p_{1/2}$ corresponding to $CaCl_2$,[51] that of the CO_2-laser-carbonized chitin nanopaper exhibited additional peaks at 347.4 eV for $2p_{3/2}$ and 350.9 eV for $2p_{1/2}$ corresponding to $CaCO_3$ **(Fig. 3–3)**.[52,53] The formation of $CaCO_3$ upon the CO_2-laser-induced carbonization is due to the presence of $CaCl_2$, CO_2, and H_2O, where CO_2 and H_2O can be generated by the combustion chain reaction of chitin upon its carbonization.[54]

The CO_2-laser-induced carbonization of the $CaCl_2$-treated chitin nanopaper can be ascribed to the generation of thermal energy (high temperatures) through the photothermal effect derived from the lattice vibrations of chitin molecules, as reported for polyimide.[27] Although the original chitin nanopaper burned out upon CO_2 laser irradiation, such combustion could be suppressed in the presence of $CaCl_2$ **(Fig. 3–1c)**. The combustion-inhibiting effect of $CaCl_2$ can be explained as

follows. During carbonization of polymeric materials, reactive radicals, such as ·OH and ·H, are continuously generated, promoting the combustion reaction of polymeric materials.[55] The Ca and Cl ions can reportedly scavenge these radicals,[36–39] thereby inhibiting the combustion of polymeric materials. Hence, the CO_2-laser-induced carbonization of chitin nanopaper was successfully achieved in the presence of $CaCl_2$.

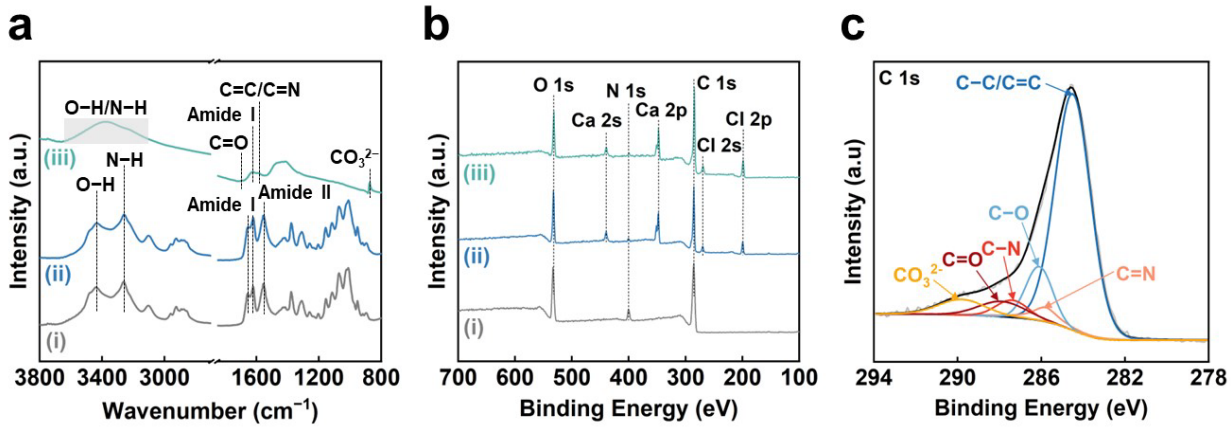

Fig. 3–2 Chemical structures of the CO_2-laser-carbonized chitin nanopaper. (a) FT-IR and (b) wide XPS spectra of the (i) original chitin nanopaper, (ii) $CaCl_2$-treated chitin nanopaper, and (iii) CO_2-laser-carbonized chitin nanopaper. (c) C 1s XPS spectrum of the CO_2-laser-carbonized chitin nanopaper.

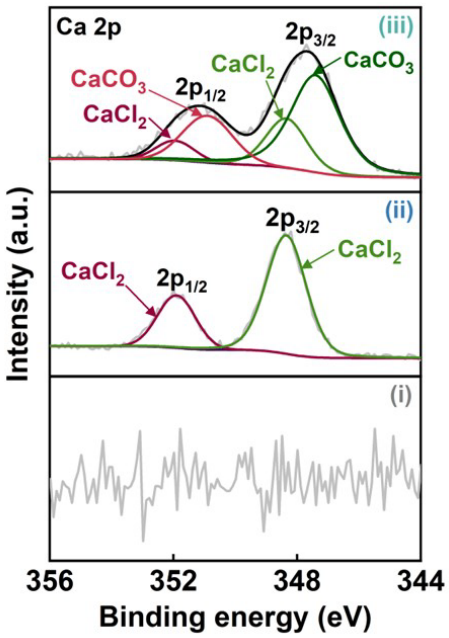

Fig. 3–3 Ca 2p XPS spectra of the (i) original chitin nanopaper, (ii) $CaCl_2$-treated chitin nanopaper, and (iii) CO_2-laser-carbonized chitin nanopaper.

Morphologies of CO_2-laser-carbonized chitin nanopaper

The morphologies of the chitin nanopapers were observed by field-emission scanning electron microscopy (FE-SEM) **(Fig. 3–4)**. The original chitin nanopaper had smooth surfaces derived from the densely packed chitin nanofibers **(Fig. 3–4a)**. Smooth surface structures were maintained after $CaCl_2$ treatment **(Fig. 3–4b)**. After CO_2-laser-induced carbonization, the surface structures became rough and porous **(Fig. 3–4c)**, forming coralline-like microstructures, as observed in the CO_2-laser-carbonized polybenzoxazine resin film (**Fig. 3–4c–e**).[33] The thicknesses of the original and $CaCl_2$-treated chitin nanopapers were approximately 100 and 105 μm, respectively. The CO_2-laser-carbonized chitin nanopaper had two layers comprising a chitin nanopaper and a CO_2-laser-carbonized area with thicknesses of approximately 70 and 160 μm, respectively **(Fig. 3–4d,f)**. These results suggest that approximately 35 μm of the surface layer of the $CaCl_2$-treated chitin nanopaper was carbonized by CO_2 laser irradiation to form a carbonized layer of approximately

160 μm. Such a relatively thick CO_2-laser-carbonized layer was formed owing to a "bombing" effect;[56] byproduct gases were released quickly upon the rapid CO_2-laser-induced carbonization to form a porous and thick carbonized layer.

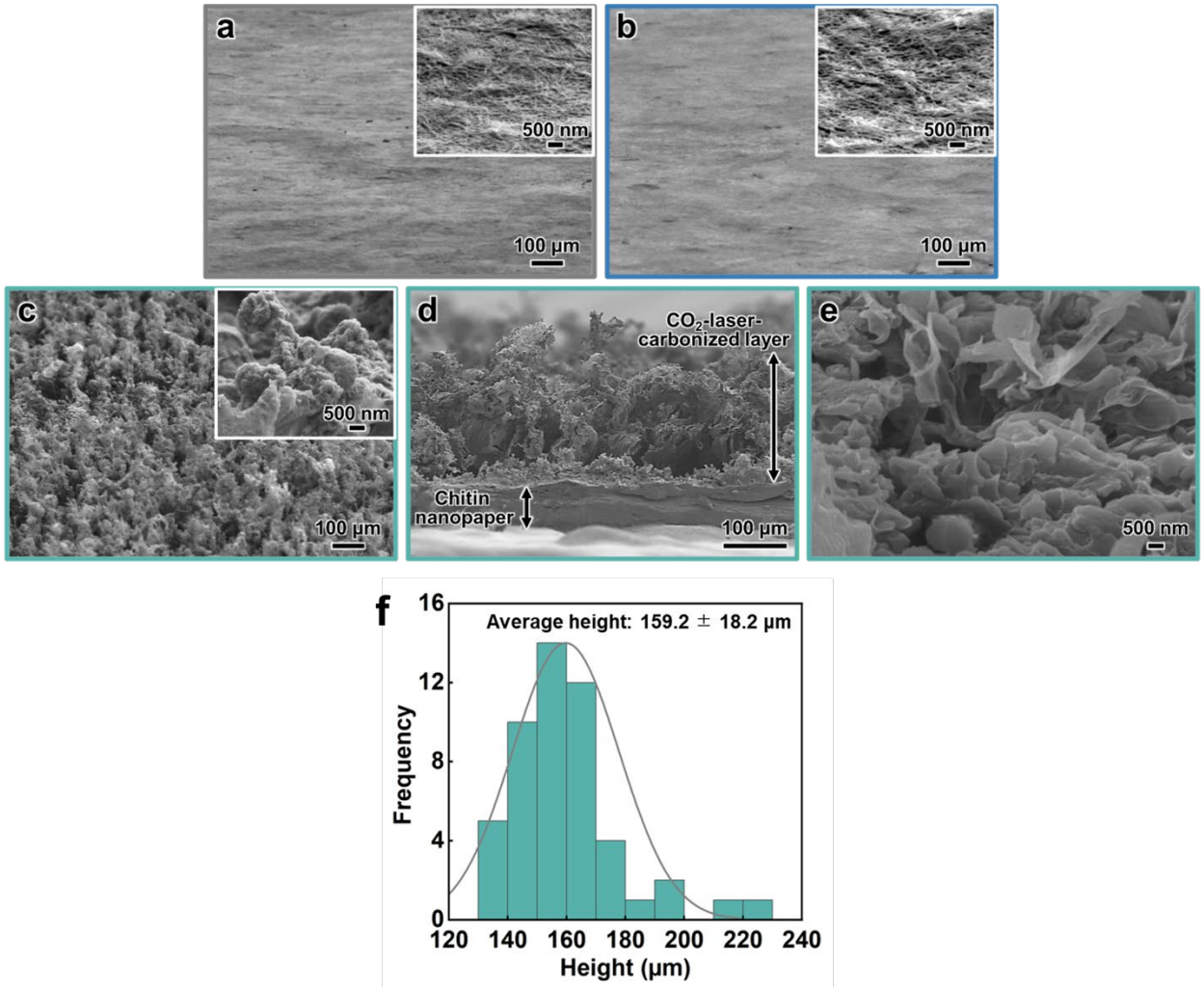

Fig. 3–4 Morphologies of the CO_2-laser-carbonized chitin nanopaper. Oblique-view FE-SEM images of the (a) original chitin nanopaper, (b) $CaCl_2$-treated chitin nanopaper, and (c) CO_2-laser-carbonized chitin nanopaper. (d, e) Cross-section FE-SEM image of the CO_2-laser-carbonized chitin nanopaper and (f) Height distribution histogram of the CO_2-laser-carbonized layer.

Solar absorption and solar thermal heating performances of CO_2-laser-carbonized chitin nanopaper

CO_2-laser-carbonized chitin nanopaper was applied as a photothermal material for solar thermal heating. The solar thermal heating performance of photothermal materials is determined by their capacity to absorb and convert solar light into heat.[18] Accordingly, the light absorption properties of the CO_2-laser-carbonized chitin nanopaper were first evaluated. **Fig. 3–5a–c** shows the ultraviolet-visible-near infrared (UV-vis-NIR) absorption, reflection, and transmission properties of the original chitin nanopaper, $CaCl_2$-treated chitin nanopaper, and CO_2-laser-carbonized chitin nanopaper. The original and $CaCl_2$-treated chitin nanopapers exhibited poor light absorption owing to their high light reflection and transmission. In contrast, the CO_2-laser-carbonized chitin nanopaper achieved much higher light absorption by suppressing reflection and transmission; the light absorption ranged from approximately 98 to 94% in the wavelength range of solar light from 300 to 2500 nm (AM1.5G).

For a clearer discussion, the solar absorption was estimated from the UV-vis-NIR absorption spectra, according to the following equation:[57]

$$\bar{\alpha} = \frac{\int_{\lambda_{min}}^{\lambda_{max}} I_{solar}(\lambda) \cdot \alpha_{solar}(\lambda) d\lambda}{\int_{\lambda_{min}}^{\lambda_{max}} I_{solar}(\lambda) d\lambda} \qquad (1)$$

where $\bar{\alpha}$ denotes the solar absorption (%), λ denotes the wavelength (nm), λ_{min} and λ_{max} are 300 and 2500 nm, respectively, $I_{solar}(\lambda)$ denotes the AM1.5G solar spectral irradiance at λ, and $\alpha_{solar}(\lambda)$ denotes the light absorption (%) at λ. The solar reflection and transmittance were estimated in a similar manner.

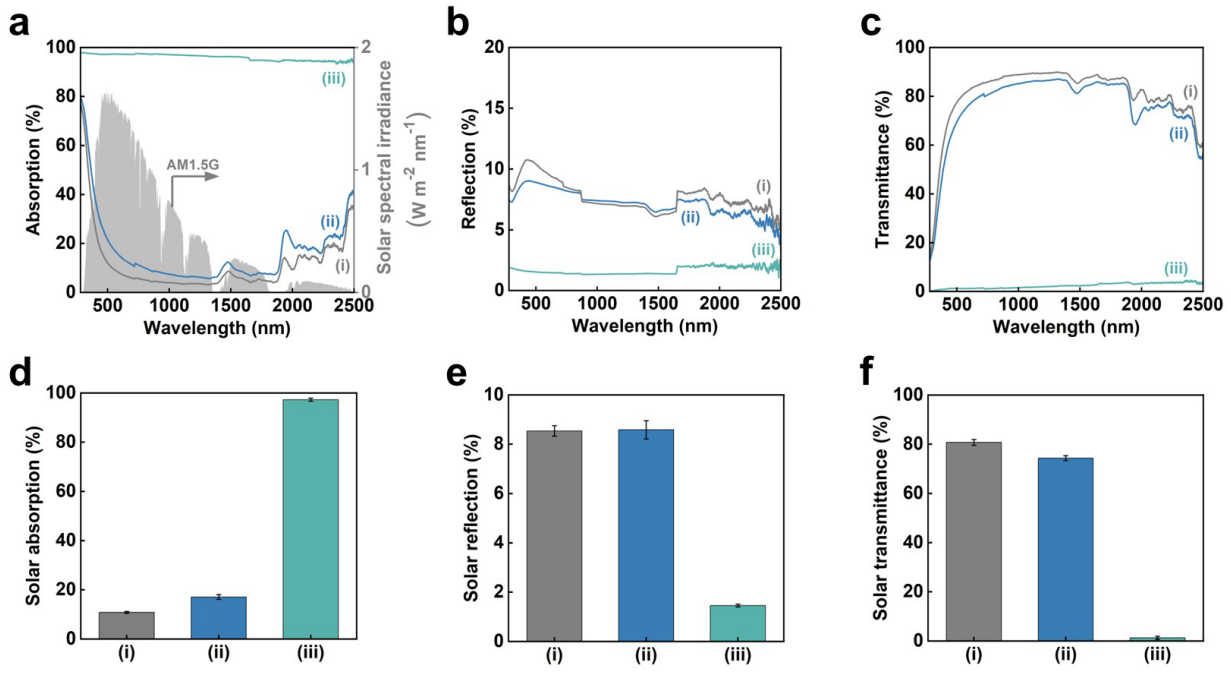

Fig. 3–5 Solar absorption of the CO_2-laser-carbonized chitin nanopaper. (a) Solar spectral irradiance (AM1.5G) and UV-vis-NIR absorption, (b) reflection, (c) transmittance spectra, solar (d) absorption, (e) reflection, and (f) transmittance of the (i) original chitin nanopaper, (ii) $CaCl_2$-treated chitin nanopaper, and (iii) CO_2-laser-carbonized chitin nanopaper.

Fig. 3–5d–f displays the estimated solar absorption, reflection, and transmittance values of the original chitin nanopaper, $CaCl_2$-treated chitin nanopaper, and CO_2-laser-carbonized chitin nanopaper. The solar absorption, reflection, and transmittance of the original chitin nanopaper were 10.8, 8.5, and 80.7%, respectively, whereas those of the $CaCl_2$-treated chitin nanopaper were 17.1, 8.6, and 74.3%, respectively. These results indicate that the solar absorption properties of the chitin nanopaper did not change significantly after $CaCl_2$ treatment, because the original chemical structure of chitin nanopaper remained unchanged after the $CaCl_2$ treatment **(Fig. 3–2a)** and the $CaCl_2$ itself exhibited low solar absorption. Notably, solar absorption was drastically improved to 97.3% by CO_2-laser-induced carbonization, while solar reflection and transmission decreased to

1.5 and 1.2%, respectively. Solar absorption of the CO_2-laser-carbonized chitin nanopaper is owing to (1) its N- and O-doped carbon structures and (2) its coralline-like porous microstructure, as follows: (1) While the original and $CaCl_2$-treated chitin nanopapers had high optical bandgap values (approximately 5 eV), the CO_2-laser-carbonized chitin nanopaper had a much lower optical bandgap (approximately 0.5 eV) **(Fig. 3–6)**, facilitating light absorption at lower energies (i.e., longer wavelengths). The original and $CaCl_2$-treated chitin nanopapers possessed a wide $\sigma-\sigma^*$ bandgap derived from the sp^3-hybridized carbon structure of chitin. The CO_2-laser-carbonized chitin nanopaper with graphitic sp^2-hybridized carbon structures **(Fig. 3–1c)** has $\pi-\pi^*$ bandgap, which is located within the $\sigma-\sigma^*$ bandgap.[58] Moreover, the CO_2-laser-carbonized chitin nanopaper contained the N- and O-containing functional groups (n-orbital) **(Fig. 3–2)**, where the n energy level is located within the $\pi-\pi^*$ bandgap[59] and, thus, can further decrease the optical bandgap.[16] (2) The coralline-like porous microstructures **(Fig. 3–4c,d)** can also enhance light absorption[33] by facilitating multiple light reflections inside the CO_2-laser-carbonized chitin nanopaper (i.e., by suppressing the light reflection to its outer surface), as in a light confinement effect.[60]

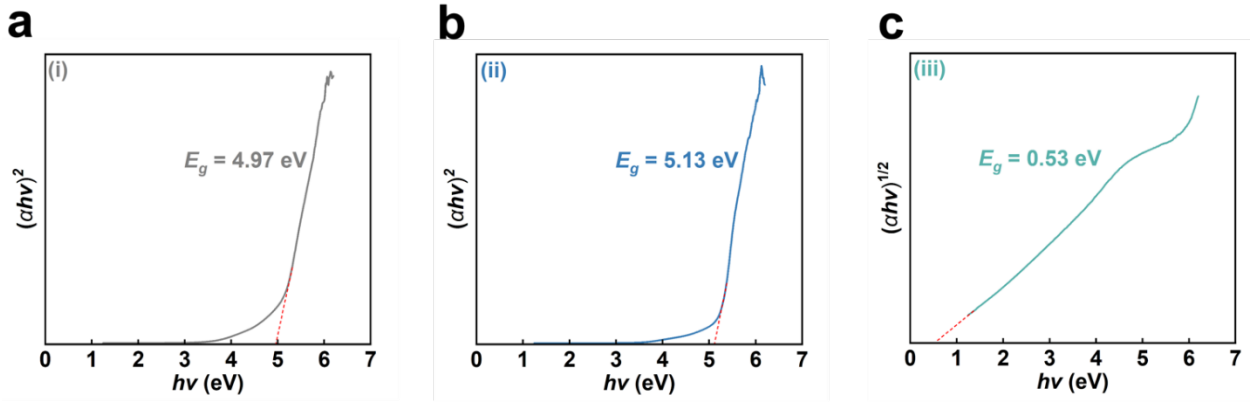

Fig. 3–6 Tauc plots and estimated optical bandgap values of the (a) original chitin nanopaper, (b) $CaCl_2$-treated chitin nanopaper, and (c) CO_2-laser-carbonized chitin nanopaper.

Subsequently, the solar thermal heating performance of the CO_2-laser-carbonized chitin nanopaper was investigated. Change in the surface temperature during simulated solar irradiation (light intensity: 1.0 kW m^{-2} (1 sun), AM1.5G) was monitored using a thermal imaging camera **(Fig. 3–7a)**. As shown in **Fig. 3–7b**, the surface temperature of the CO_2-laser-carbonized chitin nanopaper sharply rose upon 1 sun irradiation and reached up to 77.7 ± 0.99 °C within 600 s, which was much higher than those of the original and $CaCl_2$-treated chitin nanopapers (36.1 ± 0.35 and 36.1 ± 0.19 °C, respectively). The original and $CaCl_2$-treated chitin nanopapers exhibited poor solar thermal heating performances, due to the low solar absorption of the chitin nanopaper and $CaCl_2$ **(Fig. 3–5d)**. The high solar thermal heating performance of the CO_2-laser-carbonized chitin nanopaper was attributed to its effective solar absorption (97.3%).

The effects of the $CaCl_2$ pretreatment time (spraying time of the 25 wt% $CaCl_2$/ethanol solution) and CO_2 laser power on the solar thermal heating performance of the CO_2-laser-carbonized chitin nanopaper were investigated **(Fig. 3–7c)**. The CO_2-laser-carbonized chitin nanopaper prepared with a $CaCl_2$ pretreatment time of 10 s exhibited a higher surface temperature (i.e., higher solar thermal heating performance) than those prepared with $CaCl_2$ pretreatment times of 5 and 20 s, regardless of the examined laser power (1.5, 3.0, 4.5, or 6.0 W). Hence, the optimal $CaCl_2$ pretreatment time for providing the best solar thermal heating performance was determined to be 10 s (addition amount of $CaCl_2$ for approximately 400 mg and 38.5 cm^2 of the chitin nanopaper: approximately 78 mg). This is possibly because $CaCl_2$ pretreatment for 10 s can balance the combustion inhibition during carbonization and the surface exposure of the carbonized layer. Regardless of the $CaCl_2$ pretreatment time, the solar thermal heating performance of the CO_2-laser-carbonized chitin nanopaper was increased with increasing laser power from 1.5 to 4.5 W, while the solar thermal heating performance was decreased with increasing laser power from 4.5 to 6.0

W. Hence, the optimum laser power was considered as 4.5 W. This is possibly because a laser power of 4.5 W can balance the progress of carbonization and the suppression of combustion. The equilibrium surface temperature of the CO_2-laser-carbonized chitin nanopaper upon 1 sun irradiation (77.7 ± 0.99 °C) was higher even than those of the commercial carbon nanotube (55.0 °C)[15] and graphene oxide (69.4 °C) films,[15] high-temperature carbonized cellulose nanopaper (73.9 °C),[15] and high-temperature carbonized chitin nanopaper (75.9 °C).[16] Thus, the CO_2-laser-carbonized chitin nanopaper is expected to be a high-performance photothermal material for solar thermal heating.

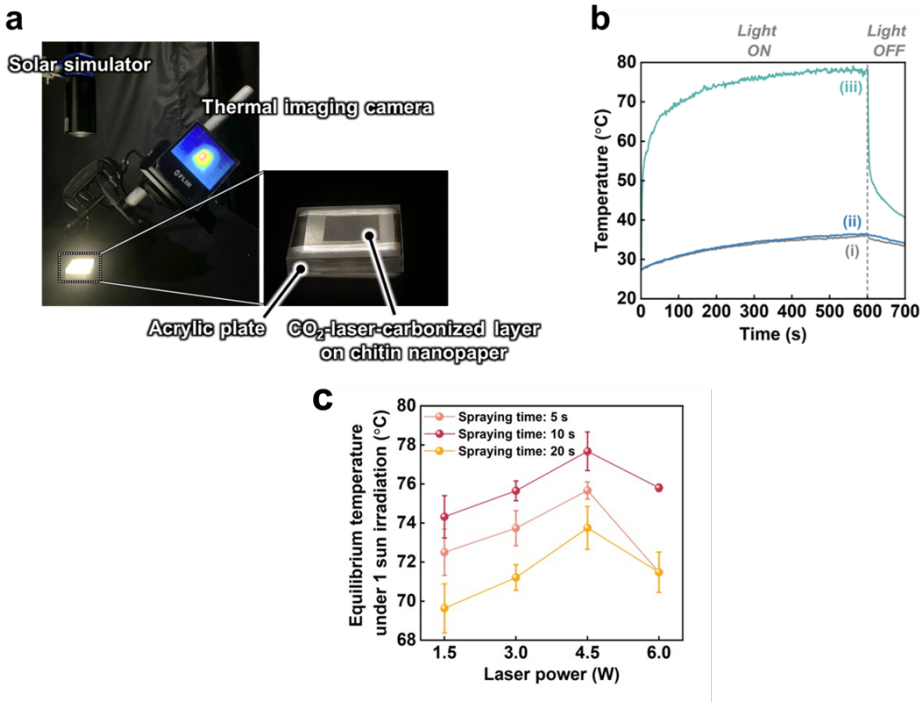

Fig. 3–7 Solar thermal heating performance of the CO_2-laser-carbonized chitin nanopaper. (a) Experimental setup for the surface temperature measurement during 1 sun irradiation by a solar simulator, (b) surface temperature versus 1-sun irradiation time of the (i) original chitin nanopaper, (ii) $CaCl_2$-treated chitin nanopaper, and (iii) CO_2-laser-carbonized chitin nanopaper. (c) Equilibrium surface temperature under 1 sun irradiation of CO_2-laser-carbonized chitin nanopaper prepared with different spraying times different CO_2 laser powers.

3.4 Conclusions

In conclusion, the fast carbonization of chitin nanopaper was successfully achieved by CO_2 laser irradiation. Pretreatment of chitin nanopaper with $CaCl_2$ as a combustion inhibitor is the key to achieve the CO_2-laser-induced carbonization. While conventional hydrothermal and high-temperature carbonization require time-consuming hour-scale processes, CO_2-laser-induced carbonization can be performed on a second timescale. The CO_2-laser-carbonized chitin nanopaper has N- and O-doped carbon structures and coralline-like microstructures, affording a high solar absorption of up to 97.3%. Furthermore, the CO_2-laser-carbonized chitin nanopaper provided the excellent solar thermal heating performance (equilibrium surface temperature under 1 sun irradiation: 77.7 °C). Further functional designs and applications of the CO_2-laser-carbonized chitin nanopaper can be expected. This study opens the door for the facile fabrication of carbonized biomass materials as sustainable photothermal materials toward the effective utilization of renewable solar energy as thermal energy.

3.5 References

1 Z. Bi, Q. Kong, Y. Cao, G. Sun, F. Su, X. Wei, X. Li, A. Ahmad, L. Xie and C.-M. Chen, *J. Mater. Chem. A*, 2019, **7**, 16028–16045.

2 G. Singh, K. S. Lakhi, S. Sil, S. V. Bhosale, I. Kim, K. Albahily and A. Vinu, *Carbon*, 2019, **148**, 164–186.

3 D. Li, W. Chen, J. Wu, C. Q. Jia and X. Jiang, *J. Mater. Chem. A*, 2020, **8**, 24977–24995.

4 H. Koga, K. Nagashima, K. Suematsu, T. Takahashi, L. Zhu, D. Fukushima, Y. Huang, R. Nakagawa, J. Liu, K. Uetani, M. Nogi, T. Yanagida and Y. Nishina, *ACS Nano*, 2022, **16**, 8630–8640.

5 S. Dutta, A. Bhaumik and K. C.-W. Wu, *Energy Env. Sci*, 2014, **7**, 3574–3592.

6 L.-F. Chen, Z.-H. Huang, H.-W. Liang, H.-L. Gao and S.-H. Yu, *Adv. Funct. Mater.*, 2014, **24**, 5104–5111.

7 Y. Wang, R. Liu, Y. Tian, Z. Sun, Z. Huang, X. Wu and B. Li, *Chem. Eng. J.*, 2020, **384**, 123263.

8 J. You, M. Li, B. Ding, X. Wu and C. Li, *Adv. Mater.*, 2017, **29**, 1606895.

9 L. Zhu, Y. Huang, Y. Morishita, K. Uetani, M. Nogi and H. Koga, *J. Mater. Chem. C*, 2021, **9**, 4444–4452.

10 B. Duan, X. Gao, X. Yao, Y. Fang, L. Huang, J. Zhou and L. Zhang, *Nano Energy*, 2016, **27**, 482–491.

11 X. Li, L. Zhu, T. Kasuga, M. Nogi and H. Koga, *Chem. Eng. J.*, 2022, **450**, 137943.

12 Y. Li, Y. A. Samad, K. Polychronopoulou, S. M. Alhassan and K. Liao, *J Mater Chem A*, 2014, **2**, 7759–7765.

13 Y. Geng, W. Sun, P. Ying, Y. Zheng, J. Ding, K. Sun, L. Li and M. Li, *Adv. Funct. Mater.*, 2021, **31**, 2007648.

14 Y. Sun, Z. Zhao, G. Zhao, L. Wang, D. Jia, Y. Yang, X. Liu, X. Wang and J. Qiu, *Carbon*, 2021, **179**, 337–347.

15 T. Yeamsuksawat, Y. Morishita, J. Shirahama, Y. Huang, T. Kasuga, M. Nogi and H. Koga, *Chem. Mater.*, 2022, **34**, 7379–7388.

16 T. Yeamsuksawat, L. Zhu, T. Kasuga, M. Nogi and H. Koga, *Nanomaterials*, 2023, **13**, 1480.

17 ASTM G173-03., *Standard Tables for Reference Solar Spectral Irradiances: Direct Normal and Hemispherical on 37° Tilted Surface*, ASTM International: West Conshohocken, PA, 2012.

18 M. Gao, L. Zhu, C. K. Peh and G. W. Ho, *Energy Environ. Sci.*, 2019, **12**, 841–864.

19 R. Fillet, V. Nicolas, V. Fierro and A. Celzard, *Sol. Energy Mater. Sol. Cells*, 2021, **219**, 110814.

20 W. Guan, Y. Guo and G. Yu, *Small*, 2021, **17**, 2007176.

21 A. M. Saleque, N. Nowshin, Md. N. A. S. Ivan, S. Ahmed and Y. H. Tsang, *Sol. RRL*, 2022, **6**, 2100986.

22 S. Zhou, L. Zhou, Y. Zhang, J. Sun, J. Wen and Y. Yuan, *J. Mater. Chem. A*, 2019, **7**, 4217–4229.

23 Y. Long, Y. Yu, Y. W. Chua and H. Wu, *Fuel*, 2017, **193**, 460–466.

24 B. Hu, Q. Lu, Y. Wu, W. Xie, M. Cui, J. Liu, C. Dong and Y. Yang, *J. Energy Chem.*, 2020, **43**, 78–89.

25 R. J. White, M. Antonietti and M.-M. Titirici, *J. Mater. Chem.*, 2009, **19**, 8645.

26 M. Sevilla and A. B. Fuertes, *Carbon*, 2009, **47**, 2281–2289.

27 J. Lin, Z. Peng, Y. Liu, F. Ruiz-Zepeda, R. Ye, E. L. G. Samuel, M. J. Yacaman, B. I. Yakobson and J. M. Tour, *Nat. Commun.*, 2014, **5**, 5714.

28 P. I. C. Claro, A. C. Marques, I. Cunha, R. F. P. Martins, L. M. N. Pereira, J. M. Marconcini, L. H. C. Mattoso and E. Fortunato, *ACS Appl. Nano Mater.*, 2021, **4**, 8262–8272.

29 S. Lee and S. Jeon, *ACS Sustain. Chem. Eng.*, 2019, **7**, 2270–2275.

30 L. Zhu, X. Li, T. Kasuga, K. Uetani, M. Nogi and H. Koga, *J. Mater. Chem. C*, 2022, **10**, 3712–3719.

31 Y. Chyan, R. Ye, Y. Li, S. P. Singh, C. J. Arnusch and J. M. Tour, *ACS Nano*, 2018, **12**, 2176–2183.

32 C. H. Dreimol, H. Guo, M. Ritter, T. Keplinger, Y. Ding, R. Günther, E. Poloni, I. Burgert and G. Panzarasa, *Nat. Commun.*, 2022, **13**, 3680.

33 Y. Peng, W. Zhao, F. Ni, W. Yu and X. Liu, *ACS Nano*, 2021, **15**, 19490–19502.

34 Y. Huang, Y. Morishita, K. Uetani, M. Nogi and H. Koga, *Nanoscale Adv.*, 2020, **2**, 2339–2346.

35 J. Tauc, R. Grigorovici and A. Vancu, *Phys. Status Solidi B*, 1966, **15**, 627–637.

36 D. H. Cotton and D. R. Jenkins, *Trans. Faraday Soc.*, 1971, **67**, 730.

37 B. Li, H. Lv, J. Deng, L. Ye, W. Gao and M. Bi, *Fuel*, 2021, **304**, 121451.

38 Y. Koshiba and Y. Hirakawa, *Case Stud. Therm. Eng.*, 2021, **25**, 100984.

39 G. T. Linteris, M. D. Rumminger and V. I. Babushok, *Prog. Energy Combust. Sci.*, 2008, **34**, 288–329.

40 G. K. Ramesha and S. Sampath, *J. Phys. Chem. C*, 2009, **113**, 7985–7989.

41 Z. H. Ni, T. Yu, Y. H. Lu, Y. Y. Wang, Y. P. Feng and Z. X. Shen, *ACS Nano*, 2008, **2**, 2301–2305.

42 Y. Wang, L. Zhu, J. You, F. Chen, L. Zong, X. Yan and C. Li, *ACS Sustain. Chem. Eng.*, 2017, **5**, 10673–10681.

43 J. D. Goodrich and W. T. Winter, *Biomacromolecules*, 2007, **8**, 252–257.

44 N. U. Nguyen-Thai and S. C. Hong, *Macromolecules*, 2013, **46**, 5882–5889.

45 J. Liu, S. Liu, A. Zhao, D. Bi, D. Yao and R. Kong, *J. Anal. Appl. Pyrolysis*, 2023, **169**, 105863.

46 F. Reig, *Talanta*, 2002, **58**, 811–821.

47 H. Yu, L. Shang, T. Bian, R. Shi, G. I. N. Waterhouse, Y. Zhao, C. Zhou, L.-Z. Wu, C.-H. Tung and T. Zhang, *Adv. Mater.*, 2016, **28**, 5080–5086.

48 Z.-H. Sheng, L. Shao, J.-J. Chen, W.-J. Bao, F.-B. Wang and X.-H. Xia, *ACS Nano*, 2011, **5**, 4350–4358.

49 C.-M. Chan, J. Wu, J.-X. Li and Y.-K. Cheung, *Polymer*, 2002, **43**, 2981–2992.

50 S. L. Stipp and M. F. Hochella, *Geochim. Cosmochim. Acta*, 1991, **55**, 1723–1736.

51 M. Nie, M. Azizi, I. Keresztes, A. Kierulf and A. Abbaspourrad, *ACS Appl. Polym. Mater.*, 2021, **3**, 1415–1425.

52 J. Gong, W. Zhang, T. Liu and L. Zhang, *Nanoscale*, 2011, **3**, 3123.

53 D. R. Baer and J. F. Moulder, *Surf. Sci. Spectra*, 1993, **2**, 1–7.

54 I. Corazzari, R. Nisticò, F. Turci, M. G. Faga, F. Franzoso, S. Tabasso and G. Magnacca, *Polym. Degrad. Stab.*, 2015, **112**, 1–9.

55 S. T. Lazar, T. J. Kolibaba and J. C. Grunlan, *Nat. Rev. Mater.*, 2020, **5**, 259–275.

56 S. Luo, P. T. Hoang and T. Liu, *Carbon*, 2016, **96**, 522–531.

57 J. Mandal, D. Wang, A. C. Overvig, N. N. Shi, D. Paley, A. Zangiabadi, Q. Cheng, K. Barmak, N. Yu and Y. Yang, *Adv. Mater.*, 2017, **29**, 1702156.

58 C. Mathioudakis, G. Kopidakis, P. C. Kelires, P. Patsalas, M. Gioti and S. Logothetidis, *Thin Solid Films*, 2005, **482**, 151–155.

59 M. Li, S. K. Cushing, X. Zhou, S. Guo and N. Wu, *J. Mater. Chem.*, 2012, **22**, 23374.

60 J. Wang, J. Zhao, Y. Li, M. Yang, Y. Q. Chang, J. P. Zhang, Z. Sun and Y. Wang, *ACS Macro Lett.*, 2015, **4**, 392–397.

Concluding Remarks

In this dissertation, bio-nanofiber-derived carbon materials were successfully prepared using conventional high-temperature carbonization and CO_2-laser carbonization. The resulting bio-nanofiber-derived carbon materials exhibited a promising performance in solar thermal heating. Chapter 1 compared the solar thermal heating performance of carbonized cellulose nanopapers with dense and nanoporous structures. To maintain the nanoporous structure, an I_2 pretreatment was performed to suppress carbon removal during high-temperature carbonization. It was confirmed that the nanoporous structure enhanced the light absorption and improved the solar thermal heating performance. The carbonized cellulose nanopapers with nanoporous structures were then carbonized at various temperatures to control their chemical structures. The semi-carbonized structure obtained at 500 °C provided the best solar thermal heating performance, as it was suitable for light absorption. However, the I_2 pretreatment was time-consuming and potentially harmful.

To address the pretreatment issue, chitin was introduced in Chapter 2 as an alternative carbon precursor to cellulose due to its reported high thermal stability and the presence of the acetyl-amino group, which provides an opportunity to prepare N-doped carbon structures by carbonization. As a result, the carbonized chitin nanopaper exhibited a better solar thermal heating performance than the carbonized cellulose nanopaper due to both its N- and O-doped carbon structure and subwavelength nanoporous structure. The optimal carbonization temperature for the chitin nanopaper was found to be 400 °C, as this provided a balance between the carbon-based chemical structure and nano/microscale morphology, thereby facilitating effective solar thermal heating.

Considering that conventional high-temperature carbonization processes are time-consuming, Chapter 3 explored the CO_2-laser carbonization of the chitin nanopaper as a rapid and facile method. The CO_2-laser carbonization was achieved by the addition of $CaCl_2$ as a combustion inhibitor. The resulting CO_2-laser-carbonized chitin nanopaper exhibited an outstanding solar-thermal heating performance, owing to its N- and O-doped carbon structure and coralline-like microstructure. Its performance was comparable to that of cellulose and chitin nanopaper carbonized at high temperatures. In summary, this study demonstrates the fabrication of carbonized bionanofiber materials as sustainable photothermal materials for the effective utilization of renewable solar energy as thermal energy.

List of Publications

1. Semicarbonized Subwavelength-Nanopore-Structured Nanocellulose Paper for Applications in Solar Thermal Heating

Thanakorn Yeamsuksawat, Yoshitaka Morishita, Jun Shirahama, Yintong Huang, Takaaki Kasuga, Masaya Nogi, Hirotaka Koga*

Chemistry of Materials, **2022**, *34 (16)*, 7379–7388.

DOI: 10.1021/acs.chemmater.2c01466

2. Chitin-Derived Nitrogen-Doped Carbon Nanopaper with Subwavelength Nanoporous Structures for Solar Thermal Heating

Thanakorn Yeamsuksawat, Luting Zhu, Takaaki Kasuga, Masaya Nogi, Hirotaka Koga*

Nanomaterials, **2023**, *13(9)*, 1480.

DOI: 10.3390/nano13091480

3. CO_2-Laser-Induced Carbonization of Calcium Chloride-Treated Chitin Nanopaper for Applications in Solar Thermal Heating

Thanakorn Yeamsuksawat, Luting Zhu, Takaaki Kasuga, Masaya Nogi, Hirotaka Koga*

RSC Advances, **2023**, *13*, 17556-17564

DOI: 10.1039/d3ra03373b

Copyright

The author has obtained the permissions to reuse contents from Wiley-VCH, Royal Society of Chemistry, Elsevier, American Chemical Society, and MDPI.

Credits

Reproduced with permission from Thanakorn Yeamsuksawat, Yoshitaka Morishita, Jun Shirahama, Yintong Huang, Takaaki Kasuga, Masaya Nogi, Hirotaka Koga, Chemistry of Materials, **2022**, *34 (16)*, 7379–7388. Copyright 2022, American Chemical Society.

Reproduced with permission from Thanakorn Yeamsuksawat, Luting Zhu, Takaaki Kasuga, Masaya Nogi, Hirotaka Koga, Nanomaterials, **2023**, *13(9)*, 1480.

Reproduced with permission from Thanakorn Yeamsuksawat, Luting Zhu, Takaaki Kasuga, Masaya Nogi, Hirotaka Koga, RSC Advances, **2023**, *13*, 17556-17564 Copyright 2023, Royal Society of Chemistry

Acknowledgements

Time has flown by swiftly, and now, almost three years of my life as a student at Osaka University in Japan are coming to a close. Throughout my journey, I have experienced moments of happiness, sadness, stress, and numerous challenges. I believe everything that has come into my life is like a color, decorating a piece of fabric, making it more beautiful. Therefore, I would like to express my heartfelt gratitude to all the people who have acted as painters, adding vibrant hues to my life's canvas.

Firstly, I would like to acknowledge the invaluable financial support provided to me through the Japanese Government (MEXT) Scholarship and the Japan International Cooperation Agency (JICA). These scholarships have enabled me to pursue my degree in Japan, marking the first step toward achieving my academic goals.

I would like to express my sincere gratitude to Professor Masaya Nogi, who opened the first door and allowed me to become a part of his laboratory. I have gained lots of fundamental knowledge about cellulose nanofibers, both through his insightful teachings and the tasks he assigned me.

I would like to express my heartfelt appreciation to Associate Professor Hirotaka Koga, who has been serving as my supervisor. I am extremely grateful for his efforts, as without him, I have no idea how I would have been able to fulfill the graduation requirements. Moreover, he always lends his hand to provide support during my difficult times. I have learned so much from him, especially in terms of how to tell the story of my research in a logical manner. There were times when I doubted my ability to meet his expectations, but he always showed great patience and never gave up on pushing me to become better and better. I am truly indebted to him, and he will forever remain my role model for my future academic career.

I sincerely thank Assistant Professor Takaaki Kasuga for his kind, valuable advice and generous support in the maintenance and management of the laboratory. His kind assistance has been instrumental in ensuring a smooth and productive research environment.

I would also like to extend my heartfelt gratitude to Associate Professor Yusa Muroya for his guidance and support during the Joho and Kikaku seminars. Professor Takahiro Kozawa and Professor Akinori Saeki for serving as my vice supervisors during my graduation defense and for their assistance in preparing my dissertation. Their expertise and guidance have been invaluable, and I truly appreciate their contributions to my academic journey.

I thank all Nogi laboratory members and my Thai friends, particularly P'Koen, Snook, and Mew, for their unwavering support. The moments we shared, filled with laughter, are truly unforgettable. I treasure our friendships and sincerely wish them all success and happiness in their future endeavors.

Last but certainly not least, I would like to express my heartfelt gratitude to my Daddy, Mommy, Bright, and Beam for their unwavering support and encouragement. During moments of despair and when I felt like giving up, they were always there to uplift my spirits. Their love and belief in me have constantly motivated me throughout my journey.

June 2023

Thanakorn Yeamsuksawat